POLITECNICO DI MILANO
Scuola di Ingegneria Industriale e dell'Informazione
Corso di Laurea magistrale in Ingegneria Biomedica

Tesi di laurea

Live imaging and analysis of the embryonic heart to study tissue dynamics and calcium signaling in cardiogenesis

Relatore: **Prof.ssa Ing. Maria Laura Costantino**
Correlatori: **Dott. Julien Vermot**
                  Dott. Ing. Francesco Boselli

                              Laureando
                              Paola Lamperti
                              823979

Anno accademico: 2014-2015

II

Acknowledgement

Table of contents

List of figures

Introduction

VII

Results

XI

List of tables

Riassunto

Introduzione

I difetti congeniti del cuore sono alterazioni della struttura e della funzione cardiaca che nascono quando il normale processo di sviluppo del cuore viene compromesso. Si stima che tra tutte le malattie congenite, quelle cardiache rappresentino la prima causa di morte nei neonati. Nel tentativo di sviluppare tecniche di diagnosi precoce e di cura, molti sforzi sono attualmente rivolti allo studio della cardiogenesi e dei processi che possono alterarla.

I modelli animali comunemente utilizzati sono il pollo, il topo e lo *zebrafish*, grazie al fatto che le prime fasi dello sviluppo cardiaco sono comuni in tutti i vertebrati. Il cuore nasce, infatti, come una struttura tubolare formata da tre strati: il miocardio (il tessuto contrattile esterno), l'endocardio (il tessuto endoteliale a diretto contatto con il sangue) e la gelatina cardiaca o *cardiac jelly* (lo strato intermedio di matrice extracellulare). Nelle successive fasi di sviluppo, il cuore si ripiega su se stesso e le porzioni laterali del tubo si espandono formando due camere divise dal canale atrioventricolare. Nei mammiferi, le due camere andranno poi incontro al processo di septazione e la struttura finale del cuore prevedrà due atri e due ventricoli. Nello *zebrafish*, la forma del cuore a questo stage è già molto simile a quella definitiva, con un atrio e un ventricolo.

Negli ultimi anni, molti ricercatori hanno dimostrato il ruolo fondamentale che la meccanica dei tessuti e la fluidodinamica del cuore rivestono in tutte le fasi dello sviluppo cardiaco. Le forze meccaniche, infatti, innescano una serie di risposte biologiche, chimiche e elettriche che portano al rimodellamento delle cellule e dei tessuti. I processi con cui questo avviene vanno sotto il nome di meccanismi di meccanotrasduzione.

Tra questi, un meccanismo da tempo oggetto di studio nel cuore adulto è quello che contribuisce all'attivazione del calcio nei cardiomiociti grazie alla deformazione del miocardio. Questo tipo di meccanotrasduzione e il suo possibile impatto sulla dinamica del calcio e della contrazione cardiaca nel cuore embrionale non sono ancora stati investigati.

Nello studio dello sviluppo fisiologico e patologico del cuore, lo *zebrafish* offre diversi vantaggi rispetto agli altri modelli animali. Il principale riguarda la possibilità di ricorrere a tecniche genetiche che permettono di aumentare o bloccare l'espressione di geni fondamentali nel processo di sviluppo del cuore e di alterare la biomeccanica del cuore *in vivo* per indagarne il ruolo nella cardiogenesi. Il limite dello *zebrafish* nella ricerca cardiovascolare sta nella struttura finale del cuore, che risulta una versione semplificata del

cuore a quattro camere dell'uomo. Tuttavia il problema non si pone se si considerano le prime fasi dello sviluppo cardiaco, che, come detto, sono comuni.

Nello *zebrafish*, l'uso di strumenti genetici consente, inoltre, di esprimere proteine fluorescenti in strutture di interesse quali i tessuti cardiaci. Grazie alla trasparenza ottica degli embrioni, poi, il segnale fluorescente può essere osservato e acquisito al microscopio *in vivo* e l'immagine del cuore così ottenuta può essere analizzata.

Il presente lavoro si focalizza sul cuore tubolare nelle prime fasi di sviluppo, poco dopo che la contrazione cardiaca ha avuto inizio. In questo stadio, le valvole cardiache non sono ancora presenti; tuttavia il cuore riesce a pompare il sangue senza rigurgiti significativi. Il meccanismo con cui questo avviene non è ancora stato compreso. I lavori presenti in letteratura sull'argomento descrivono alcuni aspetti del funzionamento del cuore in maniera per lo più qualitativa e quasi nessun tentativo è stato fatto per combinare risultati di meccanica dei tessuti, fluidodinamica e elettrofisiologia.

In questo contesto, il presente lavoro si pone come obiettivo lo studio del cuore dell'embrione di *zebrafish* a 28-30 ore post fecondazione (hpf), cioè appena prima che il tubo cardiaco inizi a piegarsi su se stesso. L'analisi si basa sui dati ottenuti dall'*imaging* del cuore battente *in vivo* e comprende lo studio, per mezzo di algoritmi dedicati, della dinamica dei tre strati che compongono il cuore durante il ciclo cardiaco, della velocità dei globuli rossi e della propagazione dell'impulso elettrico in condizioni fisiologiche. Oltre a fornire un punto di partenza nella comprensione del meccanismo di funzionamento del tubo cardiaco, questo permette di correlare la dinamica del calcio nel cuore battente con la dinamica del miocardio embrionale e perciò indagare l'accoppiamento elettromeccanico e l'esistenza di un eventuale processo di meccanotrasduzione che moduli la dinamica del calcio in funzione dalla deformazione del tessuto, come osservato nei cardiomiociti adulti.

Materiali e metodi

Il presente studio del cuore nelle prime fasi di sviluppo è basato sui dati ottenuti dall'*imaging* del cuore *in vivo* in embrioni transgenici che esprimono molecole fluorescenti in modo specifico nelle strutture di interesse. Per studiare la dinamica del cuore e la velocità dei globuli rossi, l'*imaging* è stato condotto al microscopio confocale, che vanta un'ottima risoluzione spaziale, su cuori geneticamente modificati per emettere fluorescenza verde nel miocardio e rossa nell'endocardio e nei globuli rossi. Per studiare la

dinamica del calcio nel miocardio, l'*imaging* è stato condotto al microscopio a fogli di luce (*light sheet microscope*), caratterizzato da un'elevata risoluzione temporale, su cuori geneticamente modificati per esprimere *gcamp5.0*, un reporter del calcio, che emette un segnale verde proporzionale alle variazioni di calcio nei cardiomiociti. Nello stesso cuore, una proteina fluorescente rossa, non sensibile al calcio, è stata utilizzata come controllo per l'analisi del segnale del *gcamp5.0*.

L'*imaging* prevede che sezioni del cuore battente a diversa profondità siano consecutivamente acquisite. Attraverso algoritmi dedicati, poi, le sezioni sono assemblate per ricostruire il volume tridimensionale del cuore e il suo movimento durante il ciclo cardiaco.

Per studiare il comportamento del cuore nello spazio e nel tempo, per prima cosa il volume acquisito è stato ricostruito con un nuovo algoritmo di segmentazione semiautomatica implementato *ad hoc* in Matlab: ad ogni istante temporale del ciclo cardiaco, il volume viene sezionato con piani equidistanti tra loro e perpendicolari all'asse longitudinale del tubo cardiaco in tutta la sua lunghezza e le sezioni di cuore risultanti vengono fittate con ellissi. La curva che connette tutti i centri delle ellissi e approssima l'asse del cuore (*centreline*) è stata usata per parametrizzare la geometria del tubo.

La dinamica del cuore è stata indagata nel miocardio, endocardio e *cardiac jelly*. Per descrivere il miocardio sono stati utilizzati due parametri: l'area delle ellissi che rappresentano le sezioni del tessuto e la distanza tra cardiomiociti adiacenti. L'analisi è stata condotta su tre cuori a 28 hpf e sei cuori a 30 hpf. L'endocardio è stato studiato considerando l'area delle ellissi in due cuori a 28 hpf; il *cardiac jelly* prendendo come parametro la differenza tra l'area del miocardio e dell'endocardio in due cuori a 28 hpf.

Per correlare il movimento e l'eiezione del cuore, la velocità dei globuli rossi è stata calcolata in due cuori a 28 hpf.

Per studiare la propagazione dell'impulso elettrico nel miocardio, per prima cosa è stato analizzato un cuore non battente come suggerito da letteratura. La contrazione muscolare è stata inibita usando BDM prima dell'*imaging*. Il segnale acquisito emesso dal *gcamp5.0* descrive la variazione di calcio nei cardiomiociti. L'attività muscolare del cuore è stata poi riattivata e il segnale del calcio nel cuore battente analizzato. Per tale analisi, si è considerato il rapporto tra l'intensità del segnale emesso dal *gcamp5.0* e il segnale di controllo del miocardio, in modo da correggere artefatti dovuti a variazioni di intensità

relativi ai movimenti dei tessuti cardiaci. La strategia adottata per rimuovere tali artefatti è stata verificata in un cuore di controllo che esprime due transgeni fluorescenti non sensibili al calcio. Il confronto tra la dinamica del calcio e quella del miocardio è stato fatto per indagare l'accoppiamento elettromeccanico del cuore.

Risultati e discussione

Dall'analisi delle aree di miocardio e endocardio, il miocardio risulta avere una forma ellittica durante tutto il ciclo cardiaco, mentre l'endocardio presenta invaginazioni che permettono al lumen di espandersi e contrarsi. Infatti l'endocardio si restringe molto più del miocardio: l'*Area Fractional Shortening*, un indice che misura quanto l'area cambia passando dalla condizione di rilassamento a quella di contrazione, è risultato tra -50 e -80% nell'endocardio e tra -30 e -60 % nel miocardio.

L'analisi della velocità dei globuli rossi nel tubo cardiaco ha mostrato rigurgiti nella prima metà del cuore, in cui l'AFS è minore, che sembrano sparire procedendo verso la zona finale del cuore, caratterizzata invece dal massimo AFS. Queste osservazioni suggeriscono che sia la costrizione del lumen a determinare o meno questi retroflussi.

L'analisi della dinamica del miocardio ha mostrato risultati confrontabili sia dall'analisi dell'area che della distanza tra cardiomiociti adiacenti. La contrazione propaga dall'*inflow* all'*outflow* con un ritardo nella propagazione nella zona finale. Questo ritardo determina la simultanea contrazione di *inflow* e *outflow,* probabilmente per aumentare la pressione nella zona centrale del cuore. Per quanto riguarda l'endocardio, l'analisi dei due cuori ha dato risultati diversi: in un cuore la contrazione propaga linearmente e con velocità uniforme; nell'altro l'onda è più irregolare. Queste differenze sembrano essere dovute al *fitting* non ottimale delle sezioni dell'endocardio.

Confrontando la dinamica di miocardio e endocardio, la contrazione dei due tessuti avviene contemporaneamente, suggerendo che la forza che parte dal miocardio e dà inizio alla contrazione nell'endocardio si trasmette instantemente nello stadio evolutivo analizzato. La dinamica del *cardiac jelly,* invece, sembra in controfase. La massima area è infatti raggiunta durante la contrazione del cuore e la minima area durante il rilassamento. Lo strato potrebbe quindi alternativamente accumulare e restituire energia elastica aiutando la contrazione delle sezioni dei due tessuti dopo la diastole e l'espansione dopo la sistole.

La durata della contrazione e del rilassamento cambia lungo il cuore sia nel miocardio che nell'endocardio: la prima metà del tubo cardiaco rimane rilassata più a lungo (40-60% del

ciclo cardiaco) e contratta per meno tempo (20%); mentre l'*outflow* rimane contratta più a lungo (30-40%) e rilassata per meno tempo (20-30%). La prolungata contrazione della zona finale del cuore potrebbe permettere il riempimento della regione a monte, che invece rimarrebbe a lungo rilassata per consentire al sangue di entrare e alla pressione di aumentare.

Dallo studio della propagazione dell'impulso elettrico nel cuore non battente, l'onda del calcio propaga linearmente dall'*inflow* (in cui lavori presenti in letteratura indicano l'esistenza di un pacemaker) all'*outflow*.

Dal confronto tra la dinamica del calcio e quella del miocardio nel cuore battente si è osservato che lungo tutto il cuore, il calcio intracellulare raggiunge il massimo livello durante l'accorciamento del tessuto, come ci si aspetta dal fatto che la contrazione muscolare è attivata dall'aumento di calcio nel citoplasma. In alcuni cardiomiociti, tuttavia, un aumento del livello di calcio è stato osservato anche in corrispondenza di condizioni di allungamento del tessuto, suggerendo che un meccanismo di meccanotrasduzione simile a quello di attivazione del calcio a seguito della deformazione del miocardio osservato nei cardiomiociti adulti esista anche nel cuore dell'embrione.

Conclusione

Nel presente lavoro, la dinamica dei tessuti, del calcio nel miocardio e l'accoppiamento elettromeccanico nel cuore embrione sono stati investigati *in vivo* usando lo *zebrafish* come modello animale.

Degli algoritmi sono stati sviluppati e implementati per quantificare i dati ottenuti dall'*imaging* del cuore battente e hanno permesso di ottenere molte informazioni sugli strati che compongono il cuore. Anche se i risultati ottenuti dovranno essere verificati su un campione più ampio, i risultati preliminari presentati in questa tesi suggeriscono l'esistenza di un meccanismo di meccanotrasduzione nel cuore embrionale che regola l'accoppiamento tra la deformazione del miocardio e l'attivazione del calcio.

L'analisi, condotta su campioni sani, vuole essere un punto di partenza nello studio di condizioni patologiche. Gli stessi algoritmi e protocolli sperimentali sviluppati in questa tesi potranno essere applicati in futuro su cuori affetti da alterazioni genetiche o fisiche per capire come queste anomalie influenzino l'anatomia e il normale funzionamento del cuore.

Abstract

<u>Introduction</u>

Congenital cardiovascular diseases are structural problems that form when cardiac morphogenetic process is altered. They represent the most common cause of infant deaths from birth malformations. In the hope that one day early diagnosis and cure will be possible, many researches are trying to understand why and how cardiogenesis is impaired. Animal models commonly used to study cardiovascular morphogenesis are zebrafish, chick and mouse since the early mechanisms of heart formation are evolutionary conserved among vertebrates. At the onset of cardiogenesis, heart forms as a linear tube made up of three layers: the myocardium (the contractile outer tissue made of cardiomyocytes), the cardiac jelly (an acellular layer of extracellular matrix) and the endocardium (in direct contact with the blood flow). During the development, the heart loops, expands and two chambers appear, divided by the atrioventricular canal, where the precursor of the atrioventricular valve forms. From this stage on, heart develops differently according to the animal. In mammals, common chambers undergo the septation process and two distinct atria and two ventricles form. In zebrafish, the final structure of the heart is almost already achieved with a single atrium and a ventricle.

In the last decade, mechanical forces have been proved to affect all the steps of cardiac morphogenesis and be involved in abnormal development of the heart. In fact, they are converted in biological, chemical and electrical responses that lead to structural and functional remodelling of cells and tissues through mechanotransduction pathways.

Among these, a cardiac mechanotransduction mechanism has been studied for a long time in the adult heart: the stretching of adult cardiomyocytes contributes to trigger calcium signaling and to control calcium spark rate. Until now, this mechanism and its effect on calcium signaling and heart contraction in the embryonic heart has never been investigated. In the study of mechanotransduction pathways leading to physiological and abnormal cardiac development, zebrafish offers several advantages compared to other vertebrate animal models. In fact, genetic tools are available to overexpress or knock down genes involved in cardiogenesis and the heart mechanics can be altered *in vivo* to study its effect on cardiac morphogenesis. Furthermore its transparency allows high resolution imaging at high temporal resolution. Considering all these advantages, and even though the final

structure of the heart corresponds to a simplified version of the four-chambered mammal heart, zebrafish is considered as an excellent model in cardiovascular research.

In zebrafish, fluorescence can be expressed in precise regions of the heart using genetic tools. Thanks to the optical transparency of the embryos, then, the physiological or pathological beating heart can be observed under microscope, acquired and analysed.

The present work focuses on the zebrafish primitive heart tube. At this stage, valves are not present yet; however the heart produces a unidirectional blood flow which is sufficient to promote blood circulation in the whole embryo. The pumping mechanism is still not understood. The papers available in literature provide mainly a qualitative description of some aspects of heart pumping, and few efforts have been done to investigate the biomechanics underlying its working mechanism, in particular how the layers interact with each other, along with blood flow and the electrical control of myocardial contraction.

In this context, the present work aims to study the embryonic heart in zebrafish model at the onset of the looping stage (28-30 hpf), using the data acquired from four-dimensional live imaging of the beating heart.

The analysis considers the dynamics of the three layers composing the heart during the cardiac cycle, the velocity of red blood cells along the tube and the calcium dynamics in the myocardium in physiological condition.

This represents a starting point to understand the working mechanism of the primitive valveless heart and allows to correlate calcium and myocardium dynamics in the embryonic heart to search for the stretch-dependent calcium activation documented in adult isolated cardiomyocytes.

Materials and methods

The study of the primitive heart tube is based on the analysis of the data obtained from *in vivo* 4-D imaging of transgenic zebrafish hearts at 28-30 hours post fecundation (hpf), that express fluorescent molecules in the structures of interest.

To study heart dynamics and red blood cells velocity, the imaging was performed with the confocal microscope on embryos expressing green fluorescence in myocardium and red fluorescence in endocardium and red blood cells. To study calcium dynamics in the myocardium, the imaging was performed with the light sheet microscope on embryos in which the calcium reporter *gcamp5.0* was genetically encoded. The *gcamp5.0* expresses in green a signal proportional to calcium variations in cardiomyocytes and, at the same time,

a non-calcium-sensitive red fluorescent protein was used as control to study the *gcamp5.0* signal.

Four-dimensional live imaging is based on the separate acquisition of slices of the heart over the cardiac cycle at different depths; slices sequences are then put together to reconstruct the whole moving volume using a dedicated algorithm.

To study the behaviour of the heart tube in space and in time, at first the 3D moving volume was reconstructed on the base of the images acquired by means of a new semi-automatic segmentation algorithm implemented using Matlab: at each time step of the cardiac cycle, the acquired volume of the heart is cut with equidistant planes perpendicular to the longitudinal axis of the heart and the resulting cross-sections are fitted with ellipse. The centreline of the heart was defined as the line that connects the centres of all the ellipses and was used to parametrize the geometry of the heart.

Heart dynamics was studied by analysing myocardium, endocardium and cardiac jelly motion. For the myocardium, the area of the cross-sectional ellipses of the layer and the distance between neighbouring cardiomyocytes were considered. Three hearts at 28 hours (hpf) and six hearts at 30 hpf were studied. The endocardium was analysed in two hearts at 28 hpf considering the area of the cross-sectional ellipses of the layer as parameter. The cardiac jelly dynamics was investigated calculating the difference between myocardium and endocardium areas in two hearts at 28 hpf.

To find relationships between heart wall movements and blood ejection, red blood cells velocity was calculated in a plane in two hearts at 28 hpf.

To study the electric impulse propagation in the myocardium, at first a heart where contraction was blocked by drugs (non-beating heart) was considered as suggested by literature. Electro-mechanical isolation was achieved by putting the embryo in BDM before the imaging and the *gcamp5.0* signal (that represents calcium variation in cardiomyocytes) was analysed.

The contraction was then restarted in the same heart and the calcium signal was calculated in the beating heart as the ratio between *gcamp5.0* intensity and the control signal (myocardium baseline signal) to delete the artefacts due to movement of the heart.

The strategy adopted was verified in a control heart that expressed two fluorescent proteins in a non-calcium-dependent manner.

The comparison between calcium and myocardium dynamics was done to investigate the electromechanical coupling and the mechano-electric feedback in the heart.

<u>Results and discussion</u>

From the analysis of myocardium and endocardium cross-sections, the myocardium has an elliptical shape during the whole cardiac cycle, while endocardium shows evaginations to allow the lumen expansion and contraction. In fact, the endocardium constricts more than the myocardium: the Area Fractional Shortening (an index that measures how much the area changes from the relaxed to the contracted condition) was found to be between -50 and -80% for the endocardium and between -30 and -60% for the myocardium.

The analysis of red blood cells velocity in the tube showed that regurgitations characterize the inflow region, that has lower AFS, while they seem to disappear in the final part of the heart, with larger AFS. These observations suggest that the presence of reversing flows is determined by the constriction of the lumen.

The analysis of myocardium dynamics showed similar results considering both the cross-sections areas and the distance between neighbouring cardiomyocytes. The contraction wave propagates almost linearly from the inflow to the outflow, with a delay in the final part of the tube. This slowdown in the propagation makes the contraction wave start at the inflow while the outflow is still contracted, probably to increase the pressure in the central part.

As regards the endocardium, the two hearts analysed gave different results: in one heart the contraction travels linearly along the tube with uniform speed, in the other the wave velocity changes several times and the contraction pattern results more irregular. The differences seem to be due to the ellipse fitting of the endocardium cross-sections, that is not optimal.

By comparing myocardium and endocardium dynamics, the contraction of the two layers occurs simultaneously and the transmission of the force that starts the contraction from the outer to the inner compartment seems immediate. Cardiac jelly dynamics, on the contrary, is in counterphase to myocardium and endocardium and this central layer may help the expansion of the cross-sections of the two tissues after the contraction and the shortening after the relaxation, by accumulating and returning elastic energy.

The duration of the contraction and of the relaxation changes along the heart both in the myocardium and in the endocardium: the first half of the heart remains expanded the

longest (40-60% of the entire cardiac cycle) and contracted the shortest (20%) while the outflow region remains contracted the longest (30-40%) and expanded the shortest (20-30%). A longer contraction status of the outflow region of the heart may allow the first part of the tube being filled with blood and the longer relaxation upstream may help the blood enter the tube and the pressure increase for the ejection.

From the study of the electric impulse propagation in the non-beating heart, the calcium wave was found to propagate almost linearly from the inflow of the heart (the pacemaker region, according to works in literature) to the outflow.

In order to investigate the electromechanical coupling in the heart *in vivo,* calcium dynamics and myocardium dynamics were compared in the beating heart. In the whole heart, the calcium reached the maximum level during the contraction of the tissue as expected from the fact that the contraction in muscles normally occurs thanks to the increase of calcium concentration in cells cytoplasm. In some cardiomyocytes, however, an increase in calcium was observed also in correspondence to a stretched condition of the myocardium, suggesting that a mechanotransduction mechanism similar to the stretch-dependent calcium activation observed in adult cardiomyocytes may exist also in the embryonic heart.

Conclusion

In the present work, tissue dynamics and calcium signaling of the primitive heart tube were investigated using the zebrafish animal model.

New tools were developed *ad hoc* to analyse the dynamics of the three layers composing the heart, the calcium in the myocardium and the electro-mechanical coupling in the beating heart.

The algorithms provided several information on the heart dynamics and, even if the results obtained are still preliminary, they suggest the existence of a mechanotransduction mechanism that controls the coupling of myocardium strain and calcium activation in the embryonic heart.

The analysis, performed on healthy embryos, corresponds to the starting point for the study of pathological conditions. The same analysis could be conducted in the future on hearts affected by genetic or physical alterations to understand how these anomalies impact on the anatomy and on the normal working mechanism of the heart.

1. Introduction

1.1 Congenital heart diseases

Congenital heart diseases are structural and functional problems due to an abnormal formation of the heart. Defects may affect new-borns and require interventions in the first year of life or be detected only in adulthood. For this reason, an accurate estimation of the incidence is difficult. According to the last data from the American Heart Association, the occurrence of congenital heart defects is around 8 per 1000 live births in the United States, 6.9 per 1000 births in Europe; 9.3 per 1000 in Asia, resulting in the most common cause of infant deaths from birth malformations (24%) [1].

Congenital heart defects form when cardiac morphogenetic processes are altered, often together with perturbed mechanical cues. However genetic and environmental causes remain largely unknown. Several efforts have been made to investigate all the mechanisms involved in cardiac development in high hope that diagnostic and therapeutic techniques will be found soon.

1.2. Cardiac development

Animal models commonly used to study cardiovascular morphogenesis are zebrafish, chick and mouse since the mechanisms of heart formation are evolutionary conserved among vertebrates and differences can be seen only at later stages. Until atrial and ventricular septation, heart developmental stages are exactly the same (Figure 1), except obviously the timing (Table 1), and even the depolarization impulse initiates and propagates similarly.

In all vertebrates, the heart forms at first as a linear tube without valves, from the fusion of two endocardial tubes surrounded by myocardium. During the fusion, myocardial cells produce the extracellular matrix that composes the cardiac jelly, so that the heart tube is made up of three layers: the myocardium, the outer contractile tissue made of cardiomyocytes, the cardiac jelly, the acellular layer of extracellular matrix in the middle, and the endocardium, the inner endothelial tissue in direct contact with the blood flow. In the early heart tube, cardiomyocytes have a primitive phenotype; they depolarize spontaneously and slowly conduct the impulse before myocardium contraction begins [2].

1

At this stage, the electrocardiogram results sinusoidal (Figure 2). Soon the heart tube starts beating. At first the rhythm is irregular and slow but it is quickly replaced by a synchronous unidirectional contraction once the blood stars flowing. The heart undergoes the looping process needed for the proper alignment of the future chambers and at the same time, its length increases by addition of cardiomyocytes that rapidly acquire a pacemaker phenotype at the venous pole. The pacemaker activity is thus located in the inflow tract. Simultaneously, the portions of the linear tube where the chambers will form expand in a step called ballooning and acquire a myocardial phenotype of fast conduction and high contractility. When the chambers are defined, a constriction called atrioventricular canal is clearly visible between them. A regional thickening of the cardiac jelly occurs in the atrioventricular canal and in the outflow tract and cushions, the valves precursors, form. At this stage, cardiomyocytes in the sinus venosus and atrioventricular canal retain the primitive phenotype of slow conduction. A depolarization pattern more similar to that of the adult heart is already recognizable: the electrical impulse generates at the inflow, fast propagates through the atrium during atrial contraction, is slowed down in the atrioventricular canal to allow the ventricle to fill and accelerates again in the ventricle during ventricular contraction (Figure 2) [3].

From this stage on, the heart develops differently according to the animal.

In mammals, common chambers undergo the septation process so that two distinct atria and two ventricles form. In lower vertebrates, the final structure is almost already achieved with a single atrium and a ventricle. The two chambers will be definitely divided when the atrioventricular valve will form. In zebrafish, for example, atrioventricular and outflow cushions transform in valves between 48 and 96 hpf and become functional by 111 hpf, so that a unidirectional blood flow enters the atrium from the sinus venosus, goes to the ventricle and exits the heart through the conus arteriosus (Figure 3) [4].

In humans, the atrioventricular cushion divides the canal in two left and right atrioventricular orifices, one will separate the right atrium and ventricle, the other one the left atrium and ventricle after the chambers septations (Figure 4). At this stage, blood enters the common atrium, flows through the atrioventricular canal into the primitive left ventricle, from here to the primitive right ventricle through the intraventricular foramen (a constriction between the inlet and the outlet of the common ventricle) and exits the truncus arteriosus. During weeks 4-8 of human gestation, the aortic arch arteries remodel in the

aortic and pulmonary vessels and the truncus arteriosus divides in the pulmonary and aorta trunk; the septum primum and secundum separate the common atrium, forming the two atria and the intraventricular septum divides the two ventricles. By week 8, valves are formed and blood enters from the sinus venosus to the right atrium, goes to the left atrium thanks to the foramen ovale bypassing the pulmonary circulation, enters the left ventricle and exits the heart (Figure 4) [5] [6] [7].

Table 1: Comparative timeline of cardiac development events common in vertebrates. Developmental stages are expressed in days post-fertilization (dpf) in human and mouse, in Hamburger-Hamilton (HH) stage in chick, in hours post-fertilization (hpf) in zebrafish. Adapted from [8] and [9].

Events in heart development	Human (dpf)	Mouse (dpf)	Chick (HH)	Zebrafish (hpf)
Gestation/ Incubation period	9 months	20	21	
Fusion of heart tubes	22	7-8	7-10	
First heartbeat	22	7.5-8.5	10	24
Cardiac looping	22-28	8-10.5	10-24	28-36
First blood flow	24	8-8.5	9-12	26
First definable cushions	28-32	10-12	16-19	48
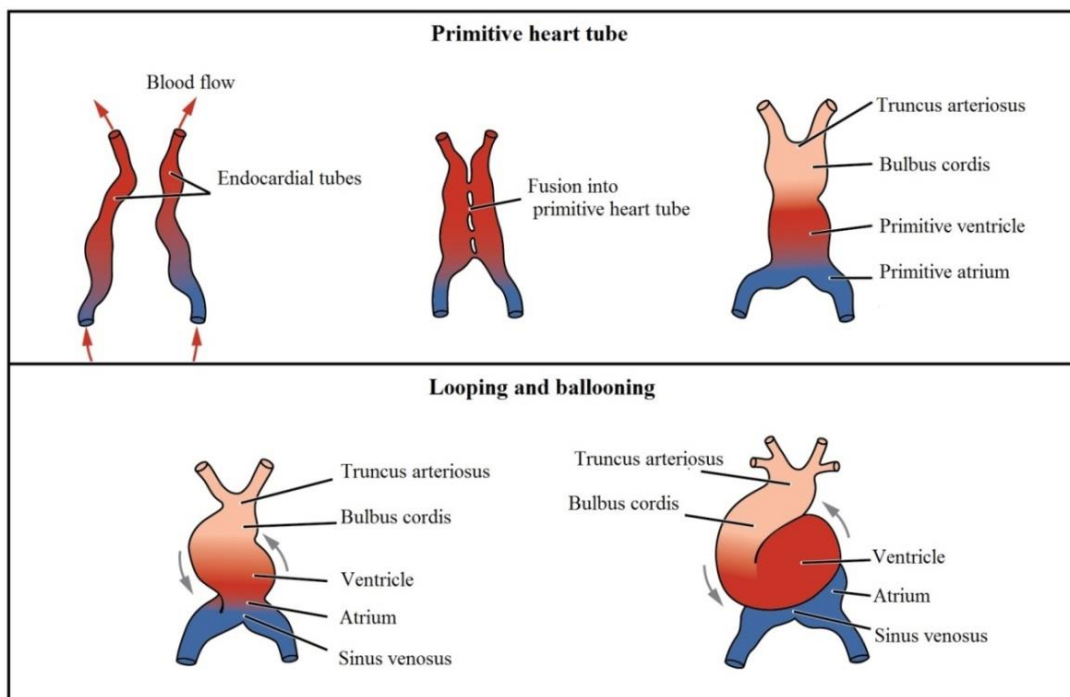
Figure 1: Stages of heart development common in all the vertebrates. Two endocardial tubes fuse in a primitive heart tube. Then the heart starts looping and two portions of the tube expand (ballooning process), until the primitive atrium and the primitive ventricle are defined. Adapted from [10].
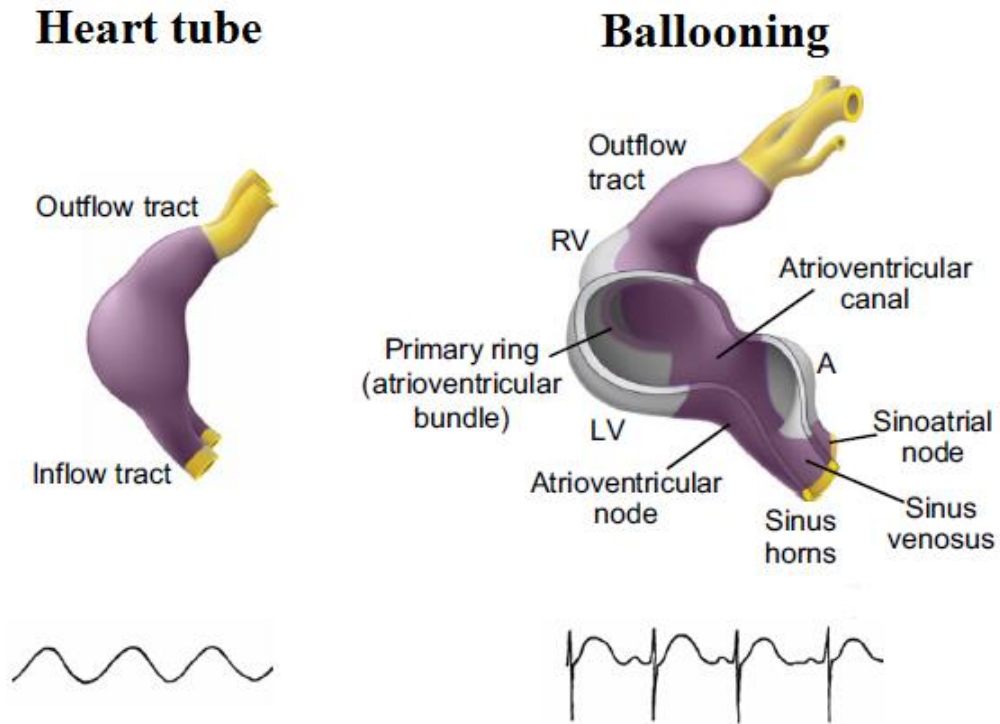
Figure 2: Electric impulse in heart development. The myocytes phenotype of the heart tube at early developmental stages determines a unidirectional wave reflecting in a sinusoidal ECG. During the ballooning, the cardiomyocytes in the chambers acquire a phenotype of fast conduction, while the sinus venosus and the atrioventricular canal retain the primitive phenotype of slow conduction, giving rise to a more mature-like ECG [3].
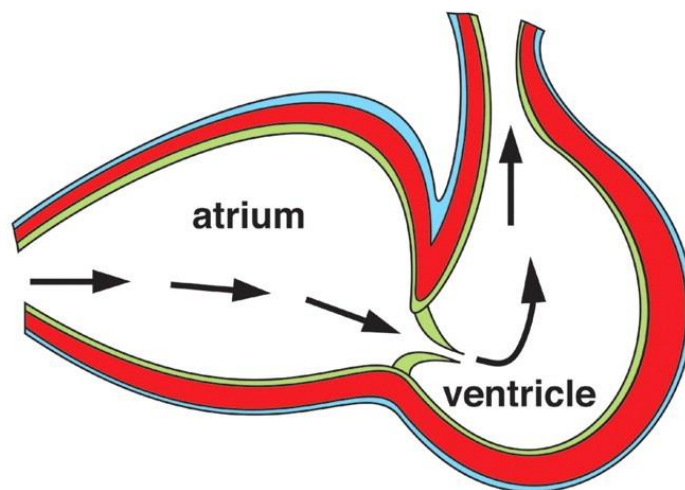
Figure 3: Schematic representation of the zebrafish adult heart. The heart has two chambers divided by the atrioventricular valve and is made up of three layers: epicardium (blue), myocardium (red) and endocardium (green). Blood flow enters the atrium from the sinus venosus, goes to the ventricle through the atrioventricular valve and exits the heart [11].
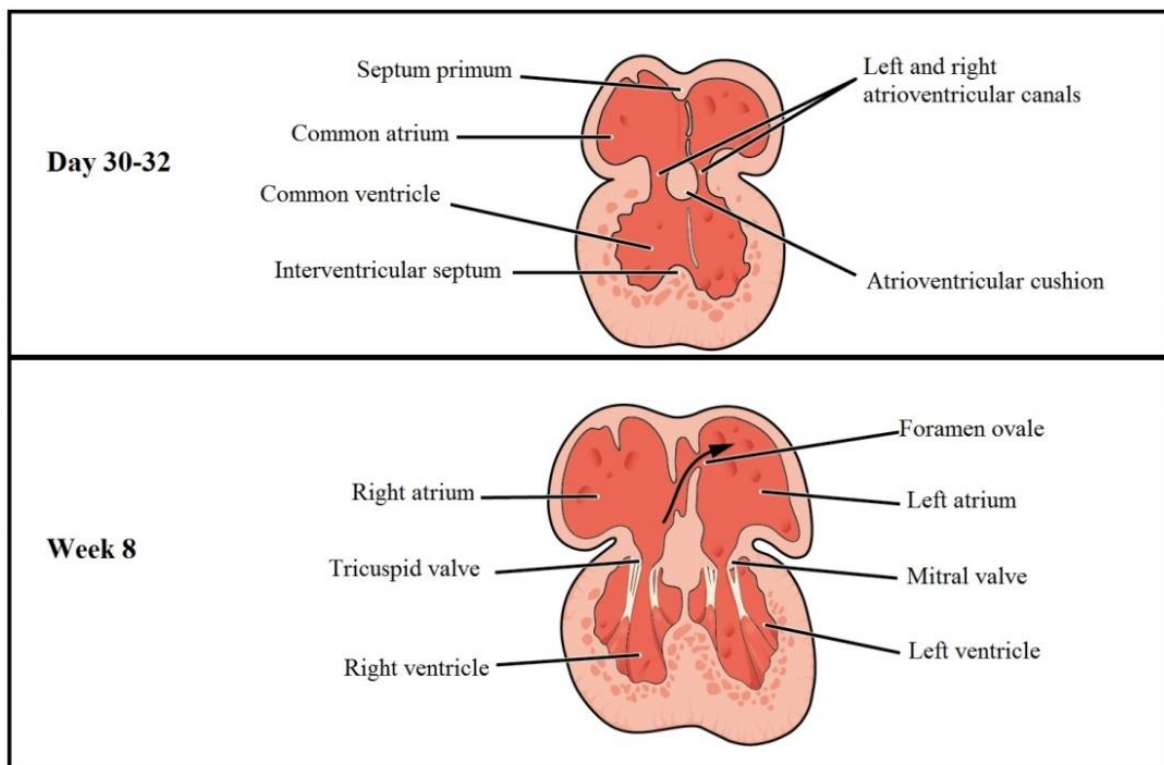
Figure 4: Partitioning of the human heart in four chambers. By day 30-32 the atrioventricular cushion divides the atrioventricular canal in left and right canals, where mitral and tricuspid valves will form. Septum primum and interventricular septum start forming to septate respectively the common atrium and ventricle. By week 8, the two atria and two ventricles are divided, but a shunt called foramen ovale is present between the atria, preventing the blood passing in the right ventricle and in the pulmonary circulation. The blood goes directly to the left ventricle end exits the heart towards the body. Adapted from [10].

1.3 Mechanotransduction: how mechanical forces regulate cardiogenesis

To study heart physiological and pathological development, a multidisciplinary approach must be adopted since tissue mechanics, fluid dynamics, genetics, electrophysiology and molecular signaling are directly involved in the process and many mechanisms simultaneously concur in a complex way. The pathways by which mechanical forces are converted in biological, chemical and electrical responses that can lead to structural and functional remodelling in cells and tissues go under the general name of mechanotransduction mechanisms.

Despite the identification of all the actors involved in mechanotransduction processes is very difficult, in the last decade, mechanical forces have been proved to affect all the steps of cardiac morphogenesis and be involved in abnormal development of the heart.

It was shown, for example, that heart looping is driven by extrinsic and intrinsic forces. Nerurkar *et al*. showed that myocardium contraction (intrinsic force) is needed in the process and that an increase of the stiffness of the tissue causes a delayed torsion of the tube [12]. No looping of the hearts was observed by Hove *et al*. in zebrafish where blood flow and shear stress (extrinsic forces) were reduced [13].

Mechanical properties and dynamics of the heart wall has been proposed to affect the ballooning process too, by controlling cells proliferation rate [14] [15] and shape changes [16] during chamber expansion. Also blood flow forces affect the process, since cellular morphology depends on shear stress [17] and vortex formation observed in blood flow patterns at this stage were suggested to influence chamber maturation [18].

Also the normal timing of the cardiac conduction system development is regulated by haemodynamic loading: a precocious development of the mature network was observed if the heart preload was increases and a delay if the preload was decreased [19]. Moreover, abnormal conduction waves were reported by Chi *et al*. in zebrafish *silent heart* mutants[1], indicating the contraction is needed for the development of the proper conduction pattern [20]. Other works suggest that mechanical forces control cardiomyocytes phenotype during the transformation from the primitive slowly conductive and poorly contractile myocardium to the fast conductive and strongly contractile tissue [21].

Blood flow forces are needed also in valvulogenesis. Starting from the observation that a reduction in physiological blood flow leads to no valve formation [13], several studies have been done on the topic. Shear stress affect the deposition of extracellular matrix in atrioventricular and outflow tract cushions [22], determines cells orientation in valves [23] and controls the expression of flow responsive genes directly involved in the normal and altered valves formation [24]. Other authors showed mechanical stimuli may promote valvular morphogenesis in combination with molecular signaling [25] and that endothelial-mesenchymal transformation, a crucial process in valve formation, is regulated by cyclic strain of the valve tissue in a magnitude and directionally dependent manner [23].

---

[1] In *silent heart* mutants, hearts fail to contract because of a mutation in the *cardiac troponin T* gene.

1.4 Electromechanical coupling in the heart

In the adult heart, cardiomyocytes depolarization leads to myocardium contraction in a process called electromechanical coupling. Calcium is the main mediator of this mechanism. When the action potential depolarizes the sarcolemma of cardiomyocytes, calcium flows into the junctional zone of the cell through the long-lasting (L-type) current calcium channels. This calcium influx signal, called calcium sparklet, opens RyR2s (Ryanodine receptors) channels and causes calcium release from the sarcoplasmic reticulum (calcium spark). The increase of calcium concentration in cytoplasm allows the interaction between myosin and actin filaments and myocardium contraction occurs thanks to the coordinated shortening of all the cardiomyocytes (Figure 5) [26] [27] [28].

In this process, a mechano-electric feedback that regulates calcium signal through a mechanotransduction mechanism has been subject of several studies in the last decades. During cardiac cycle, the myocardium deforms by contracting and relaxing alternatively and the mechanical stretch of the tissue during diastole has been proved to contribute to modulate calcium signaling through mechanotransduction [29] and control calcium spark rate [30] [31]. The works on the topic identified some of the steps and of the actors involved: cardiomyocytes stretching actives Nox2 (a Nicotinamide Adenine Dinucleotide phosphate oxidase family of enzymes present in adult cardiomyocytes) that triggers ROS (reactive oxygen species) production in a process that require an intact microtubule network in the cell. ROS increases rapidly and reversibly calcium sensitivity of RyR2s channels thanks to an oxidative mechanism and this results in an increase of calcium sparks frequency upon stretch (Figure 6) [29] [32].

Until now, the mechanism has been investigated *in vitro* in isolated adult cardiomyocytes and no *in vivo* studies in embryos are available. However, given the importance of mechanical forces in heart development, it would not be surprising if a similar mechano-electric feedback mechanism played a role in calcium signaling regulation in the embryonic heart as well and contributed to the primitive heart tube function.
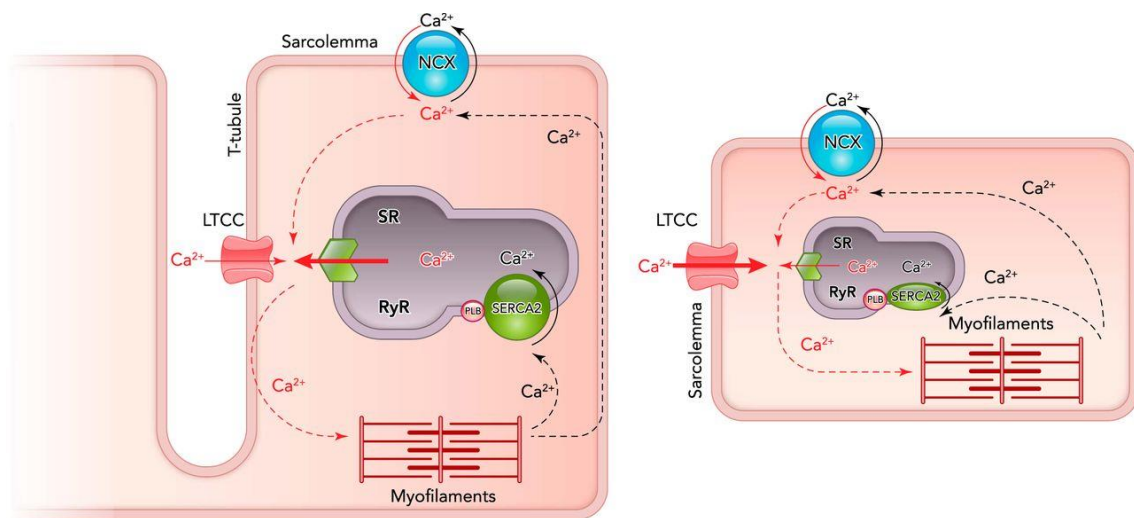
Figure 5: Excitation-contraction coupling in human (left) and in zebrafish (right) cardiomyocytes [28]. Despite the absence of a t-tubular system in zebrafish cardiomyocytes [27], the process that leads to cells contraction (red dotted line) is basically the same: Ca^{2+} influx through L-type calcium channels (LTCC) and Na^+/Ca^{2+} exchanger (NCX) causes calcium release from the sarcoplasmic reticulum (SR) via the ryanodine receptors (RyR). The increase of cytoplasmic calcium causes the sliding of the cardiomyocyte myofilaments and thus the contraction of the cell.

Ca^{2+} dissociation from the myofilaments and sequestration into the SR via the SR Ca^{2+} ATPase (SERCA2) or across the membrane via the NCX causes cardiomyocytes relaxation (black dotted line).
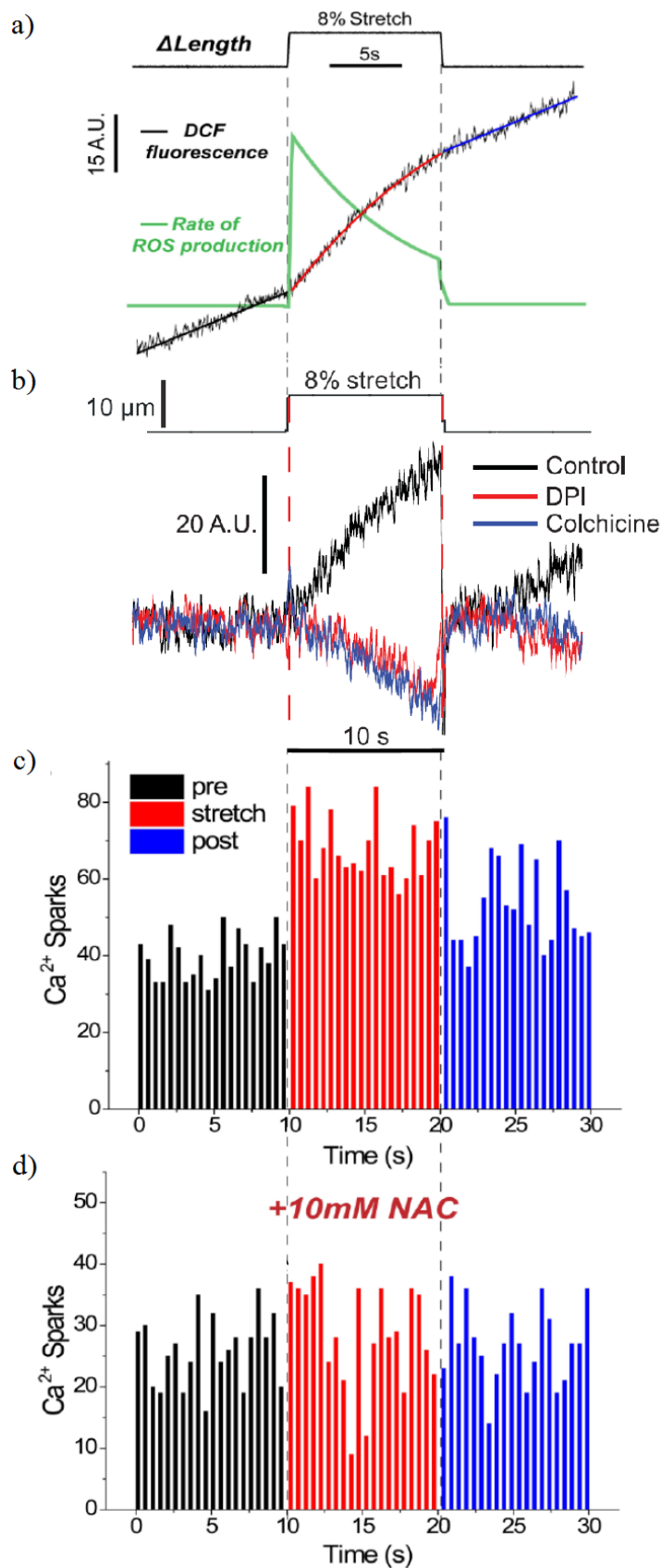
Figure 6: Summary of stretch-dependant Ca^{2+} signaling. a) If a single cardiomyocyte is stretched, ROS generation in cell, reported by the rate of change of DCF (2',7'-Dichlorofluorescein Diacetate) fluorescent signal, increases immediately, gradually decreases during the prolonged stretch duration and returns to the prestretched level during relaxation. ROS is produced by a NOX family of enzyme, since b) the use of a NOX inhibitor, DPI (Diphenyleneiodonium), blocks the process. Microtubules are involved in ROS production too: after the microtubules depolymerisation with Colchicine (b), DCF fluorescence is not detected anymore (ROS is not produced). c) Simultaneously with the stretching and ROS production, the frequency of $[Ca^{2+}]$ sparks increases. In the mechanotransduction pathway, an oxidative mechanism takes place, because d) the application of NAC (antioxidant N-Acetylcysteine) blocks the $[Ca^{2+}]$ sparks. Adapted from [29] [32].

9

1.5 Zebrafish as a model to study human cardiac development and diseases

In the study of mechanotransduction pathways leading to physiological and abnormal cardiac development, zebrafish offers several advantages compared to other animal models.

Thanks to fish external fertilization, access to embryos is immediate and does not require the explantation needed in mammals.

A wide range of genetic tools is available to overexpress or knock down genes and study their involvement in cardiac morphogenesis. These genes can be, for example, at the base of mechanotransduction pathways (as in the case of *klf2a* gene needed in valvulogenesis [24]) or their knock down may perturb the haemodynamics (e.g. by varying blood haematocrit [33]) or the mechanics (e.g. by inhibiting myocardium contraction [34]) of the heart. If the genes needed in the cardiogenesis process are identified and altered, the zebrafish heart will present defects. Thanks to their small size and to the passive diffusion of oxygen, nutrients, metabolic waste and hormones, zebrafish embryos can survive the initial stages of development without a functional cardiovascular system [35]. Therefore, genetically induced heart defects can be studied and analysed *in vivo* in zebrafish.

The limit of the zebrafish model in cardiovascular research is in the final structure of the heart. In fact, birds and mammals have the most complex heart, made of two atria and two ventricles, while fish only one atrium and one ventricle, resulting in a simplified version of the four chambered mammal heart. However, as previously described, many developmental stages are common and humans and zebrafish share the same structure until chambers septation. This suggests that also the early pumping mechanism is similar and mechanics affects the development in a similar way. Zebrafish is thus a unique model to investigate mechanotransduction mechanisms in cardiogenesis.

1.6 Live imaging of the zebrafish

In zebrafish, the visualization of the physiological or pathological heart can be based on direct observation under fluorescence microscope once the tissues of interest are genetically encoded with fluorescent markers. In fact, it is possible to generate zebrafish transgenic lines that stably express fluorescent proteins in specific tissues of the heart, such as the myocardium or the endocardium, by genetically encoding these proteins associated

to tissue specific genes promoters[2]. Since zebrafish embryos are transparent, it is then possible to access the heart optically, visualize the labelled structures under the fluorescence microscope and perform live imaging of the beating heart.

In vivo zebrafish embryonic imaging techniques include confocal microscopy and light sheet microscopy. In both cases, the sample is illuminated by the microscope laser to excite the fluorophores and the emitted fluorescent radiation is detected and acquired. The two microscopes image a single plane of the heart at a time and by repeating the imaging in several planes at different depths, it is possible to reconstruct the three-dimensional volume of the heart using the fluorescent staining.

The difference between the two microscopes is that, despite the imaging is limited to one plane, in confocal microscopy the stimulus goes through the all sample, while in the light sheet microscopy the radiation is specific for that plane (Figure 7). Therefore light sheet microscopy is less toxic for embryos.
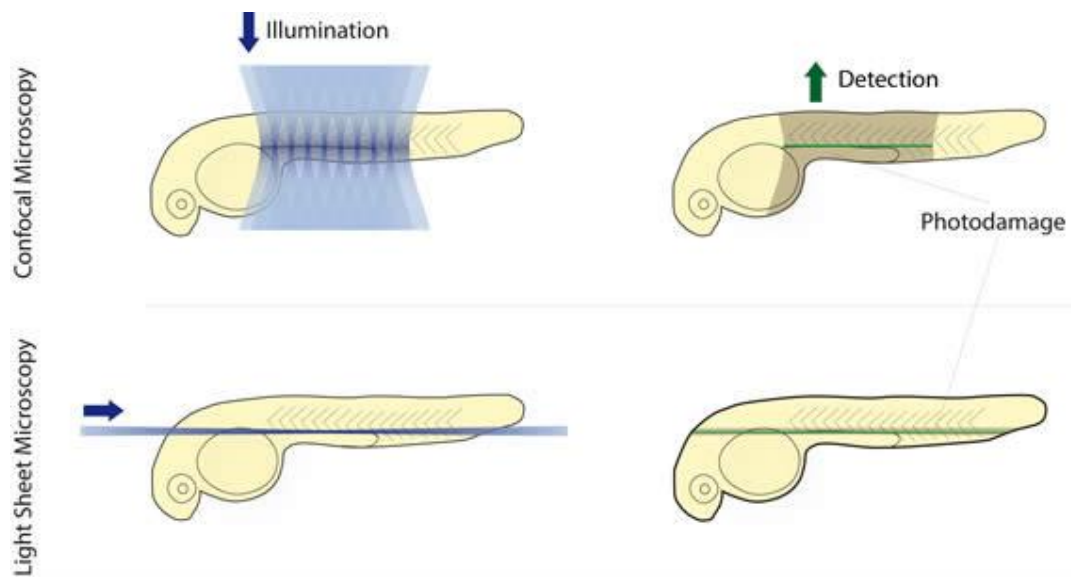
Figure 7: Sample illumination in confocal and light sheet microscopes [36]. In confocal microscopy (above), a whole region of the embryo is excited at the same time; in light sheet microscope (below), the laser illuminates only one plane of the sample.

---

[2] Promoter sequences are DNA sequences that define where transcription of a gene by RNA polymerase begins and thus which DNA strand will be transcribed and which protein will be synthetized.

1.7 Mechanics and electrophysiology in the primitive heart tube

In zebrafish, the propagation of the electrical impulse appears at 20-24 hpf [20]. By imaging *in vivo* a non-beating heart[3], Chi *et al.* found that the impulse travels as a linear and unidirectional wave from the sinus venosus, where it is generated by a pacemaker, to the outflow of the heart. An acceleration of conduction was observed in the outflow tract region where cardiomyocytes have a different morphology from the rest of the heart (Figure 8).
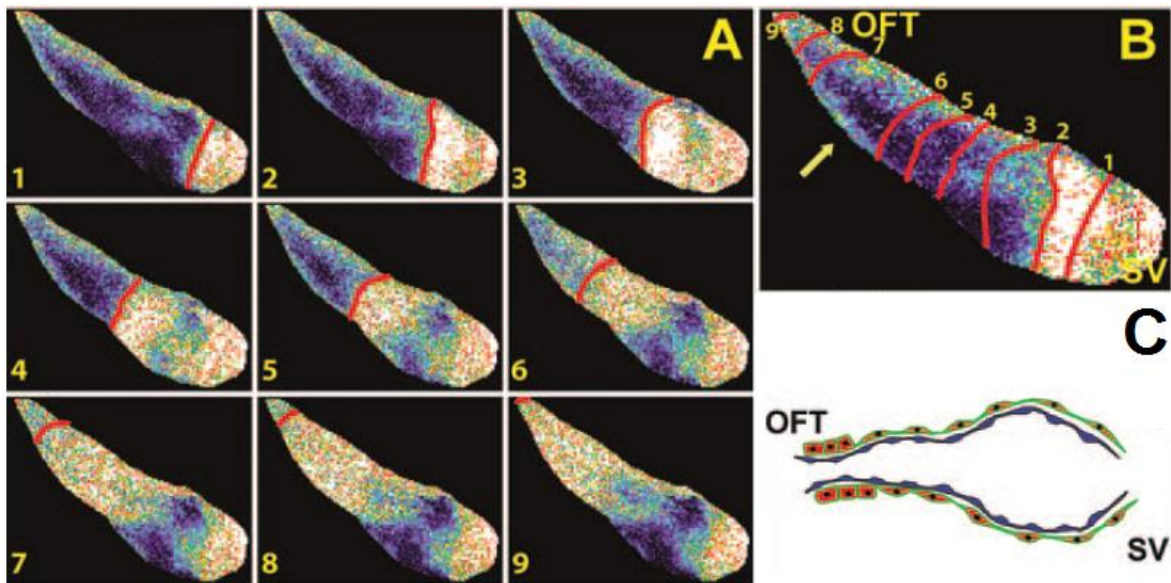
Figure 8: Cellular and *in vivo* electrophysiological analysis of the zebrafish heart at 24 hpf [20]. A) Images of the sequential calcium activation (red curves) along the heart tube from the inflow region (1) to the outflow (9); B) in the optical map of calcium excitation, an acceleration of conduction can be observed in the outflow track (yellow arrow) since the distance between the calcium curves at t=6 and t=7 is higher than in the other cases. C) In the outflow region cardiomyocytes are cuboidal. In the rest of the heart, cells have a squamous shape. The shape may thus determine the conduction velocity.

Myocardium starts contracting at 24 hpf but the opening of the endocardial lumen and the blood flow are visible only at 26 hpf [34]. At this stage, valves are not present yet; however the heart produces a unidirectional blood flow without significant regurgitation. The contraction of the endocardium propagates from the inflow to the outflow of the heart and consecutive cross-sections collapse pumping the blood into the aortic arches [4] [13] [37].

---

[3] To study the electric impulse without the contribution of the heart movement, Chi *et al.* inhibited muscles contraction using 10 mM 2,3-butanedione monoxime [20].

Endocardial lumen constriction seems to be the main factor responsible for blood pumping without regurgitations in the valveless heart tube at early stages and, on the base of direct visualization, heart tube has been proposed to act as a peristaltic pump [34], with a mechanism similar to that observed in other tubular organs without valves such as the gastrointestinal tract and the ureter, where the motion is given by the cyclic alternation of contraction and relaxation of the muscles [37].

In the 20th century, physicians and engineers started to compare the valveless heart tube to technical pumps in order to better characterize its working mechanism. Since the blood flow in the heart tube had been suggested to move thanks to peristalsis, they compared the heart to a standard technical peristaltic pump, a roller pump, and some mismatches between the two pumps were found. In particular, Forouhar *et al.* showed that the contraction propagates bidirectionally along the heart tube at 26 hpf (Figure 9), blood velocity exceeds the endocardium wave speed (Figure 10) and the relationship between flow rate and heart rate is not linear (Figure 11), three characteristics that contrast with the working mechanism of a roller pump. They thus proposed a novel mechanism based on impedance pumping [38]. In their model (shown in Figure 9), the contraction wave generates from the active compression of the venus pole and propagates passively both towards the inflow and the outflow of the heart in bidirectional waves. At the heart boundaries, the waves are hypothesized to reflect backwards thanks to an impedance mismatch due to the change in diameter and to the elasticity of the cardiac jelly. Waves reflection causes the expansion of the lumen and this creates regions at low pressure and allows the blood to enter the tube.

Also in the impedance pump model, however, some aspects contrast with the real pumping mechanism of the heart. In impedance pumps, a single site of active contraction should be present. On the contrary, Chi *et al.* observed the depolarization wave propagating along the whole heart [20]. Thus the heart contraction seems to be due to the sequential activation of all the cardiomyocytes as in the adult hearts and does not propagate simply by a passive mechanism.

Furthermore, flow direction in the impedance pump is determined by the frequency of compression at the activation site so that, changing the frequency, the flow can be reversed. Considering the physiological range of increasing beating rate in the zebrafish embryonic heart tube, if the heart worked as an impedance pump, inversions in blood

direction would be observed [37]. In addition, other factors affect flow direction and the behaviour of the impedance pump seems too unpredictable to be at the base of the unidirectional blood flow in absence of valves of the primitive heart tube [37].

For all these reasons, valveless heart works neither as a technical roller pump nor as an impedance pump.
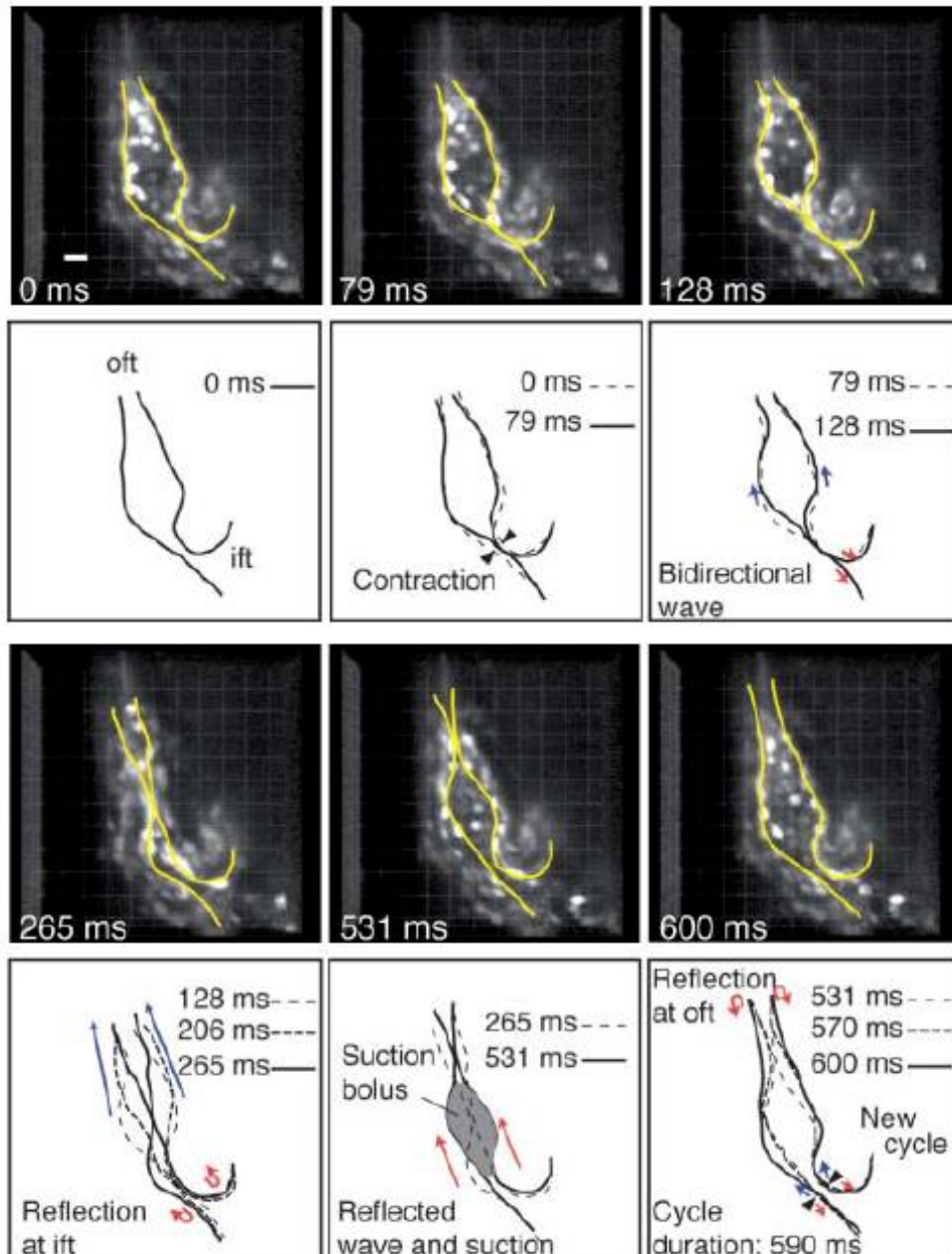
Figure 9: Pumping mechanism of the zebrafish heart tube at 26 hpf according to the impedance pump model [38]. The contraction starts from a single actuation site (black arrowheads) and propagates

14

towards the inflow (red arrows) and the outflow (blue arrows). The wave reflects at the inflow because of the impedance mismatch at the boundary, causing the suction of the blood.
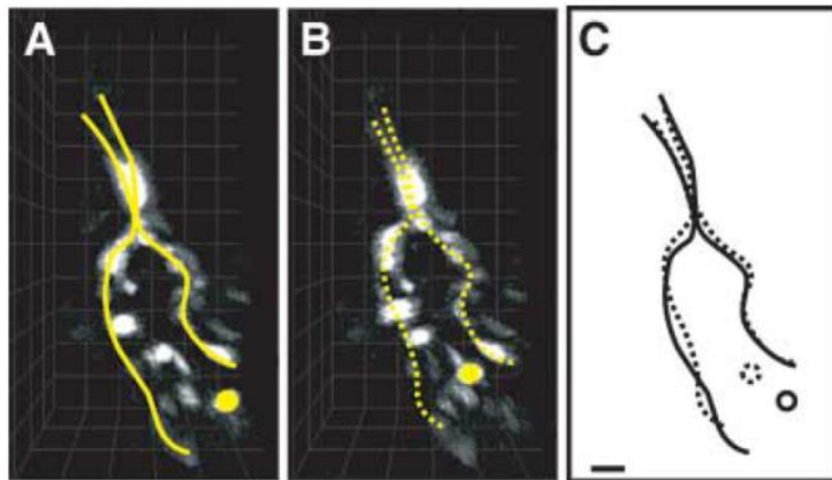
Figure 10: Comparison between red blood cells velocity and endocardium wave speed at 26 hpf [38]. A-B) Endocardial lumen (yellow curve) and one red blood cell (yellow spot) at different instants were C) superimposed. Blood cell displacement results greater than wave crest displacement.
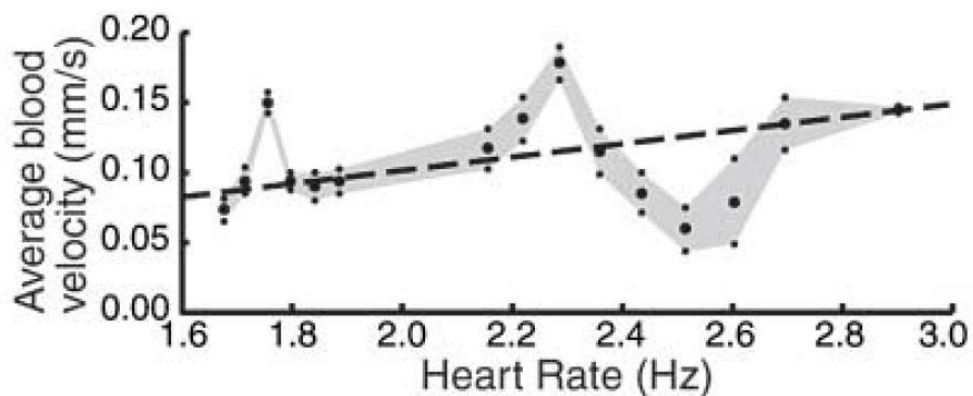
Figure 11: Comparison between blood flow rate and heart rate in zebrafish at 26 hpf [38]. The relationship (in grey) is not linear.

Except from the work of Forouhar *et al.* previously described, a quantitative analysis of the primitive heart tube pumping mechanism in zebrafish is missing. Almost all the papers available on the topic provide only a qualitative description of the heart and the few quantitative analysis present are two-dimensional.

Quantitative studies of the heart tube have been done in chick embryos between Hamburger and Hamilton developmental stages 13 and 17[4] by Garita *et al.* [39], Midgett *et al.* [40] and Butcher *et al.* [25]. However only in the first case the analysis considered the entire heart tube. In fact, Midgett and Butcher focused on the outflow tract and the atrioventricular canal, respectively.

Garita *et al.* studied the three layers of the heart and the relationships between them after performing optical coherence tomography of the living chick heart during the looping in six equidistant sections perpendicular to the blood flow (Figure 12). By measuring myocardium, endocardium and cardiac jelly cross-sections areas over the cardiac cycle, they found that:

- the inflow and midventricular regions of the heart tube (L6 and L4 cross-sections in Figure 12) are the largest to allow blood accumulation before the expulsion, and the outflow region (L2) is the smallest;
- the cardiac jelly is present in higher quantity in the ventricular region and in lower amount at the outflow;
- myocardium cross-sections result elliptical in relaxation and more circular in contraction, while endocardium cross-sections show folds and evaginations to make the lumen expand and collapse during the cardiac cycle;
- both myocardium and endocardium cross-sections area decreases in systole, but the myocardium shortening is almost the half of endocardial lumen shortening (Figure 13);
- endocardial lumen contracts sequentially from the inflow to the outflow, except for the ventricular region (L3–L5), that shows a synchronized contraction probably to help the blood ejection (Figure 14);
- the ventricular region of the heart remains longer in a relaxed state, while the outflow stays longer contracted (Figure 14) to allow the ventricular region to fill with blood and the pressure to increase;

---

[4] Chick embryos are usually staged according to Hamburger and Hamilton (HH). HH stages between 13 and 17 correspond to the looping of the heart tube (see Table 1).

- the closure of the lumen is helped by the presence of the cardiac jelly that seems to behave in counterphase to endocardium, increasing its area during heart contraction and decreasing it during relaxation (Figure 15) [39].

About the cardiac jelly, similar observations were made by Forouhar in zebrafish heart tube at the corresponding developmental stage [38] (Figure 16).
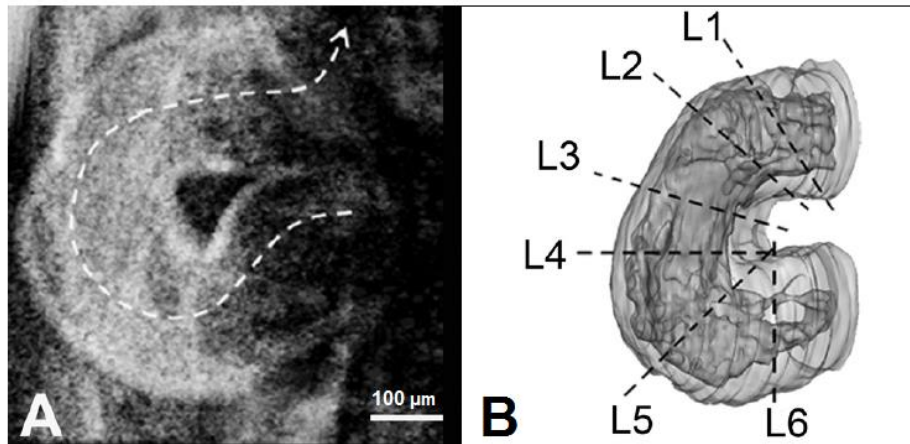
Figure 12: Optical coherence tomography of the chick embryonic heart at HH stage 13 [39]. A) The white line shows the direction of blood flow used to define B) the cross-sections perpendicular to the flow. L1 and L2 are through the outflow region; L3, L4 and L5 represent the ventricular region; L6 is at the inflow.
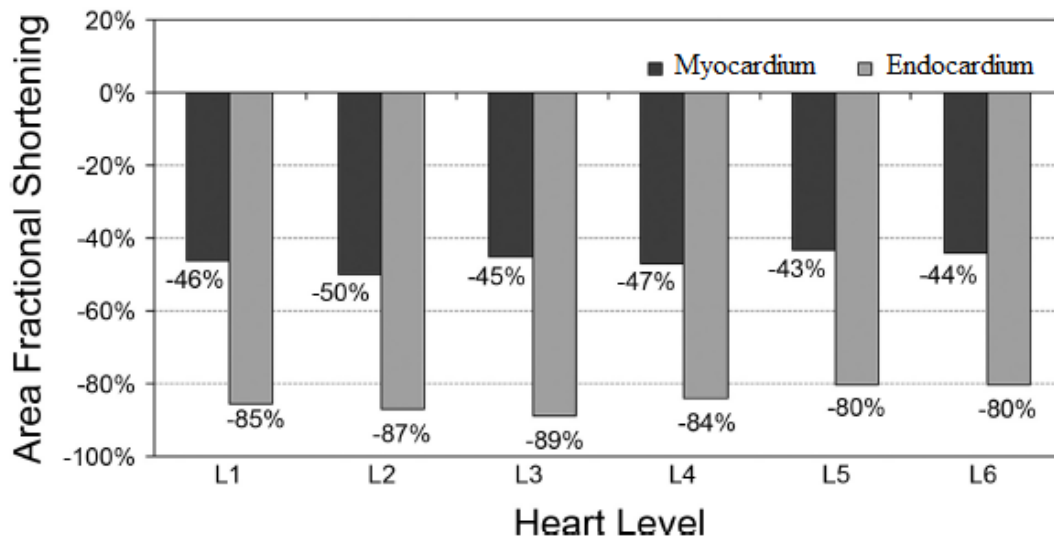
Figure 13: Area fractional shortening (AFS) of myocardium and endocardium along the heart tube in chick embryo at HH 13. AFS measures how much the cross-sections area of the two layers changes during contraction with respect to the relaxed condition. Endocardium AFS results higher. Adapted from [39].

	t1	t2	t3	t4	t5	t6	t7	t8	t9	t10	t11	t12	t13	t14	t15
L1	D								S						
L2		D							S						
L3							S								
L4					S										D
L5						S									D
L6					S									D	

Figure 14: Endocardium dynamics over the cardiac cycle in HH 13 chick heart [39]. The S (systole) and D (diastole) mark respectively the instant of minimum and maximum area; black and white blocks indicate an area within the 25% of the minimum value (thus a state of relative contraction) and within the 25% of the maximum value (thus a state of relative relaxation), respectively. Endocardium contraction propagates from the inflow (L6) to the outflow (L1) and the duration of contraction (width of the black region) increases along the heart tube, reaching the maximum at the outflow.
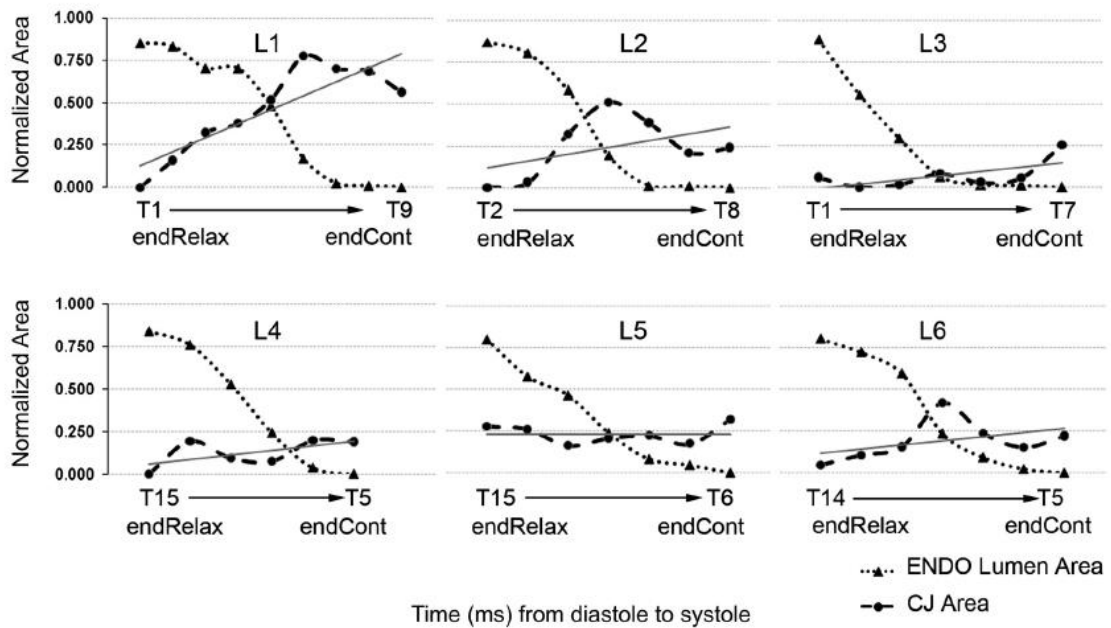
Figure 15: Comparison between endocardium and cardiac jelly dynamics from the relaxation to the contraction time in HH 13 chick heart [39]. At the inflow (L6) and in the outflow region (L1-2), cardiac jelly area increases while endocardium area decreases until the lumen has reached the 50% of its maximum value, then cardiac jelly decreases in parallel to endocardium. In the rest of the heart (L3-4-5), the area of the cardiac jelly changes poorly.
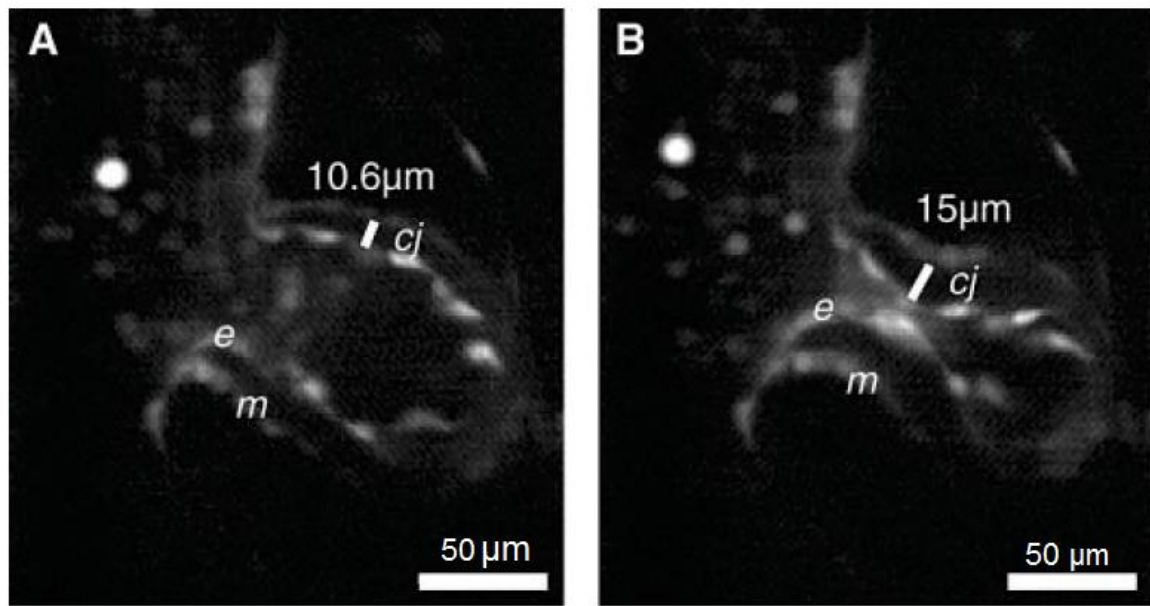
Figure 16: Cardiac jelly in the inflow region of a 26 hpf zebrafish embryonic heart during a) relaxation and b) contraction [38]. The distance between the myocardial (m) and endocardial (e) layers (white bar), representing the cardiac jelly thickness, increases during contraction.

Even if Garita *et al.* didn't supply a working model of the pumping mechanism of the heart tube, they suggested a method to study the dynamics of myocardium, endocardium and cardiac jelly and their results are one of the few examples of analytical data describing the interactions between all the layers of the heart. To fully characterize the heart, in fact, it's necessary to consider its whole structure.

Then the results should be coupled with the study of blood flow and calcium depolarization wave. Few efforts have been made, in fact, in literature to correlate all these aspects.

The investigation of how the layers interact with each other, with blood flow and electrical impulse could provide new elements in the study of the pumping mechanism of the heart tube.

1.8 Aim

In this context, the present work aims to study the embryonic heart in zebrafish model at 28-30 hpf, right before the primitive heart tube starts looping, using the data acquired from the four-dimensional live imaging of the beating heart.

Since the datasets obtained from the imaging is complex, the first goal is to develop new efficient tools for the four-dimensional analysis and quantification of the tissue dynamics,

fluid dynamics, and electric wave of the embryonic heart. The definition of a method to study the heart tube is in fact necessary to extend the analysis to a large number of samples.

The second goal is to apply these tools and to provide, for the first time in zebrafish, a quantitative description of the dynamics of the three layers composing the heart tube as well as the red blood cells flowing through it during the cardiac cycle at the developmental stage considered. This implies to study how the myocardium, the endocardium and the cardiac jelly move with respect to each other in the different regions of the heart and how red blood cells velocity changes along the heart tube.

The third goal is to study the depolarization wave of the myocardial layer of the beating heart, and its coupling with the contraction pattern of the myocardium to study the electromechanical coupling in the embryonic heart and to search the stretch-dependent calcium activation documented in adult isolated cardiomyocytes. It is the first time that the calcium response to stretch is investigated *in vivo* in embryonic cardiomyocytes. The demonstration of the existence of this mechanotransduction mechanism in the embryo may provide additional important information about the role of mechanical forces in cardiogenesis. This is probably the most innovative and challenging contribution of the work since previous analysis were limited to non-beating hearts and represents a necessary step in order to further the understanding of the working mechanism of the embryonic heart tube and to reveal possible, underling mechanotransduction pathways.

This study considers wild type animals (in physiological condition). However, the same analysis can be extended to hearts affected by genetic or physical alterations to understand how these anomalies impact on the anatomy and on the normal working mechanism of the heart. This can improve the knowledge of the role of mechanical forces in congenital heart diseases.

2. Materials and methods

The study of the primitive heart tube is based on the analysis of the data obtained from *in vivo* four-dimensional imaging of zebrafish hearts at 28-30 hpf. The work consisted of three steps:

- choice of the transgenic lines to label the structures of interest,
- sample preparation and live imaging of the heart,
- data analysis by newly developed, dedicated tools.

2.1 Choice of the transgenic lines

The first step was the identification of the zebrafish transgenic lines expressing fluorescent proteins in the structures of interest to later visualize them under the fluorescence microscope. Transgenic lines were, therefore, chosen according to the aim of the analysis. In the present work, the dynamics of the three layers composing the heart (myocardium, endocardium and cardiac jelly), the red blood cell velocity and the calcium dynamics in the myocardium were investigated. The different transgenic lines used are summarized in Table 2.

Table 2: Transgenic lines used accordingly to the fluorescent staining needed.

Transgenic line	Labelling
Tg(cmlc2:egfp)	Myocardium in green
Tg(fli:Gal4FF;UAS:kaede)	Endocardium and red blood cells in red
Tg(cmlc2:Gal4FF;UAS:RFP)	Myocardium in red
Tg(cmlc2:Gal4FF;UAS:gcamp5.0)	Myocardium in green with signal proportional to intracellular calcium concentration

In order to study the dynamics of the myocardium and the endocardium in the same fish, two transgenic lines were crossed: the *Tg(cmlc2:egfp)* and the *Tg(fli:Gal4FF;UAS:kaede)*, which give the myocardium and the endocardium specific staining, respectively.

Cardiac myosin light chain 2 (*cmlc2*) gene is a gene expressed only in cardiomyocytes. In *Tg(cmlc2:egfp)*, the green fluorescent protein e*GFP* is "attached" to the *cmlc2* promoter to obtain green florescence specifically in myocardial cells.

The transgenic line *Tg(fli:Gal4FF;UAS:kaede)*, instead, provides red fluorescent signal in the endothelium after UV excitation, exploiting the *Gal4FF-UAS* system.

Gal4FF is an engineered protein that, by binding to DNA sequences called Upstream Activation Sequence (*UAS*), activates the transcription of a reporter controlled by the *UAS* [41]. By using cell-type promoters, *Gal4FF* can be expresses in a tissue specific-manner. In this case, the binding of *Gal4FF* and *UAS* enables the *Gal4FF*-dependent transcriptional activation of the *UAS*-regulated reporter only in the regions where *Gal4FF* is expressed [42].

In *Tg(fli:Gal4FF;UAS:kaede)*, *Gal4FF* is attached to the *fli-1* (friend leukemia integration) promoter, expressed in sites of vasculogenesis, and the binding of *Gal4FF* and *UAS* determines the production, specifically in these regions, of the fluorescent protein *kaede*, which emits red fluorescence after being exposed to UV light.

The *Tg(fli:Gal4FF;UAS:kaede)* transgenic line was also used to analyse red blood cells velocity since red fluorescence is expressed in erythrocytes as well [34].

To study the calcium dynamic in the embryonic myocardium, the calcium sensitive protein *gcamp5.0* was exploited. In order to express *gcamp5.0* specifically in the myocardium, two transgenic lines were used: *Tg(cmlc2:Gal4FF;UAS:RFP)* and *Tg(UAS:gcamp5.0)*. In the former, a red fluorescence protein (*RFP*) is expressed in cardiomyocytes thanks to the binding of the *RFP*-regulating *UAS* and the transcriptional activator *Gal4FF*, that is attached to *cmlc2* promoters. In *Tg(UAS:gcamp5.0)*, instead, *UAS* controls the calcium reporter *gcamp5.0* in presence of a transcriptional activator. By crossing the two transgenic lines, the binding of *Gal4FF* (expressed in cardiomyocytes under the regulation of the *cmlc2* promoter) and *UAS* enables the activation of the transcription of both *RFP* and *gcamp5.0* in cardiomyocytes.

The resulting transgenic line *tg(cmlc2:Gal4FF;UAS:RFP;UAS:gcamp5.0)* expressed, therefore, red and green fluorescence in the myocardium. The green fluorescent signal, expressed by *gcamp5.0* was proportional to calcium variation in the cardiomyocytes. On the contrary, the red fluorescent signal, expressed by *RFP,* was not calcium-sensitive.

2.2 Collection of embryos, sample preparation and live imaging

The aim of this step was the obtainment, through the live imaging of the beating heart, of a four-dimensional dataset that contained information on the three-dimensional volume of the heart and on its movement over the cardiac cycle for the successive analysis of the heart tube.

To study the heart dynamics and red blood cells velocity, the 4D dataset (obtained with Leica TCP SP5 confocal microscope) was already available for the analysis [34]. Therefore, the following description focus on the experimental protocol developed for the calcium imaging.

To analyse calcium dynamics, female and male fish were selected from *Tg(cmlc2:Gal4FF;UAS:RFP)* and *Tg(UAS:gcamp5.0)* transgenic lines and made breed in a specific tank that prevents the fish from eating the eggs. Eggs were collected by throwing the water from the tank into a strainer, resuspended in Petri dishes and incubated at 28.5° C in 0.3% Danieau solution (a medium for zebrafish embryos [43]). About twelve hours after the collection, eggs were observed under the stereomicroscope (Leica MZ6) and dead or non fertilized eggs were identified and removed with a pipette. The remaining eggs were incubated at 28.5°C in 0.3% Danieau with 0.003% (wt/vol) 2-phenylthiourea to inhibit pigments formation and make the embryos transparent for optical observation. At 24 hpf embryos were observed under fluorescence stereo microscope (Leica M205 FA) and the brightest *tg(cmlc2:Gal4FF;UAS:RFP;UAS:gcamp5.0)* embryos among those expressing both green and red fluorescent proteins in the myocardium were selected. After the selection, the embryos were dechorionated[5] using a pair of fine-tip tweezers. The described process is shown in Figure 17.

If the experiment required to stop the heart, embryos were transferred in a 0.01 solution of 0.3% Danieau and 2,3-Butanedione monoxime (BDM), a myosin inhibitor to keep the cardiac muscle in a constant relaxed state. Otherwise for the imaging of the beating heart, embryos were anesthetized with 0.012% tricaine solution, which does not affect the heart beat but prevents the fish from moving.

Embryos were then mounted one by one in a glass bottom Petri dish and their position was chosen according to the developmental stage. At 28-30 hpf, embryos were put on their left side to allow proper illumination of the heart and its optimal exposition to the microscope camera. A transparent support made of phytogel was fabricated in the glass Petri dish to keep the embryo in the proper position.

---

[5] The chorion is the eggshell that surrounds the embryo. To increase the quality of the imaging of the embryonic heart, the membrane is removed.
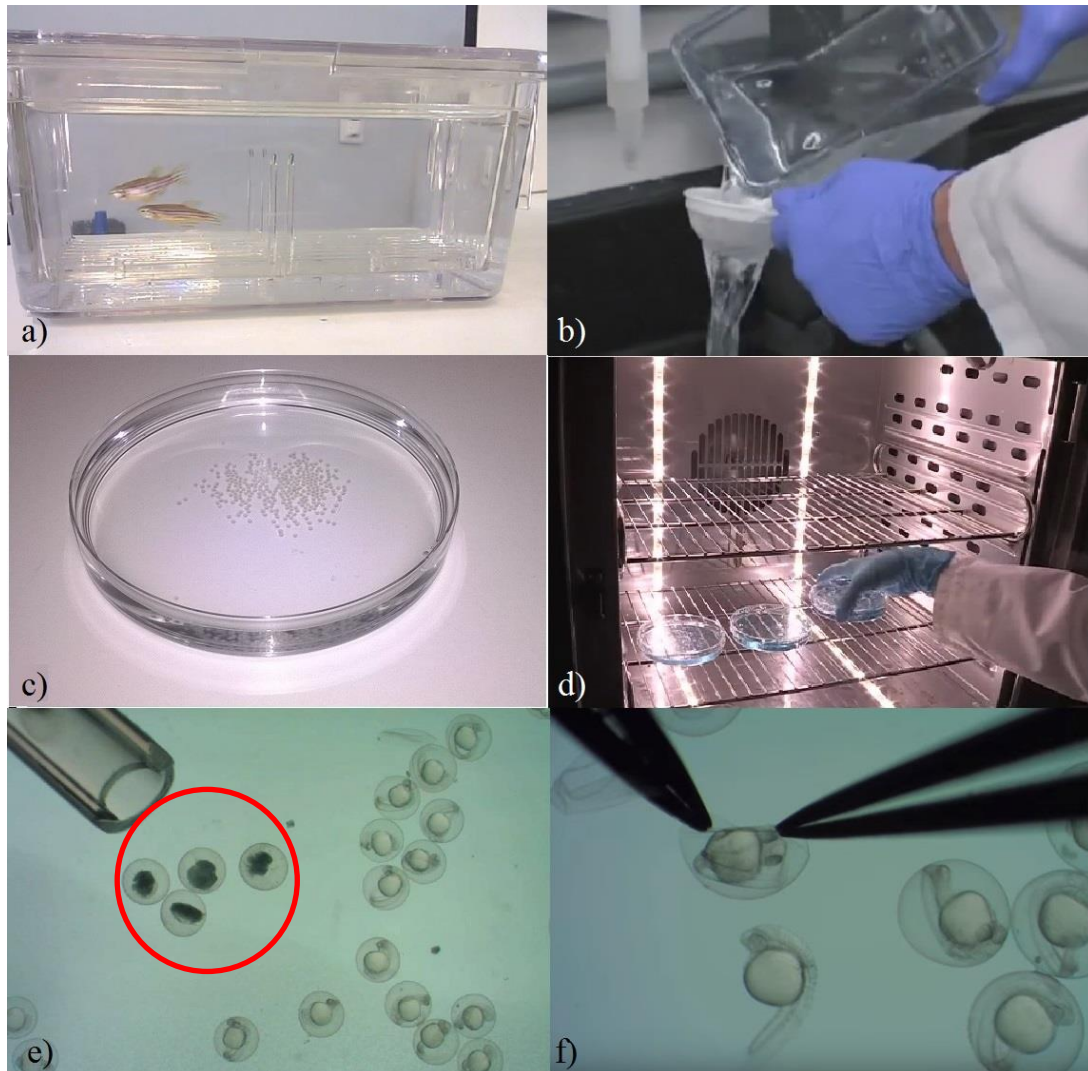
Figure 17: Zebrafish embryos preparation. a) breeding; b) eggs collection [44]; c) eggs in Danieau in the Petri dish; d) eggs incubation at 28.5°C [44]; e) dead eggs (red circle) removal [45]; f) dechorionation [46].

4D live imaging of the beating and of the non-beating myocardium was performed at Institut de Génétique et Biologie Moléculaire et Cellulaire (IGBMC) imaging center with light sheet microscope (Leica TCS SP8 DLS). During the imaging, several slices of the heart volume at different depths (z positions) were acquired over time (for 2-3 cardiac cycles) one after the other until the entire volume was processed (Figure 18). Planes were taken with a spacing of 2.4-2.6 µm between them and the frame rate of the time lapse taken at each plane was 30-60 frames per second. Then, to reconstruct the three-dimensional structure of the heart tube over the cardiac cycle, the planes acquired separately were processed. Since the acquisition of a heart plane begins at a random instant

of the cardiac cycle, the slice sequences obtained were not synchronized with each other. Thanks to the fact the heart undergoes a periodic deformation, homogeneous at different depths, the time shift between slice sequences taken at neighbouring z positions can be minimized by maximizing the similarity between them (Figure 18). Therefore, the 4D dataset was assembled with an algorithm that implements this concept to synchronize the time lapse acquired at different z-positions of the heart [47].

The same strategy was adopted to synchronize green and red fluorescence in the embryonic hearts. The two colours were acquired one after the other in each plane of the heart and synchronized post acquisition.
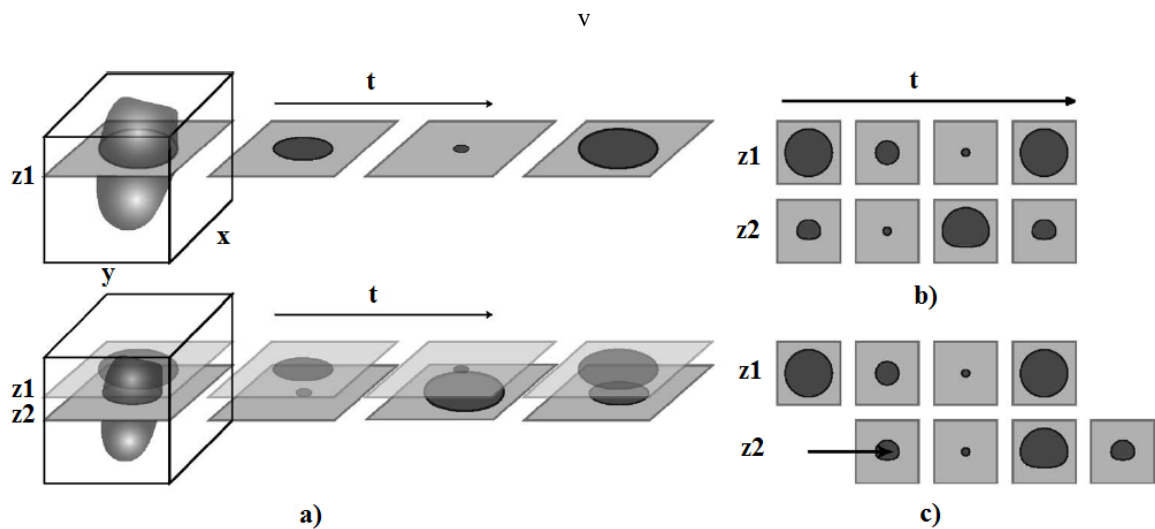
Figure 18: Live imaging and post-acquisition process [48]. a) Acquisition of heart slices at successive depths over time results in b) slice sequences not synchronized. An algorithm is used to minimize the differences between slice sequences and c) synchronize them.

2.3 Data analysis

2.3.1 Segmentation and parametrization of the anatomy of the heart

To study the behaviour of the heart tube in space and in time, at first the 3D moving volume of the heart was reconstructed using Matlab on the base of the 4D dataset obtained. The method developed and applied for the heart segmentation is described as follows:

- Reference cross-section planes definition

  Using Imaris software (Bitplane AG), the acquired image of the heart was cut with few (3-5) moving planes perpendicular to the longitudinal axis of the heart tube along its length (Figure 19). To describe each plane over the cardiac cycle, three

cells lying on it were chosen and their position over time was tracked and exported. The position of these cells was imported and used to define the centre and the normal of each reference plane at all the time step of the cardiac cycle (Figure 20) in Matlab software.

- Ellipse fitting of reference cross-sections

The cross-sections resulting from the intersection of the heart and the reference planes (Figure 19) were fitted with ellipses (Figure 21), to segment both the myocardium and the endocardium.

- Linear interpolation and new cross-section planes definition

A local reference system was defined for each ellipse using its major and minus axes and its normal unit vector. The points of the ellipses were ordered such that the normals to all the ellipses were oriented in the same way. Corresponding points of the ellipses and the centreline of the heart (defined as the line that connects the centres of the cross-sections of the heart) were linearly interpolated in space to define additional planes (100) equidistant and perpendicular to the longitudinal axis of the heart (Figure 22)

- Ellipse fitting of cross-sections

The cross-sections resulting from the intersection of the heart and the new cross-sections planes (Figure 23) were fitted as ellipses.

- Smoothing

Cubic curves connecting corresponding points of ellipses were smoothed in space (Figure 24).

This way, the anatomy of the heart was parametrized according to the centreline found (that is an approximation of the axis of the heart tube) using the arch length s of the curve (Figure 25). The position s=0 was assigned to the inflow, then s increases along the heart reaching the maximum value at the outflow.
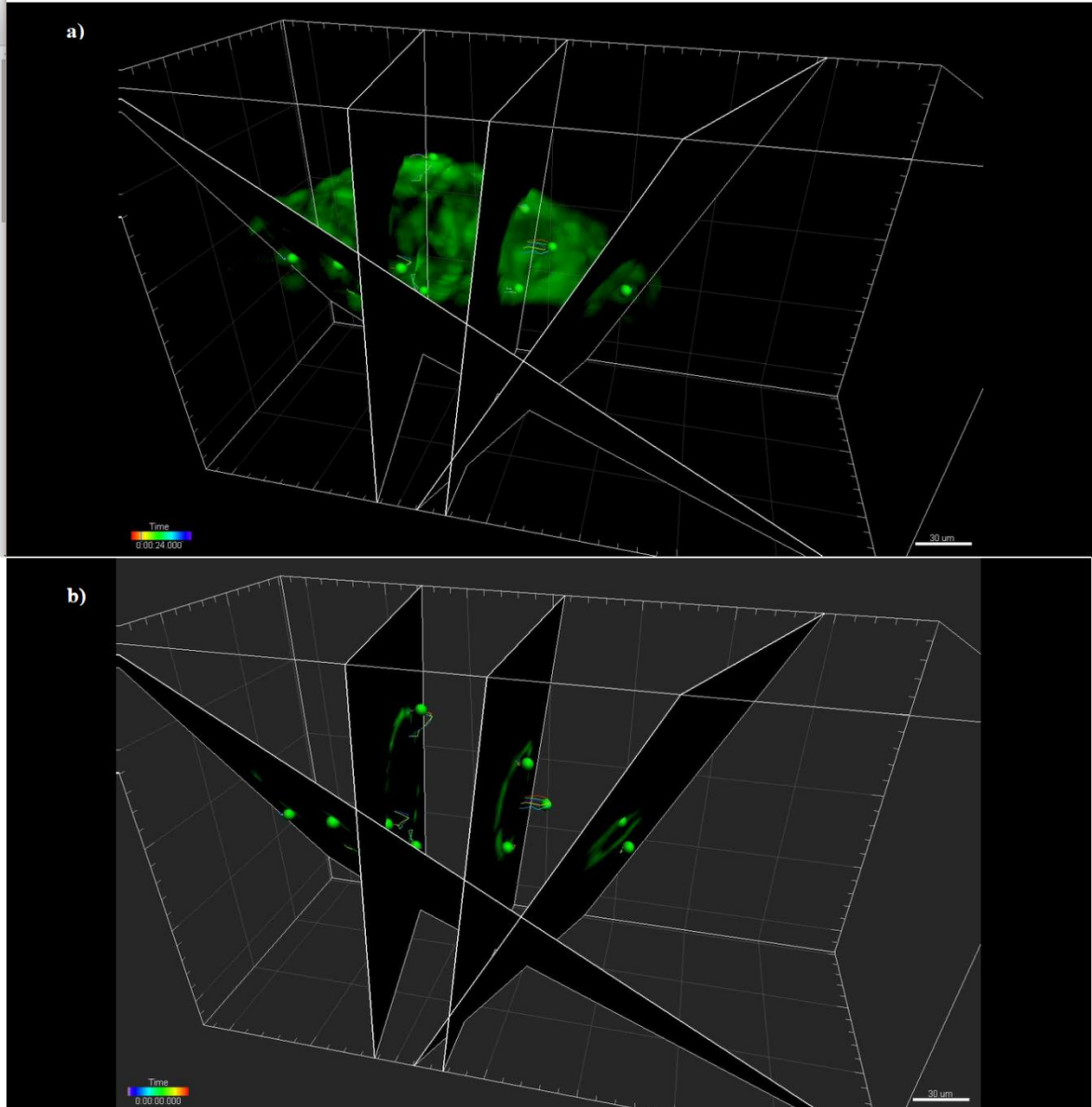
Figure 19: Reference cross-section planes definition in Imaris for the segmentation of the heart. a) Reference planes perpendicular to the longitudinal axis of the heart from the inflow (left) to the outflow (right) and b) resulting cross-sections of the myocardium. Green spots represent the cardiomyocytes moving through the reference planes during the cardiac cycle.
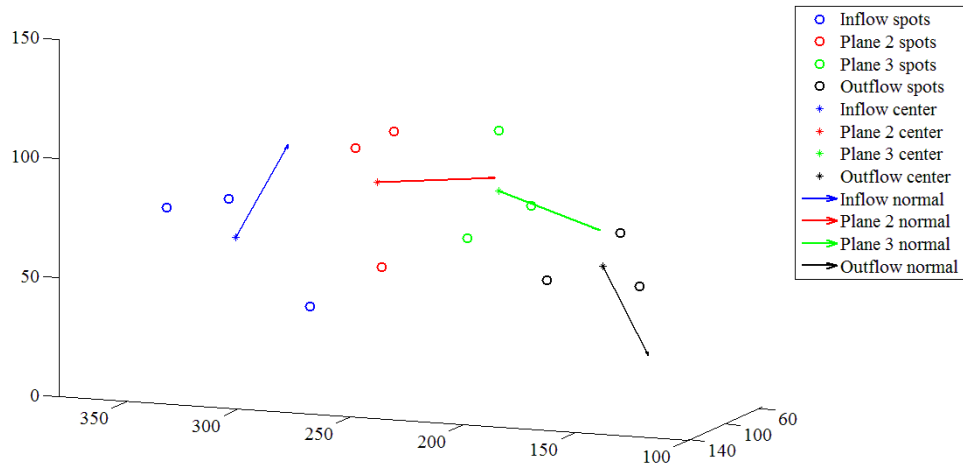
Figure 20: Reference cross-section planes definition in Matlab. The planes were defined using the position of three cardiomyocytes laying in each plane to calculate its centre and normal.
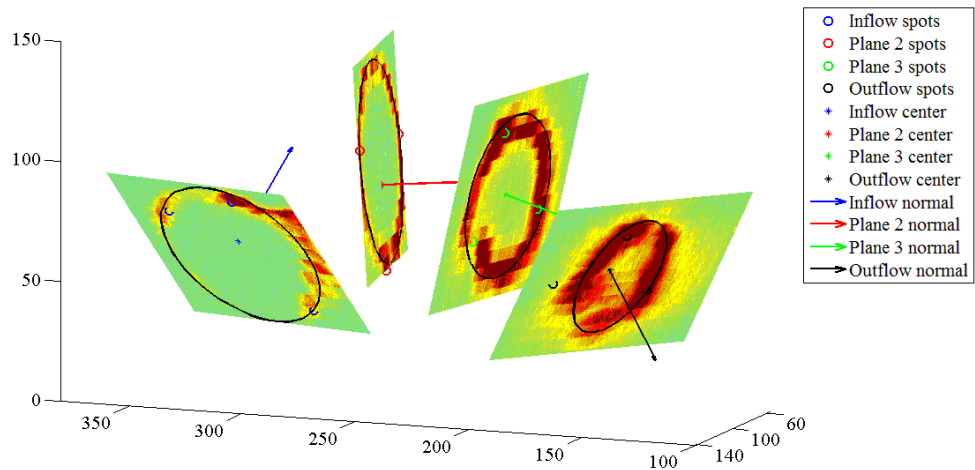
Figure 21: Ellipse fitting of reference cross-sections of the heart.
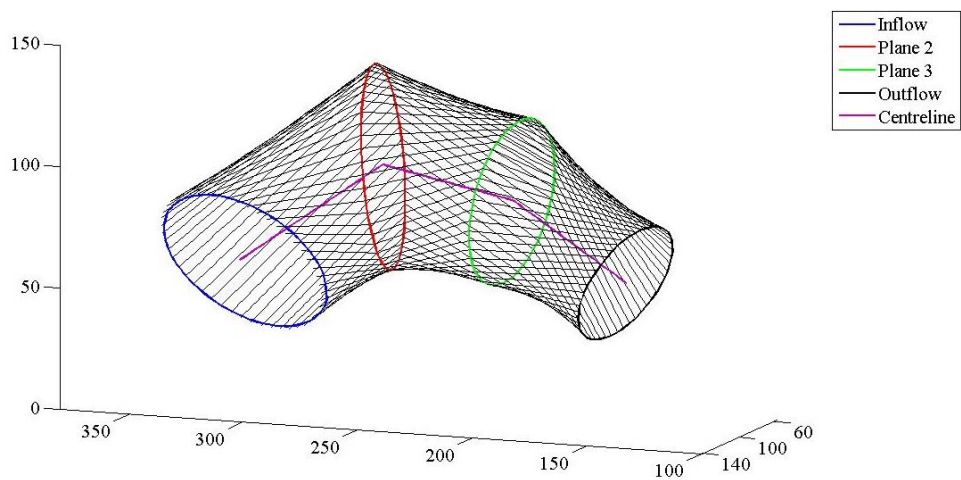
Figure 22: Linear interpolation of the centreline of the heart and of the points of cross-sectional ellipses to define new cross-section planes.

28
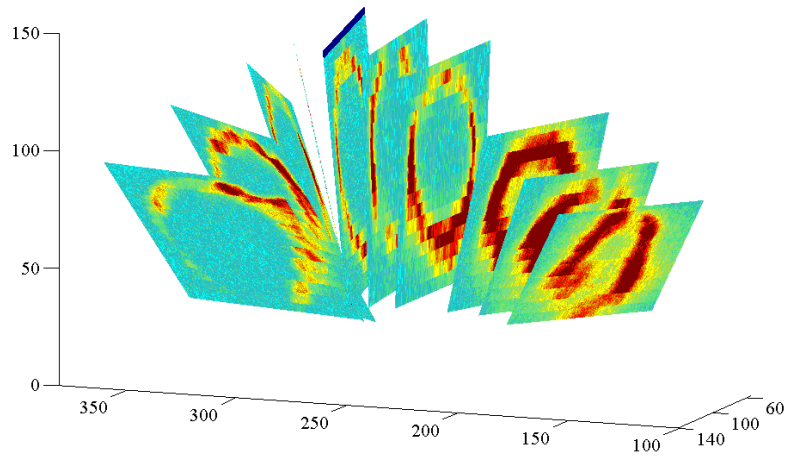
Figure 23: Cross-sections of the heart resulting from the intersection with the new planes.
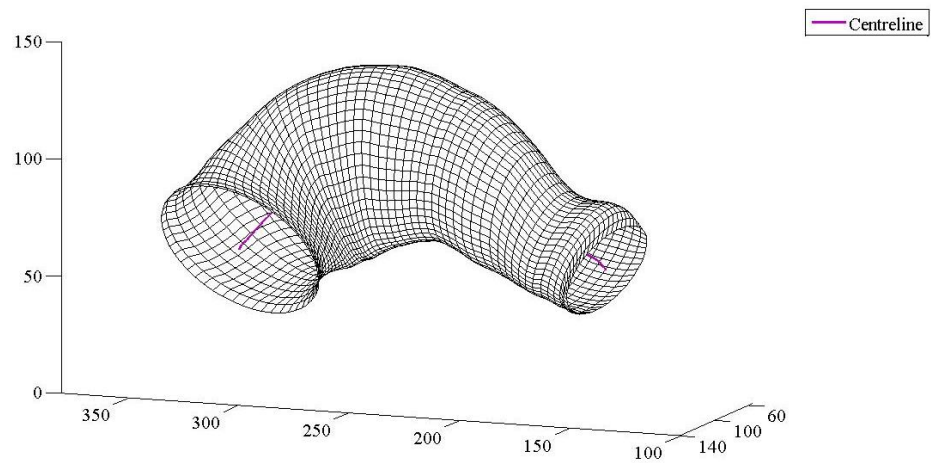
Figure 24: Smoothing of the cubic curves connecting corresponding points of the cross-sectional ellipses.
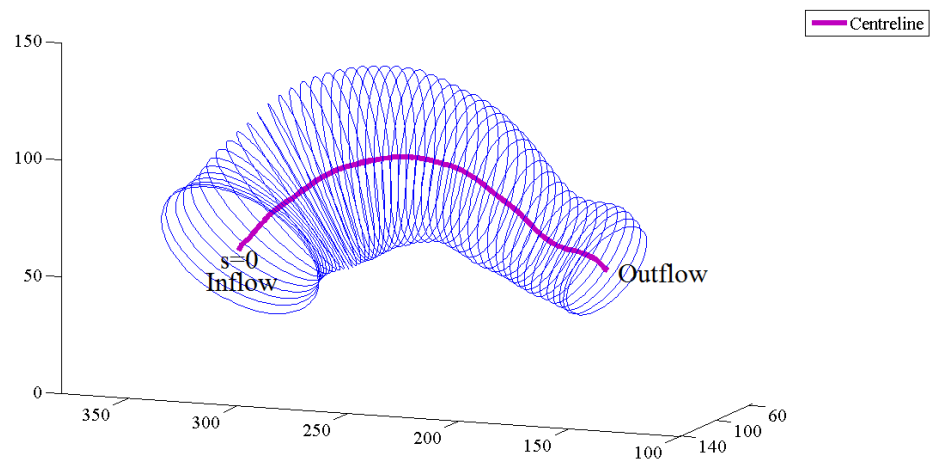
Figure 25: Parametrization of the anatomy of the heart using the arch length *s* of the centreline.

29

2.3.2   Heart dynamics

Heart dynamics was studied considering the three layers that compose the tube, myocardium, endocardium and cardiac jelly. Different parameters were used for the analysis (Table 3):

- The distance between neighbouring cardiomyocytes was used to characterize locally the myocardium;
- The area of the ellipses fitting the myocardium and endocardium cross-sections was used to describe these two cell layers;
- The difference between the area of myocardium cross-sections and the area of endocardium cross-sections was calculated to study the cardiac jelly.

Table 3: Parameters used to study the dynamics of each cardiac layer.

Layer	Parameter
Myocardium	cardiomyocytes distance; cross-sections area
Endocardium	cross-sections area
Cardiac jelly	myocardium cross-sections area – endocardium cross-sections area

2.3.2.1 Myocardium

To study the myocardium, one of the parameters used was the distance between neighbouring cardiomyocytes.

To obtain it, the 4D dataset of the moving heart was imported in Imaris Software. At each time step of the cardiac cycle, the 3D image of the heart (Figure 26) was processed with a cell detection algorithm implemented in Imaris that allowed to recognize all the cardiomyocytes present as spherical spots with diameter of 8-10 µm. Spots corresponding to the same cell over time were associated by manually connecting their centres using the particle tracking tool implemented in the software. The 3D trajectory $(x(t),y(t),z(t))$ of each cell during the cardiac cycle (Figure 26) was thus defined, exported and imported in Matlab.
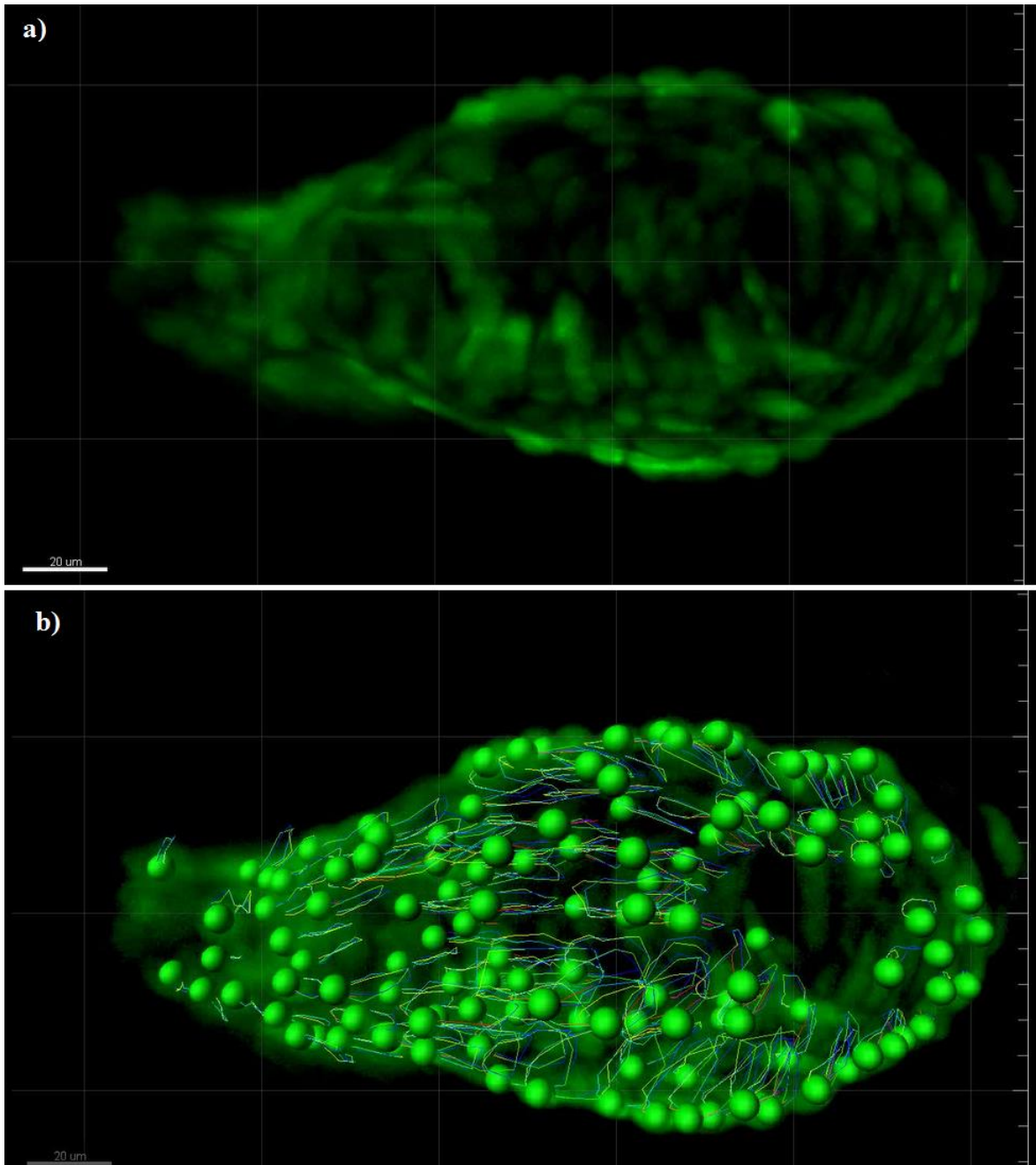
Figure 26: Tracking of the cardiomyocytes in a beating heart in Imaris. a) cardiomyocytes expressing green fluorescence; b) spherical spots used to identify the cardiomyocytes and their trajectories over time (curves).

In Matlab, two fixed coordinates $s=(p,s)$ were assigned to the centre of each spot, considering the position of the cell at the time step before the beginning of the contraction of the heart: p represents the circumferential position of the cell on the cross-section perimeter and s the archlength position on the centreline of the heart.

The Delaunay triangulation algorithm implemented in Matlab was used to define, from the set of the 2D positions of the cardiomyocytes, a network of triangles connecting the neighbouring cells. Then, the coordinates *s=(p,s)* of the centres of the segments that connect two neighbouring cells were calculated to assign to each segment a position in the heart (Figure 27).
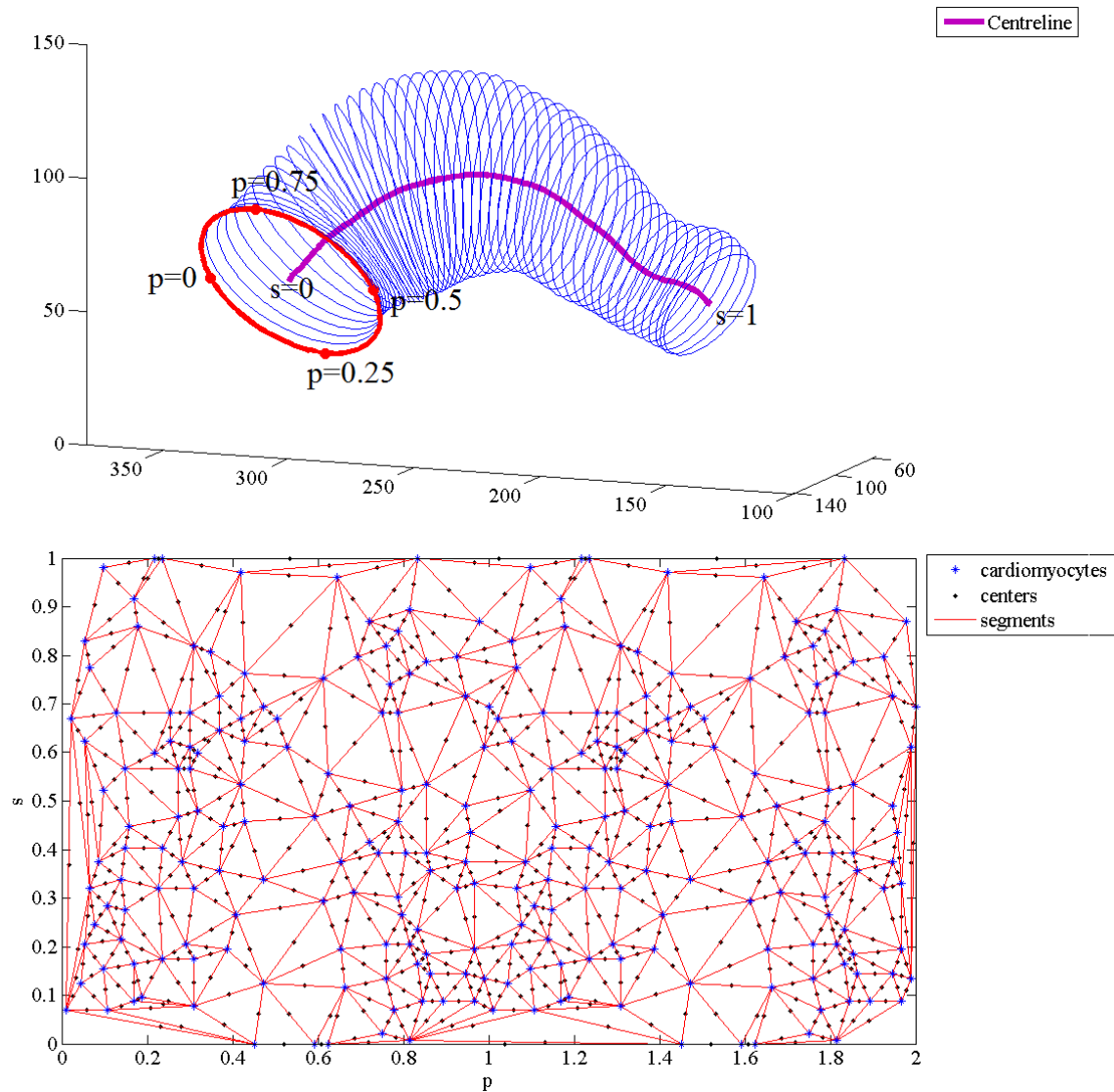
Figure 27: Identification of myocardium segments between neighbouring cardiomyocytes. After assigning two coordinates to each cell, accordingly to its positions *p* and *s* in the heart (above), Delaunay triangulation was applied to the 2D heart (unfolded tube) and the centres of the segments between two neighbouring cells were calculated (below). The centreline *s* and the circumference *p* of the heart are here normalized between 0 and 1; *p* is replicated in order to visualize also neighbouring cells at the boundaries of the unfolded tube (*p*=0 and *p*=1).

To study the dynamics of the portion of the tissue between neighbouring cardiomyocytes, the distance between the cells was normalized between 0 and 1. 0 represents the condition in which two cells are maximally closed one to the other, so the tissue is contracted; the distance is 1 when the cells are maximally distant and corresponds to a stretched condition of the myocardium. Given d the length of the segment connecting two neighbouring cardiomyocytes, $s=(p,s)$ the position of the segment centre, $t_{min}(s) = \min_t d(\mathbf{s}, \mathrm{t})$ the instant when the distance has the minimum value (i.e. the instant when the segment is maximally contracted) and $t_{max}(s) = \max_t d(\mathbf{s}, \mathrm{t})$ the instant when the distance reaches the maximum value (i.e. the instant when the segment is maximally stretched), the parameter d$_{normalized}$ was defined as follows:

$$d_{normalized}(\boldsymbol{s}, t) = \frac{d(\boldsymbol{s}, t) - d(\boldsymbol{s}, t_{min})}{d(\boldsymbol{s}, t_{max}) - d(\boldsymbol{s}, t_{min})}$$

$$d_{normalized} = \begin{cases} 0 \; if \; \tilde{t} = t_{min} \\ 1 \; if \; \tilde{t} = \; t_{max} \end{cases}$$

Thanks to this normalization, it is possible to identify at each time step the regions of the myocardium where segments are stretched and contracted and thus to understand how the contraction wave propagates along the heart tube over the cardiac cycle.

In order to study whether all the regions of the heart undergo the same stretching or whether differences can be found, an index called local fractional extension (LFE) was introduced. The LFE is a measure in percentage of how much the distance between neighbouring cells increases with respect to the minimum value. LFE was calculated as:

$$LFE(s) = \frac{d(\boldsymbol{s}, t_{max}) - d(\boldsymbol{s}, t_{min})}{d(\boldsymbol{s}, t_{min})} \%$$

The index was used to compare the local stretching of the tissue along the heart.

Since the myocardium was segmented using ellipses to fit the cross-sections, the second parameter used to study this cell layer was the area of the ellipses. The position of the ellipses along the heart centreline was defined as a function of the archlenght s and the area of the cross-sections was studied over the cardiac cycle.

In analogy with d$_{normalized}$, the ellipse area A of the cross-section in position s was normalized according to its minimum and maximum values:

$$A_{normalized}(s,t) = \frac{A(s,t) - A(s,t_{min})}{A(s,t_{max}) - A(s,t_{min})}$$

$$A_{normalized} = \begin{cases} 0 \ if \ \tilde{t} = t_{min} \\ 1 \ if \ \tilde{t} = t_{max} \end{cases}$$

$A_{normalized}$ assumes values between 0 and 1. The parameter is equal to 0 when the area reaches the minimum value and to 1 when the maximum expansion occurs.

An index called area fractional shortening (AFS) was defined as proposed by Garita *et al.* [39] and calculated for each cross-section to measure in percentage how much the area decreases going from the relaxed state (maximum area) to the contracted condition (minimum area):

$$AFS(s) = \frac{A(s,t_{min}) - A(s,t_{max})}{A(s,t_{max})}\%$$

This index was used to study if the cross-section shortening is homogeneous along the heart or if there are differences between regions.

Three hearts at 28 hpf and six hearts at 30 hpf were analysed.

2.3.2.2 Endocardium

Since endocardial cells displacement was much higher than cardiomyocytes displacement, tracking the fast movements of the cells between two successive time steps in Imaris was difficult. Furthermore, in the acquired images, the endocardium was covered by the outer layer (the myocardium) and cells were less visible. For these reasons, the tracking of single endocardial cells was not possible and the distance between neighbouring cells was not considered as a parameter to study endocardium dynamics.

Instead, it was possible to segment the endocardium using ellipses to fit the cross-sections and the area of the ellipses was used to study the layer. As for the myocardium, the position of the ellipses was defined as a function of the archlength *s* on the centreline of the heart and ellipses areas over time were studied. $A_{normalized}$ (area between 0 and 1) and the AFS index were used as well to study the layer. Two hearts at 28 hpf were analysed.

2.3.2.3 Cardiac jelly

To analyse the cardiac jelly, the difference between myocardium and endocardium areas was used as a parameter. Since the cross-sections of the two cell layers are not perfectly

elliptic, an error can arise from their too approximate description using an ellipse fitting. In the attempt to calculate more accurately the cardiac jelly area, the inner perimeter of the myocardium and the outer perimeter of the endocardium were drawn manually using Imagej software (Figure 28) in five equidistant cross-sections along the heart tube (Figure 29).
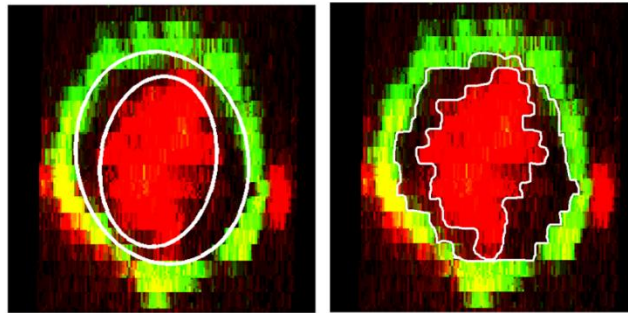
Figure 28: Cardiac jelly area calculation. To reduce the errors in the calculation of cardiac jelly area due to the ellipse fitting (left), the inner perimeter of myocardium and the outer perimeter of endocardium were drawn manually (right).
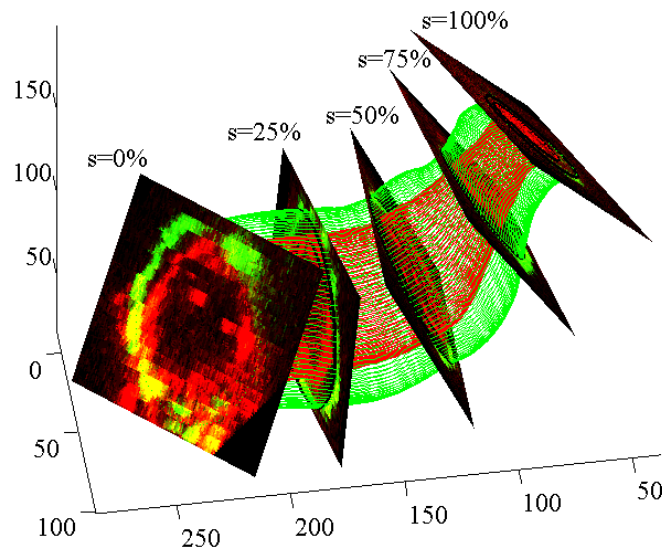
Figure 29: Myocardium and endocardium cross-sections used to analyse the cardiac jelly layer. The cross-sections are equidistant along the centreline of the heart. The myocardium is in green, the endocardium in red. The area of the cardiac jelly was calculated as the difference between myocardium and endocardium areas.

Two hearts at 28 hpf were studied. The area and $A_{normalized}$ were used for the analysis.

2.3.3 Red blood cells velocity

To find relationships between heart movement and blood ejection, red blood cells velocity was investigated.

A single red blood cell entering the inflow, passing through the whole heart tube and leaving the outflow can not be tracked. This is because of the method used for the acquisition of the heart. The trajectory of a red blood cell is three-dimensional, that means that the cell does not travel in a single plane of the heart but moves at different depths. Since the heart was acquired plane by plane at different cardiac cycles, the imaging allows to follow a single cell only as long as it remains in the plane acquired at that cardiac cycle. For this reason the analysis of red blood cells velocity was done in a single plane of the heart. All the red blood cells passing in that plane during the acquisition time were tracked with Imaris software (Figure 30) and blood mean velocity was calculated in Matlab. The analysis was done in two hearts at 28 hpf, considering a plane where most of the heart length was visible.
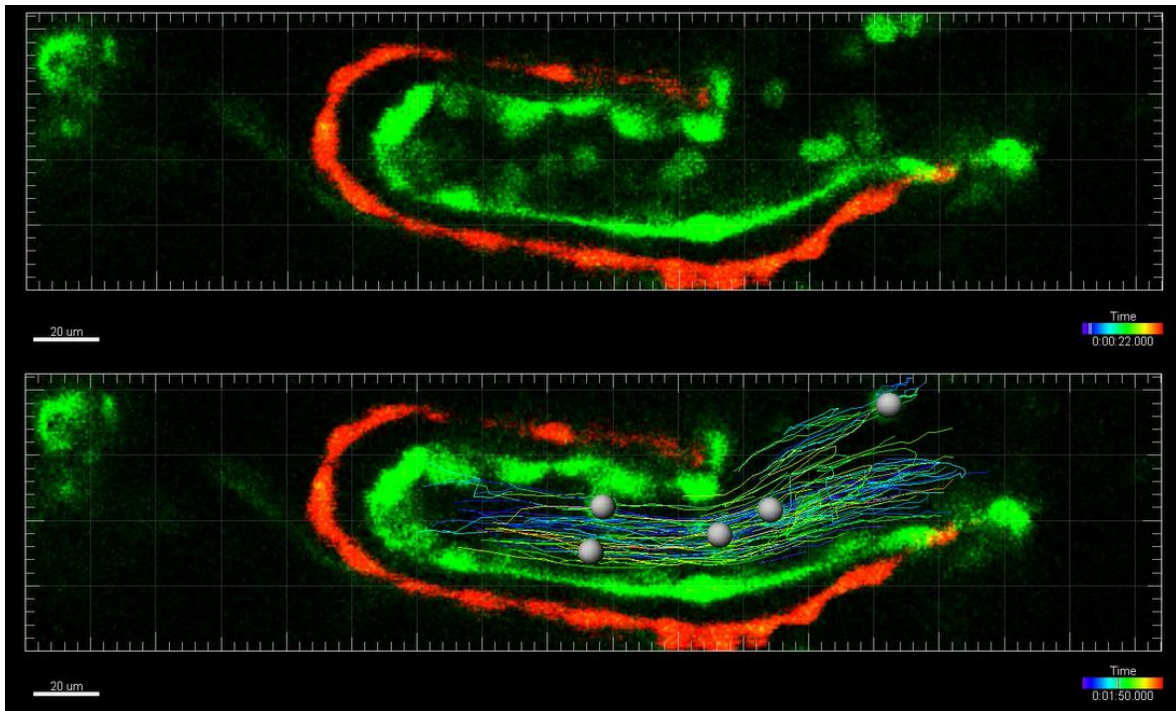
Figure 30: Example of red blood cell tracking in a plane of the heart in Imaris.

2.3.4 Calcium dynamics in myocardium

2.3.4.1 Non-beating heart

To study the calcium dynamics in the myocardium, at first a *tg(cmlc2:Gal4FF;UAS:RFP;UAS:gcamp5.0)* non-beating heart was considered. One selected embryo was put in BDM 0.01 for one hour before the imaging to reversibly inhibit the contraction of the cardiac muscle. The heart expressed green and red fluorescence in myocardial cells and both colours were acquired.

In Imaris, cardiomyocytes were identified as spherical spots using the cells detection algorithm of the software and spots corresponding to the same cell over the cardiac cycle were manually associated and tracked as previously described (Paragraph 2.3.2.1). The mean intensity value of the colour within the spots at each time step of the cardiac cycle was calculated using a measurement algorithm implemented in Imaris.

In Matlab, the position $s=(p,s)$ of each cardiomyocyte in the heart was defined and the green and red signals intensities of the cells were analysed.

As previously mentioned, in *tg(cmlc2:Gal4FF;UAS:RFP;UAS:gcamp5.0)* transgenic line the intensity of the green colour (*gcamp5.0* signal) is sensitive to calcium variations in the cardiomyocytes, while the intensity of the red colour (*RFP* signal) does not depend on the calcium in the cells. The *RFP* signal is not supposed to change over time because the *RFP* protein expression depends on the promoter of the *cmlc2* gene in the cardiomyocytes, whose dynamics is characterized by much longer time scales than those considered in the present study. The *RFP* signal can be, therefore, described as:

$$I_{RFP}(\boldsymbol{s}, t) = I_{stopped\_myo}(\boldsymbol{s})$$

$I_{stopped\_myo}(\boldsymbol{s})$ is the constant representing myocardium baseline signal when the heart is stopped.

On the contrary, the *gcamp5.0* signal is expected to change during the cardiac cycle according to calcium variations in the cell:

$$I_{gcamp5}(\boldsymbol{s}, t) \propto I_{calcium\_stopped}(\boldsymbol{s}, t)$$

The two signals were compared to prove *gcamp5.0* reported calcium oscillations in the myocardium of the embryo and to verify that *RFP* signal intensity was constant over time in the absence of heart motion such that it could be used as a control signal. As discussed later, the latter is important for the analysis of the calcium imaging in the beating heart.

2.3.4.2 Beating heart

A method to study the calcium dynamics in the beating heart was then developed.

After testing *gcamp5.0* activity in the non-beating heart, the BDM was washed out to restart the contraction. The embryo was then transferred in tricaine and monitored under the microscope until the physiological heart rate was reached again. Live imaging was thus repeated and mean intensities of *gcamp5.0* and *RFP* signals expressed in cardiomyocytes were exported from Imaris as described in the previous paragraph.

Since the heart moves going closer to and far from the microscope light source, the intensity of the laser light on the myocardium changes during the cardiac cycle and *RFP* signal is not expected to be constant as in the case of the non-beating heart. On the contrary it is supposed to be associated with the heart movement. The *gcamp5.0* and *RFP* signals were modelled as follows:

$$I_{gcamp5}(s,t) = b * I_{beating}(s,t) * I_{calcium\_beating}(s,t)$$

$$I_{RFP}(s,t) = a * I_{beating}(s,t)$$

$I_{beating}(s,t)$ is the myocardium baseline signal when the heart is beating, $I_{calcium\_beating}(s,t)$ represents calcium variations in the cells during the cardiac cycle in the beating heart, a and b were assumed to be constants and any offset additional terms was neglected.

In the beating heart, *gcamp5.0* signal is supposed to be partly due to the calcium oscillation and partly due to artefacts associated to the heart movements. To remove this artefact, represented in the equation model by the common terms $I_{beating}(s,t)$ in *gcamp5.0* and *RFP* signals, the ratio between the two acquired signals was taken:

$$I_{calcium\_beating}(s,t) \propto \frac{I_{gcamp5}(s,t)}{I_{RFP}(s,t)}$$

Both in the case of the non-beating and of the beating heart, the intensity of the calcium signal expressed by one cardiomyocyte in position *s=(p,s)* was normalized between 0 and 1 in analogy with d$_{normalized}$ and A$_{normalized}$ to study the calcium dynamics:

$$I_{normalized}(s,t) = \frac{I(s,t) - I(s,t_{min})}{I(s,t_{max}) - I(s,t_{min})}$$

$$I_{normalized} = \begin{cases} 0 \; if \; \tilde{t} = t_{min} \\ 1 \; if \; \tilde{t} = t_{max} \end{cases}$$

I$_{normalized}$ is equal to 0 when the signal reaches its minimum intensity and to 1 when the intensity is maximum.

To verify the strategy adopted to remove the artifact of the heart movement from *gcamp5.0* signal, a control heart was obtained by crossing *Tg(cmlc2:eGFP)* and *Tg(cmlc2:Gal4FF;UAS:RFP)* transgenic lines. The two lines express respectively a green and a red fluorescent protein in cardiomyocytes and the resulting embryos had the myocardium labelled both in green and in red in a non-calcium-dependent manner. The myocardium was acquired using light sheet microscope and the intensities of the two signals (green and red colors) were exported from Imaris, exactly as for the calcium reporter line, and compered. The expression of the fluorescent proteins is constant over the acquisition time but the fluorescence intensity detected by the microscope can change over the cardiac cycle because of the movement of the heart during the acquisition. Since the green and red fluorescence proteins are expressed in the same cells, it's reasonable to assume that the two signals representing both the myocardium baseline signal change in the same way while the heart is moving:

$$I_{cmlc2_{gfp}}(\boldsymbol{s}, t) = c * I_{beating}(\boldsymbol{s}, t)$$

$$I_{cmlc2_{rfp}}(\boldsymbol{s}, t) = d * I_{beating}(\boldsymbol{s}, t)$$

Assuming that the two signals are proportional to each other, the ratio between them is supposed to be a constant. If this is verified in the control, also in the beating heart of the calcium reporter line, the ratio between *gcamp5.0* and *RFP* would be sufficient to remove the terms $I_{beating}(s,t)$ present in both the signals.

3. Results

3.1 Heart dynamics

3.1.1 Myocardium

To study myocardium dynamics, two parameters were considered, the area of the myocardium cross-sections perpendicular to the longitudinal axis of the heart and the distance between neighbouring cardiomyocytes. Myocardium dynamics was thus described as how the area of this layer or how the distance between cardiomyocytes changes over the cardiac cycle along the centreline of the heart.

Figure 31 and Figure 32 show the results respectively for three analysed hearts at 28 hpf and for six hearts at 30 hpf.

The plots allow to visualize the dynamics of the myocardium in a specific region of the heart and in the whole heart tube. In fact, focusing on one position s of the centreline and going along the y axis (i.e. over the cardiac cycle), the dynamics of that region is described (example in Figure 33); while, observing when consecutive cross-sections contract, it is possible to study how the contraction propagates along the heart. The dark blue curve describes the instant when cross-section area and distance between cardiomyocytes reach the minimum value and shows thus how the contraction propagates along the heart tube over time; the dark red areas show the regions of the tissue stretched during myocardium relaxation along the heart.

Myocardium dynamics at 28 hpf and 30 hpf is quite similar, considering both the area and the distance. The contration wave propagates almost lineary along the centerline of the heart. However, a delay can be observed in Figure 31 and Figure 32 in almost all the hearts in the last part of the centreline, where the slope of the blue curve increases indicating a slowdown in the propagation speed (see also Figure 34, Figure 35 and Figure 36). In some cases, this is more visible from the analysis of the area dynamics (as in hearts 2 and 3 at 28 hpf), in others from the distance dynamics (as in hearts 1, 2 and 3 at 30 hpf). Heart 6 at 30 hpf is an exception since the contraction propagates faster in the final region of the heart and an acceleration is visible also at the inflow. In the central part of the heart tube, instead, the wave speed is lower (Figure 37).

Figure 31: Myocardium dynamics at 28 hpf, described using cross-sections areas (left) and distances between neighbouring cardiomyocytes (right). s **represents the centreline of the heart, from the inflow (**$s=0$**) to the end of the acquired image;** t **is the current time over the duration of the whole cardiac cycle (**$t=0$ **represents the beginning of the cardiac cycle and** $t=1$ **the end). The colorbar goes from 0 to 1; 0 (dark blue) is the minimum value of the area or of the distance between cells in a certain** s **position and represents the maximum contraction in that region, 1 (dark red) is the maximum value and indicates the maximum relaxation of the heart and maximum stretching of the tissue.**

Figure 32: Myocardium dynamics at 30 hpf, described using cross-sections areas (left) and distances between neighbouring cardiomyocytes (right). *s* represents the centreline of the heart, from the inflow (*s*=0) to the end of the acquired image; *t* is the current time over the duration of the whole cardiac cycle (*t*=0 represents the beginning of the cardiac cycle and *t*=1 the end). The colorbar goes from 0 to 1; 0 (dark blue) is the minimum value of the area or of the distance between cells in a certain *s* position and represents the maximum contraction in that region, 1 (dark red) is the maximum value and indicates the maximum relaxation of the heart and maximum stretching of the tissue.
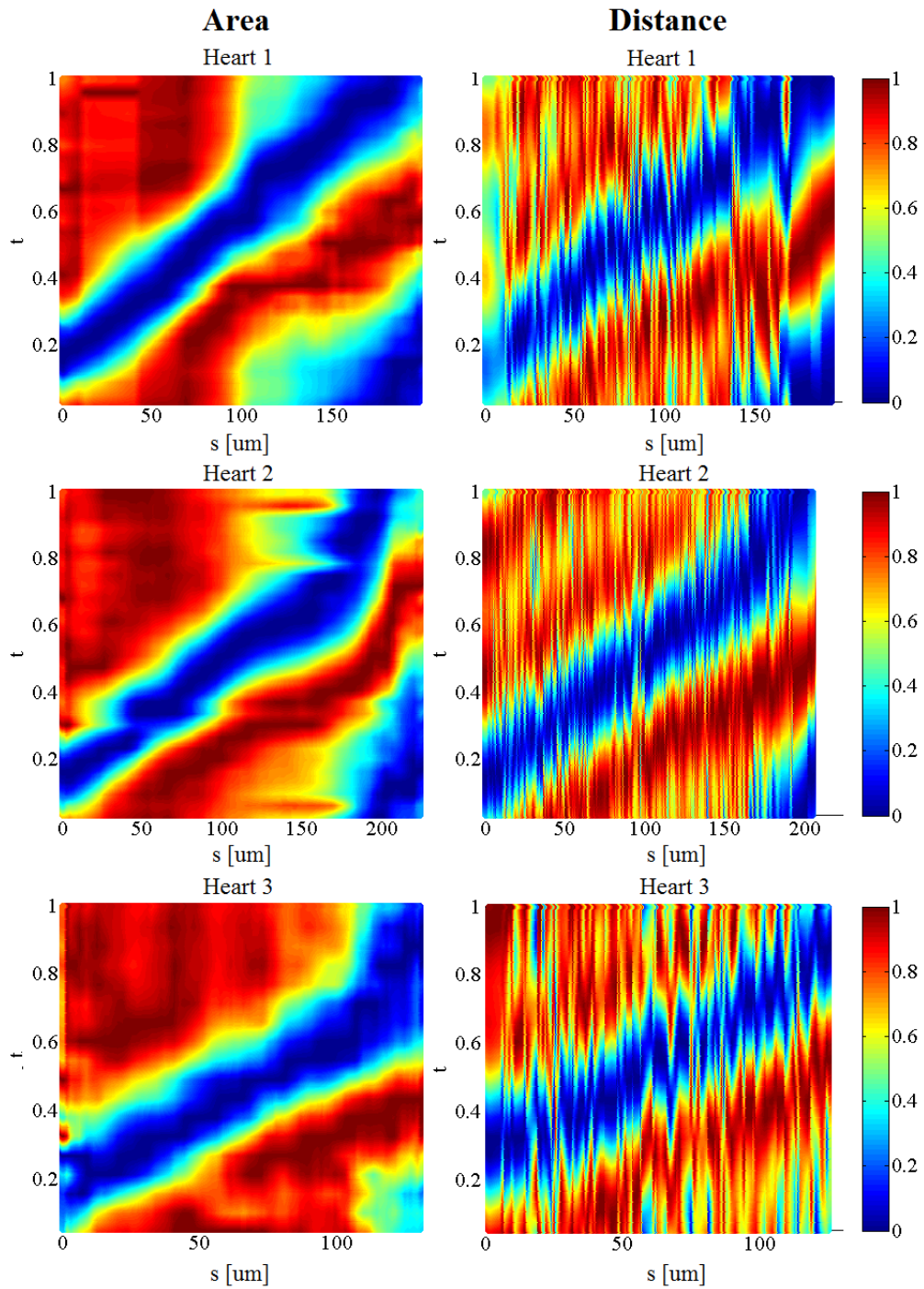
42

Figure 32 (Continue): Myocardium dynamics at 30 hpf, described using cross-sections areas (left) and distances between neighbouring cardiomyocytes (right). *s* **represents the centreline of the heart, from the inflow (*s=0*) to the end of the acquired image;** *t* **is the current time over the duration of the whole cardiac cycle (*t=0* represents the beginning of the cardiac cycle and *t=1* the end). The colorbar goes from 0 to 1; 0 (dark blue) is the minimum value of the area or of the distance between cells in a certain** *s* **position and represents the maximum contraction in that region, 1 (dark red) is the maximum value and indicates the maximum relaxation of the heart and maximum stretching of the tissue.**
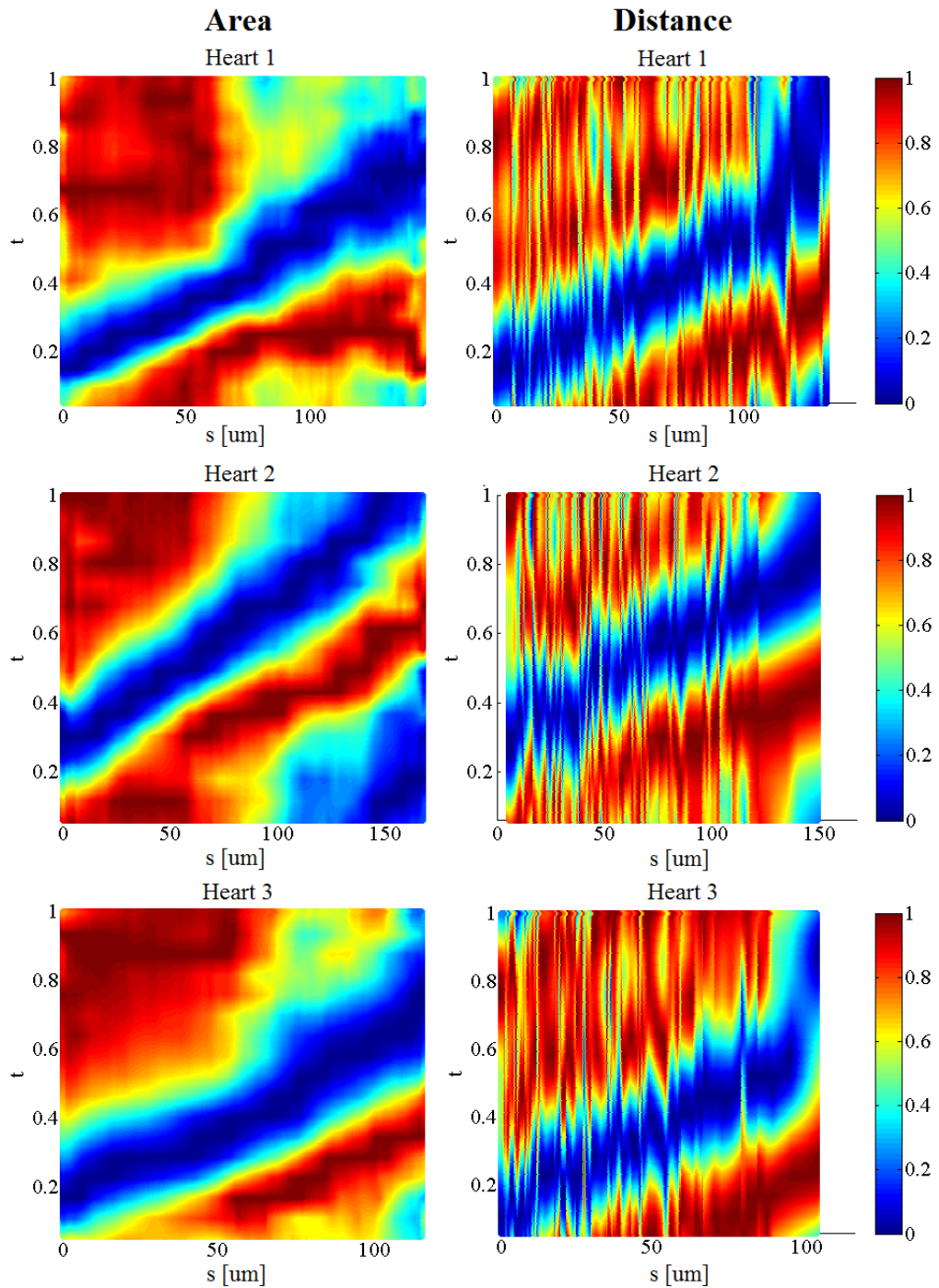
43

Figure 33: Example of myocardium dynamics in one specific region of the heart. Focusing on *s*=100 μm in heart 1 at 28 hpf (left) over the cardiac cycle (black line), the dynamics of the cross-section area (right above) and of the distance between neighbouring cardiomyocytes in that region (right below) can be extracted: both the area and the distance increase and reach a peak respectively at t=0.4 (instant of cross-section maximum expansion) and t=0.3 (instant of tissue segment maximum stretching), decrease until the contraction occurs in t≈0.55 and increase again.

Figure 34: Delay in the contraction wave propagation in the final part of the myocardium of heart 3 at 28 hpf. Considering the area dynamics at the beginning (s=0%), middle (s=50%) and ending (s=100%) of the centreline, the contraction in the three regions, corresponding to negative peaks in the curves, occurs at t≈0.25, t≈0.5 and t≈0.85, showing a delay of the wave in the final part of the heart (it needs 25% of the cardiac cycle to propagate in the first half of the heart and 35% in the second half).

Figure 35: Delay in the contraction wave propagation in the final part of the myocardium of hearts 4 and 5 at 30 hpf. Considering the area dynamics at the beginning (s=0%), middle (s=50%) and ending (s=100%) of the centreline, the contraction in the three regions, corresponding to negative peaks in the curves, occurs at t=0.2, t=0.3 and t=0.7 in heart 4 and at t=0.2, t=0.45 and t=0.9 in heart 5, showing a delay of the wave in the final part of the heart (it needs respectively 10% and 20% of the cardiac cycle to propagate in the first half of heart 4 and 5, and 40% and 45% in the second half).
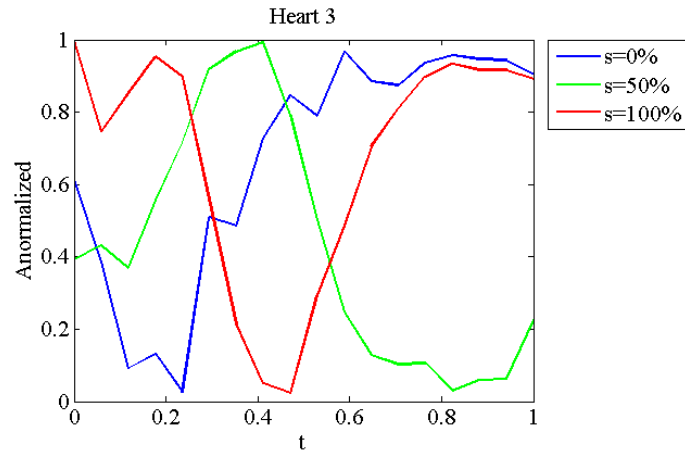
45
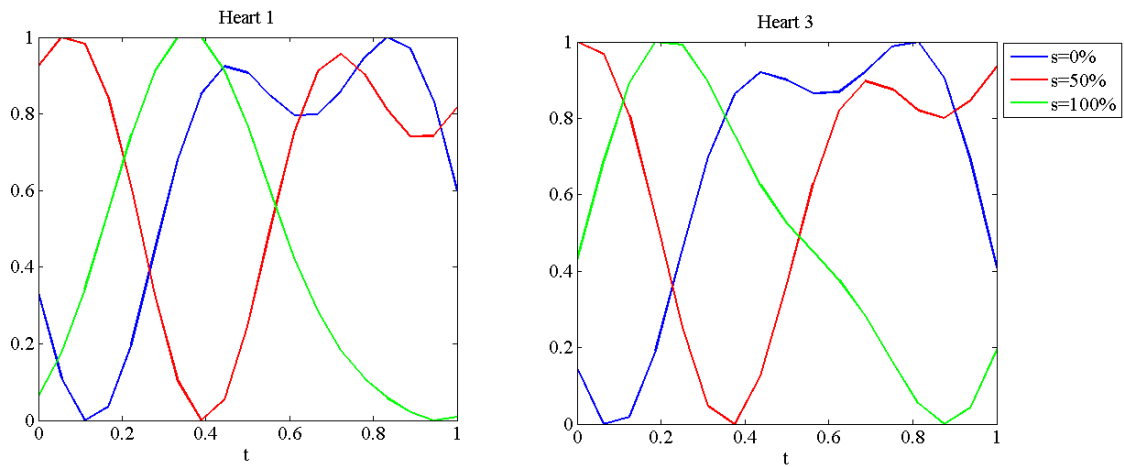
Figure 36: Delay in the contraction wave propagation in the final part of the myocardium of hearts 1 and 3 at 30 hpf. Considering the myocardium dynamics at the beginning (s=0%), middle (s=50%) and ending (s=100%) of the centreline described by d$_{normalized}$, the contraction in the three regions considered, corresponding to negative peaks in the curves, occurs at t=0.1, t=0.4 and t=0.9, showing a delay of the wave in the final part of the heart (it needs 30% of the cardiac cycle to propagate in the first half of the heart and 50% in the second half).
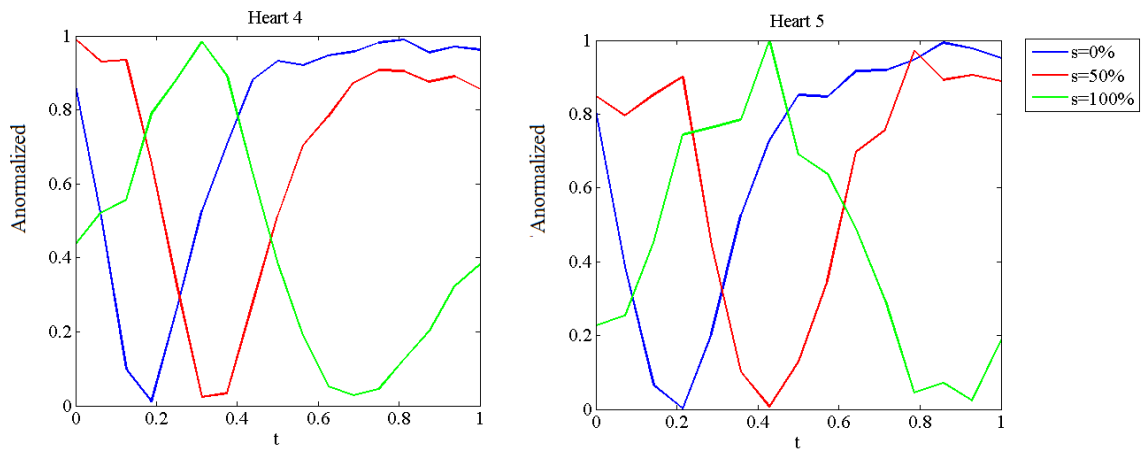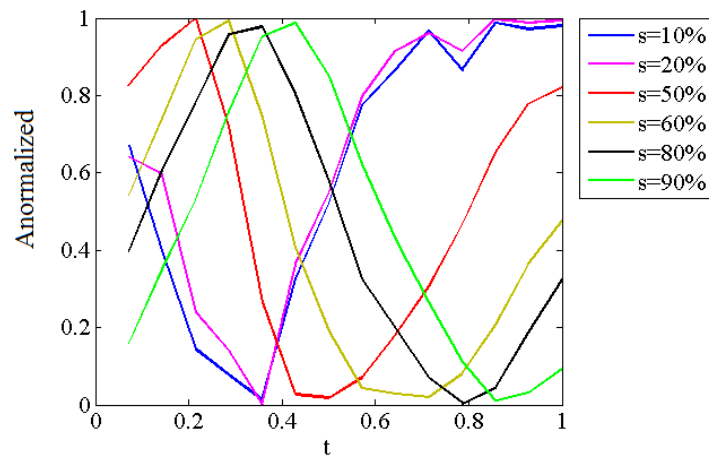

Figure 37: Contraction wave in heart 6 at 30 hpf. Considering the area dynamics along the centreline, the contraction in the different regions of the heart corresponds to the negative peaks in the curves. The propagation of the contraction results faster in the first part of the heart (the contraction occurs simultaneously in s=10% and s=20% of the centreline), then the velocity decreases in the central part of the heart and increases again in s=80-90%.

46

In hearts 1 and 2 in Figure 31 and in hearts 2, 5 and 6 in Figure 32, the inflow region starts conctacting while the final part of the myocardium is still contracted. For example, considering heart 1 at 28 hpf, $A_{normalized}$ at t=0.15 along the centreline (curve shown in Figure 38) assumes values close to 0 in the inflow region (that is contracted), startes increasing and reaches its maximus in s=70 µm (stretched region), decreases again to values close to 0 in s=190-200 µm (thus the ending region of the tube is also contracted). This means the contraction wave startes at the inflow before the wave of the previous cardiac cycle reaches the end of the heart tube. In the other hearts, on the contrary, the new contraction wave startes after the end of the previous one, since the final region of the heart is not contracted ($A_{normalized} \neq 0$) when the inflow is contracted. However, the simultaneous contraction of the two regions appears only at s>150 µm suggesting the outflow is missing in the hearts where it was not observable. In fact, while imaging the hearts, the fluorescent signal was attenuated going from the surface of the embryo to deep inside such that the outflow may not have been acquired if not sufficiently visible.
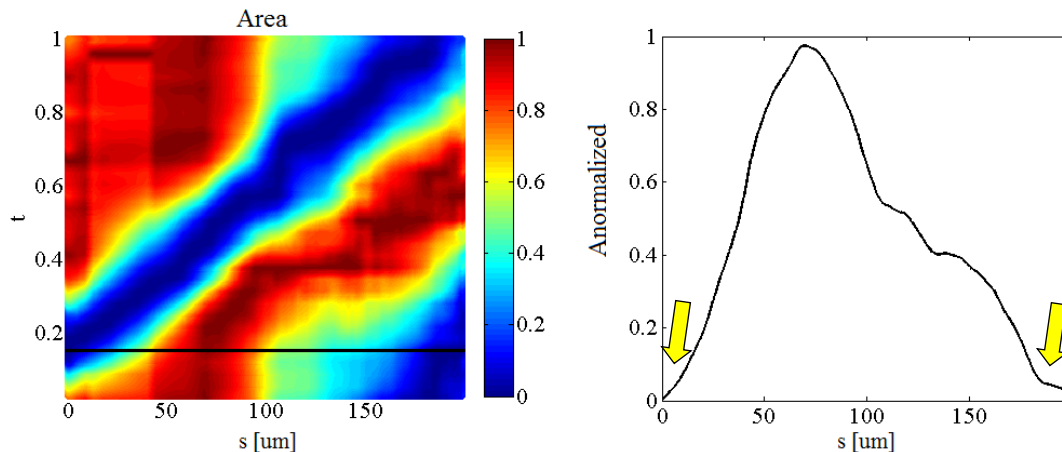
Figure 38: Simultaneous contraction of inflow and outflow regions in heart 1 at 28 hpf. Considering the area dynamics at t=0.15, the first and last regions of the myocardium are contracted (Anormalized≈0) at the same time (yellow arrow), showing that the contraction wave startes at the inflow before the wave of the previous cardiac cycle reaches the end of the heart tube.

In all the hearts analysed, it is clearly visible from Figure 31 and Figure 32 that the red region narrows starting from the second half of the heart and at the same time the blue region enlarges along the centreline. This means that the first half of the myocardium is relaxed for most of the cardiac cycle, in the second half, the situation progressively

reverses; at first the duration of the expansion and contraction is similar, then the cross-sections are longer contracted then relaxed at higher *s* (Figure 39 and Figure 40).
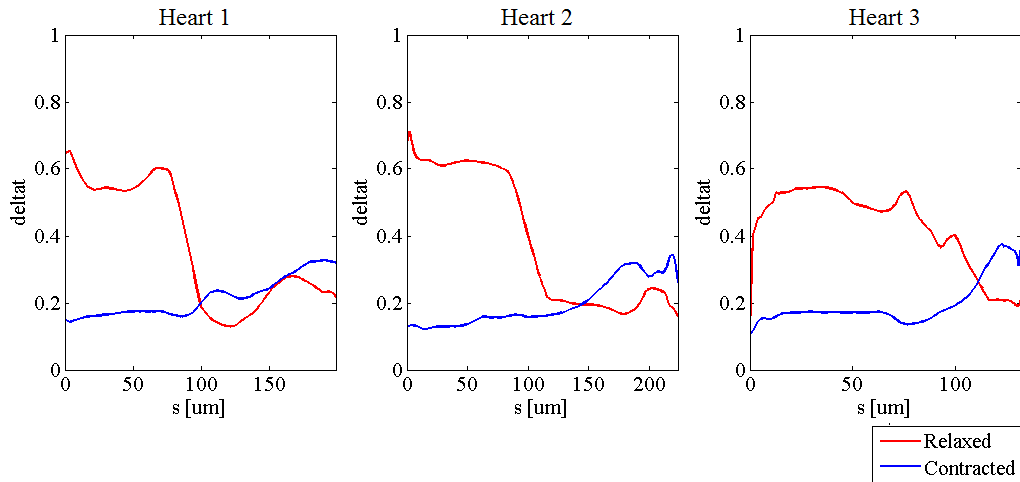
Figure 39: Duration of relaxation and contraction conditions of the myocardium along the heart at 28 hpf. In the first part of the myocardium the relaxation lasts more than the contraction but the situation reverses in the second half of the heart, where the area is longer contracted than expanded.

Figure 40: Duration of relaxation and contraction conditions of the myocardium along the heart at 30 hpf. In the first part of the myocardium the relaxation lasts more than the contraction but the situation reverses in the second half of the heart, where the area is longer contracted than expanded.

48

A comparison of the myocardium dynamics obtained with the analysis of the area and of the distance between neighbouring cardiomyocytes was done to identify possible differences. Consideri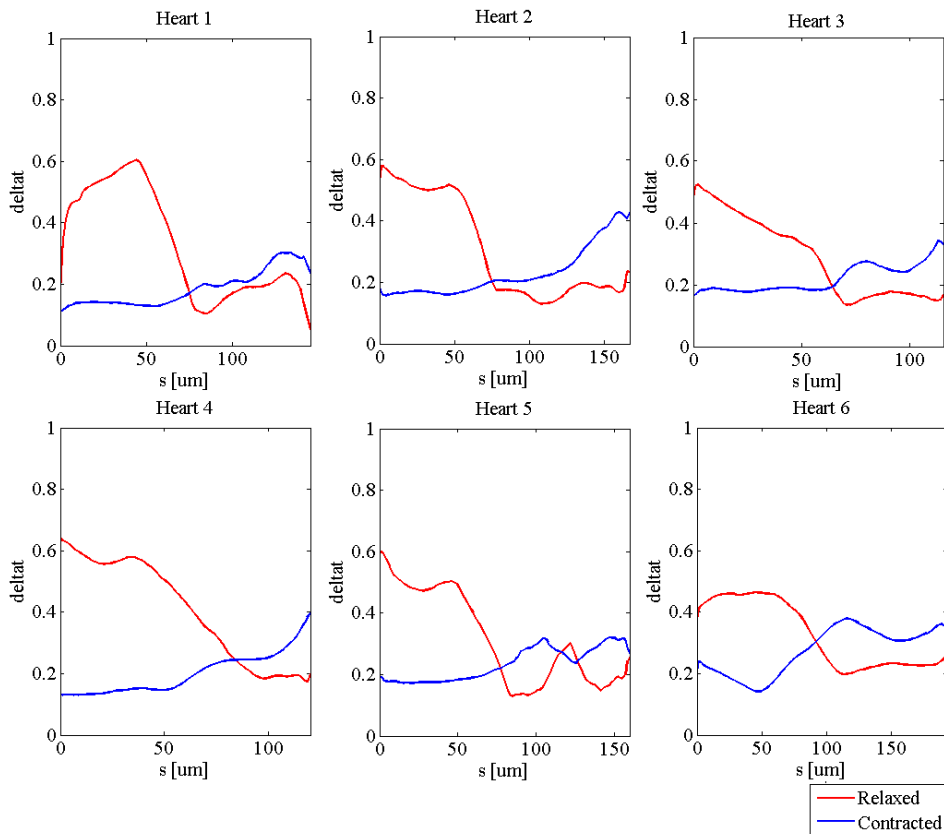ng the distance between two cells, in fact, only a small portion of the tissue is analysed and the dynamics of the myocardium is investigated locally. On the contrary, the area analysis allows to study the behaviour of the layer in a whole cross-section of the tube. The curves representing the instants of maximum contraction and of maximum stretching of the myocardium obtained with the two parameters are shown in Figure 41 and Figure 42. In general the results obtained with the two parameters are similar. The curves describing the instant of myocardium maximum area shortening and maximum segments contraction are almost superimposable; differences can be observed in curves describing areas expansion and segments stretching, especially in the first half of the heart. This can be an artefact that comes as a consequence of how long this region of the heart remains stretched. Considering, for example, the mean value of $A_{normalized}$ and $d_{normalized}$ in the inflow region of heart 2 at 28 hpf (Figure 43), it can be seen inflow area remains expanded and segments between cardiomyocytes remain stretched for $0.5<t<1$ and the two parameters show small oscillations during this period. $d_{normalized}$ has two peaks, one at $t=0.5$ (corresponding to $A_{normalized}$ peak) and one at $t=0.8$. Since this second peak is higher than the first one, $t=0.8$ results the moment of maximum segments stretching. Therefore, area and segments seem to relax at different times, while they both start stretching at $t=0.5$ and remained stretched for half of the cardiac cycle. Others factors can affect the results and cause the discrepancies observed. Errors can arise in the calculation of the area of the myocardium in the case that the cross-section planes considered in the segmentation process are not perfectly perpendicular to the longitudinal axis of the heart tube; also the manual tracking of the cardiomyocytes can generate errors because during the contraction cells get close one to the other and distinguish them is complex; furthermore, while in the analysis of the myocardium area, the dynamics of the layer is studied only in radial direction, in the analysis of the distance between neighbouring cells, the orientation of the tissue segments is not considered and the local behaviour of the tissue is investigated independently on the direction of the stretch. Thus the results obtained with the distance parameter includes also the longitudinal movement of the layer.

Therefore the discrepancies in the results seem not to be due to differences between the local and the global dynamics of the tissue, but to other reasons.
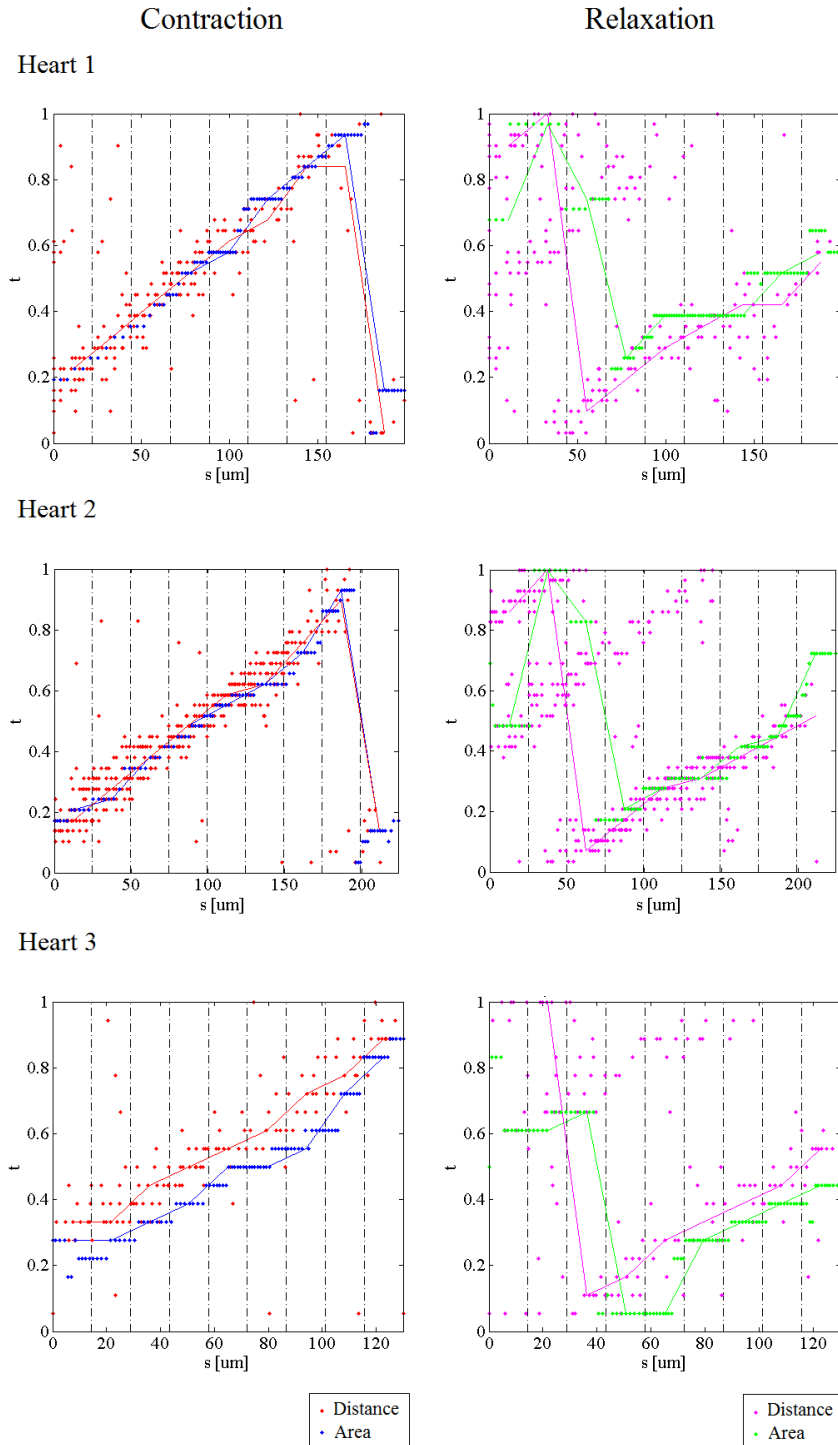
Figure 41: Comparison between myocardium contraction (left) and relaxation (right) at 28 hpf studied using two parameters: the distance between neighbouring cardiomyocytes and the cross-sections area. The points mark the time step of minimum distance (red), maximum distance (magenta), minimum area (blue) and maximum area (green). The lines represent the average values in the regions of the heart calculated after dividing the tube in nine parts.
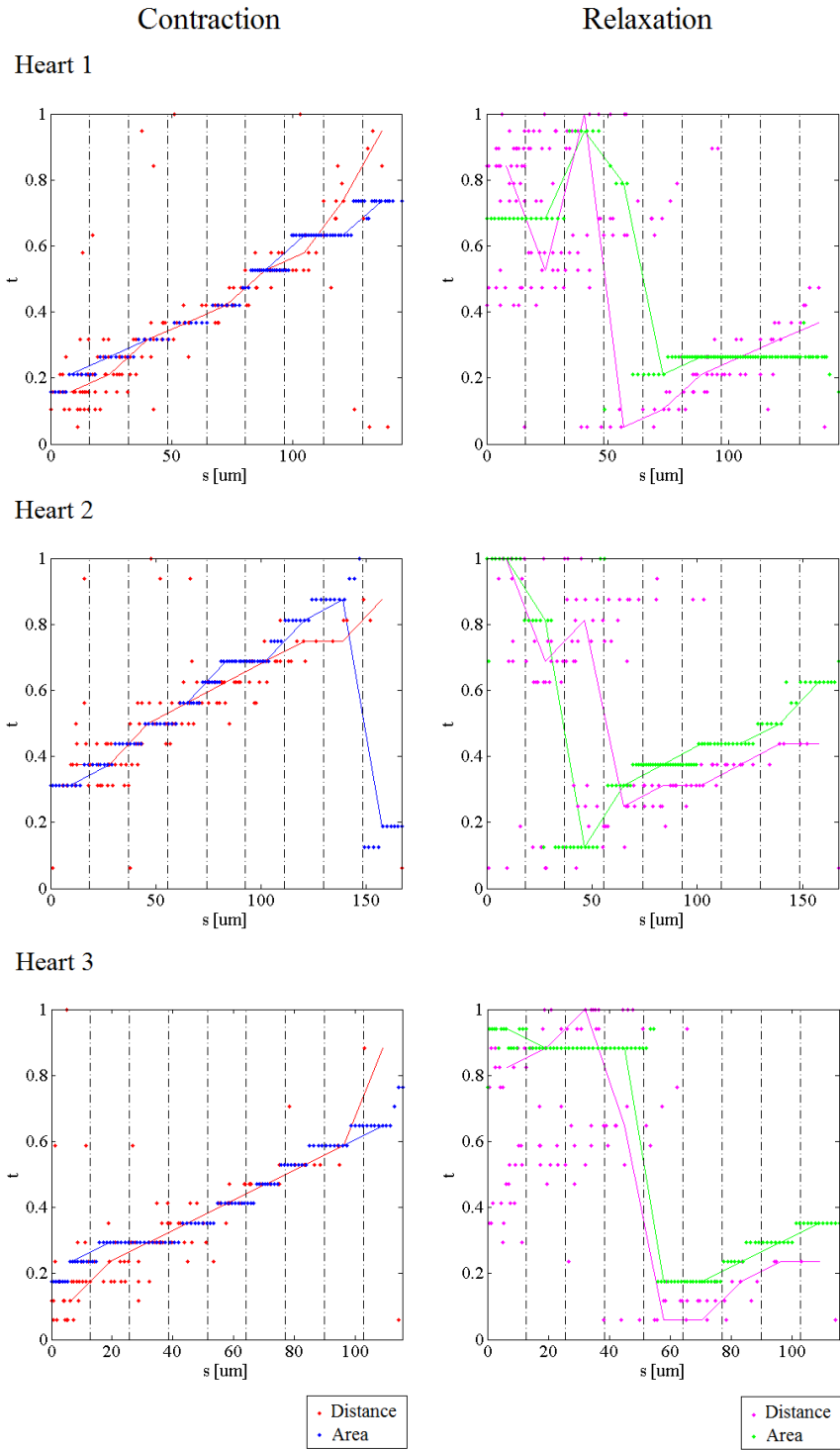
Figure 42: Comparison between myocardium contraction (left) and relaxation (right) at 30 hpf studied using two parameters: the distance between neighbouring cardiomyocytes and the cross-sections area. The points mark the time step of minimum distance (red), maximum distance (magenta), minimum area (blue) and maximum area (green). The lines represent the average values in the regions of the heart calculated after dividing the tube in nine parts.

Figure 42 (Continue): Comparison between myocardium contraction (left) and relaxation (right) at 30 hpf studied using two parameters: the distance between neighbouring cardiomyocytes and the cross-sections area. The points mark the time step of minimum distance (red), maximum distance (magenta), minimum area (blue) and maximum area (green). The lines represent the average values in the regions of the heart calculated after dividing the tube in nine parts.
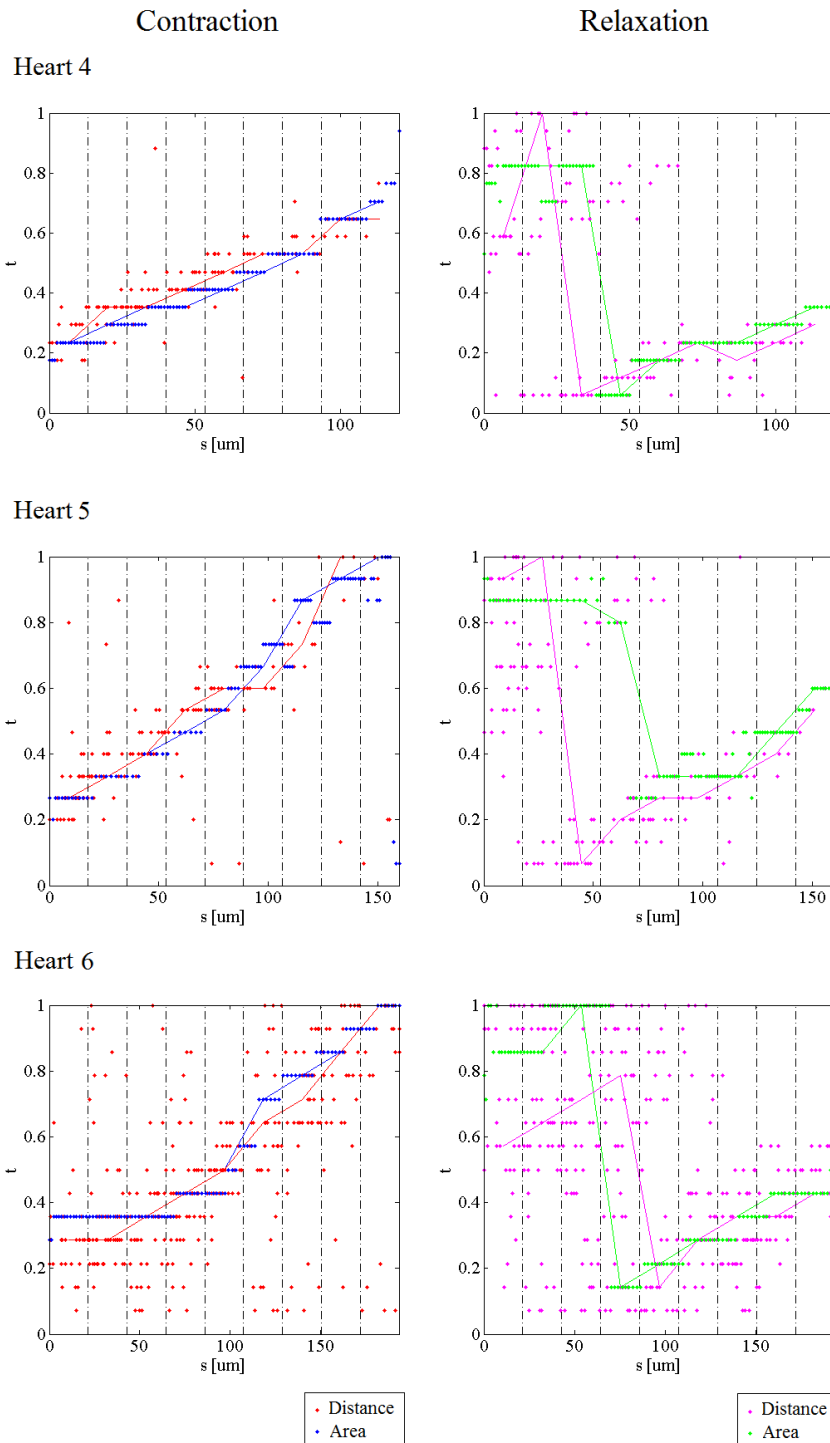
52
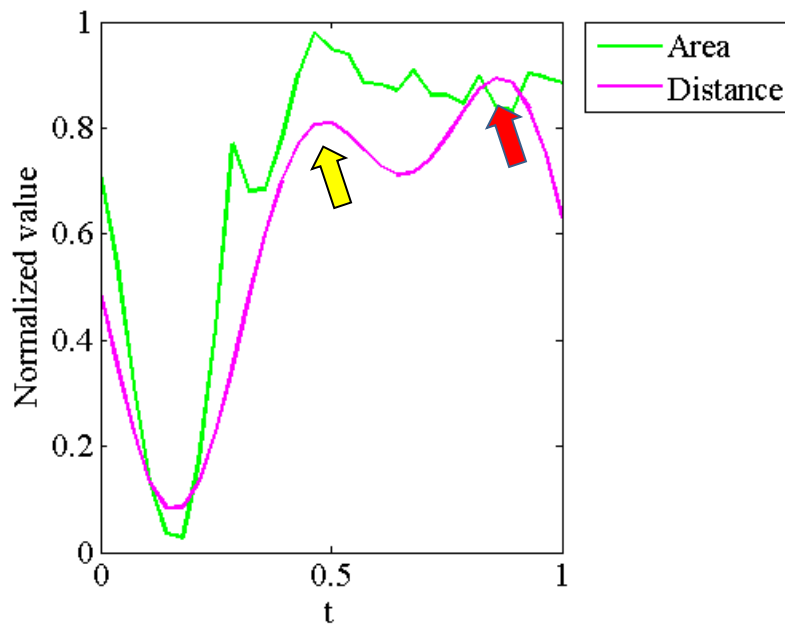
Figure 43: Comparison between myocardium dynamics at the inflow of heart 2 at 28 hpf over the cardiac cycle studied using two parameters: the cross-section area and the distance between cells. The curve relative to the distance (magenta) has two peaks (at t=0.5 and t=0.8) and the second is higher. If the relaxation time of the tissue is considered as the time step corresponding to the maximum value of the distance and of the area, the myocardium seems to relax at different times according to the parameter used. By contrast, both the signals are stretched between t=0.5 and t=1.

Considering the areas of the myocardium cross-sections (Figure 44 and Figure 45), the ending part of the heart is the smallest in all the samples considering maximum, minimum and mean values, while the region at the 20-30% of the heart length is the biggest in the hearts at 30 hpf and in heart 2 (except maximum area, that shows a peak in the second half) and heart 3 at 28 hpf. Heart 1 at 28 hpf is an exception and the area peak is reached in the second half of the heart (at the 60% of the heart length).

Focusing on the mean area, in the first half of the heart, the curve is closer to maximum than minimum area curve; the opposite is observable in the second half of the heart tube. This is a consequence of the different durations of contraction and relaxation in the two regions previously described. In the first half of the heart, cross-sections remain longer in a relaxed than in a contracted condition such that the mean values of the areas are shifted to the maximum values; vicecersa, in the second part of the heart, the myocardium spends more time contracted and areas mean values result shifted to minimum values.
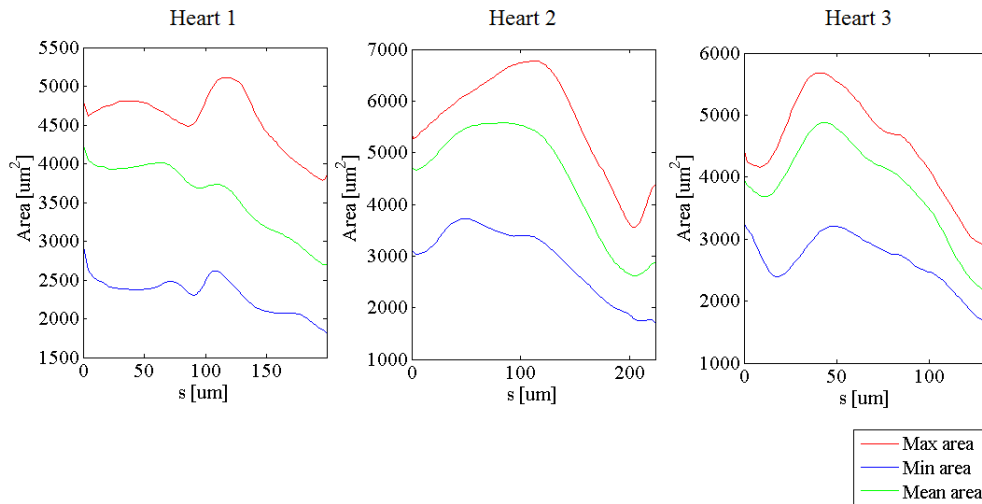
Figure 44: Maximum, mean and minimum area of myocardium cross-sections along the centreline in three hearts at 28 hpf. Outflow region has the smallest area; maximum area is reached in the three hearts respectively at the 60%, 40% and 30% of the heart tube length.
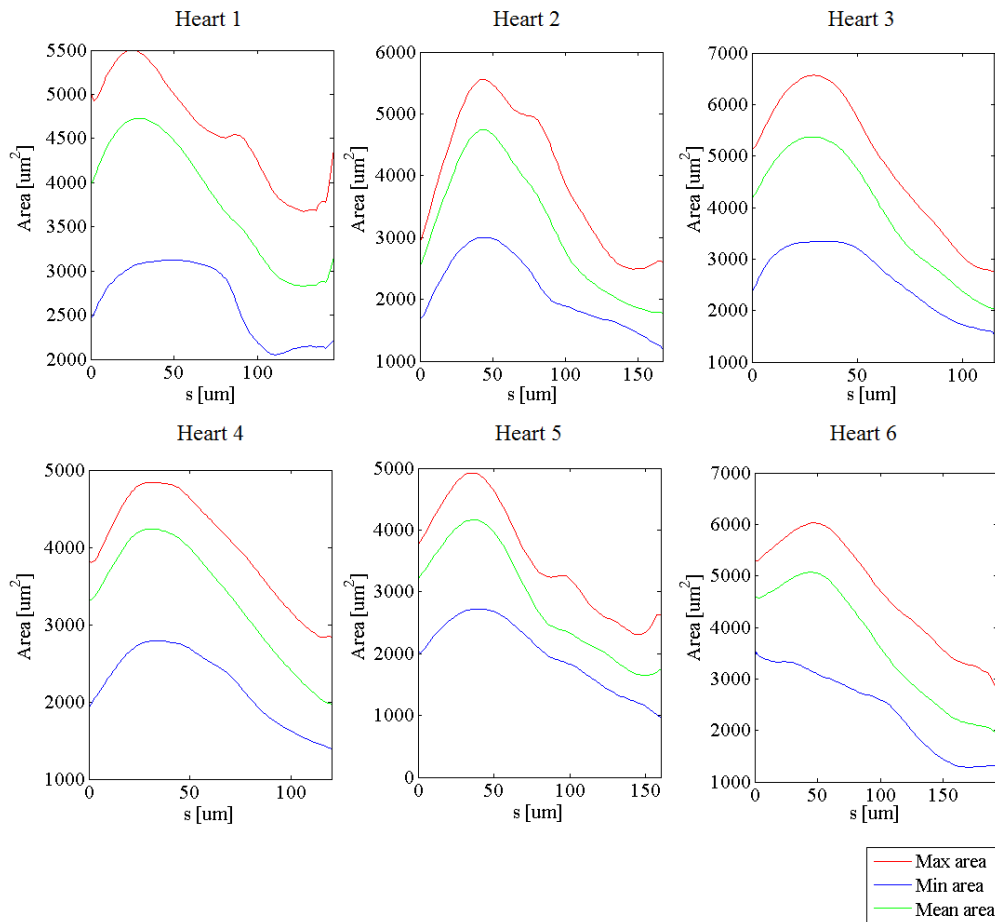
Figure 45: Maximum, mean and minimum area of myocardium cross-sections along the centreline in six hearts at 30 hpf. Outflow region has the smallest area; maximum area is reached at the 20-30% of the heart length.

Area fractional shortening (AFS) is a measure of how much the area of the cross-sections changes from the expanded to the contracted state. In the myocardium (Figure 46 and Figure 47), the AFS results between -30% and -60% (values are negative since they represents a reduction in area) and the outflow is generally the region with maximum shortening, but results along the centreline of the heart are dishomogeneous between the samples and common characteristics can not be found.
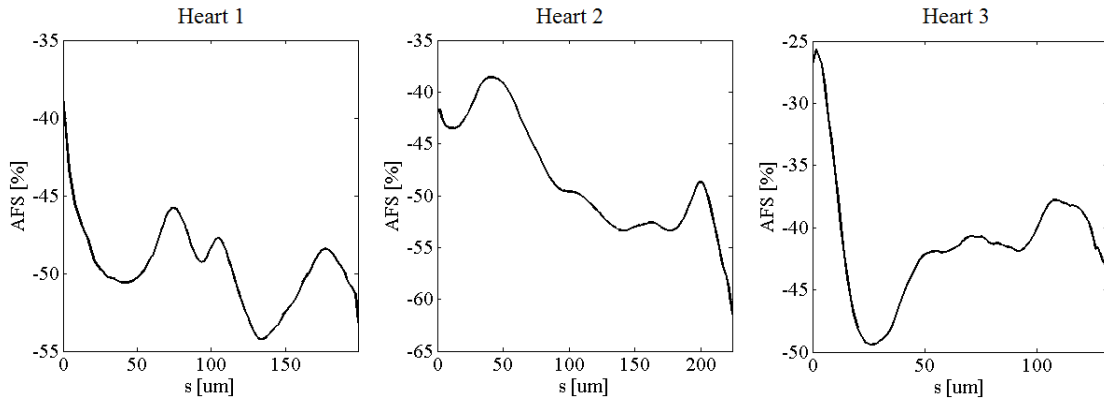
Figure 46: Myocardium area fractional shortening (AFS) along the centreline in three hearts at 28 hpf.
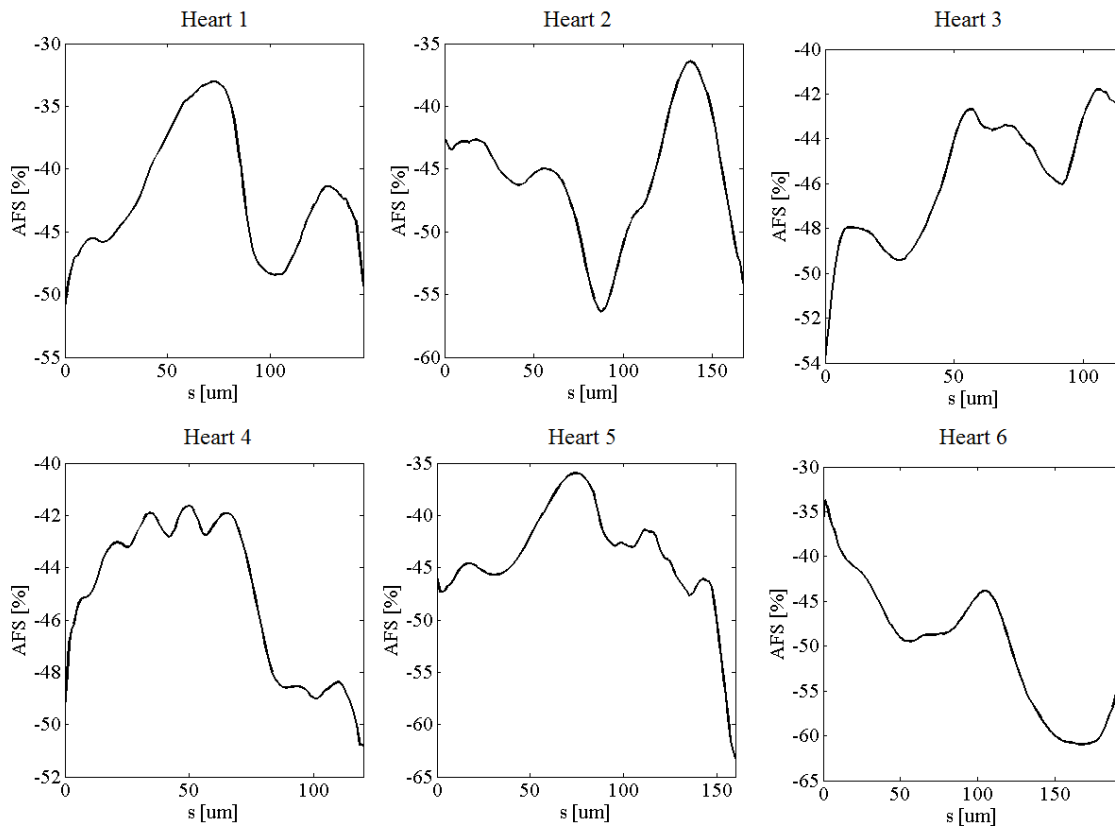
Figure 47: Myocardium area fractional shortening (AFS) along the centreline in six hearts at 30 hpf.

In addition to the area of the myocardium cross-sections, the distance between neighbouring cardiomyocytes was studied during the cardiac cycle.

This parameter gives information about the behaviour of the tissue locally, because considers only the small portion between two cells.

To search for possible differences in the stretching of the myocardium along the heart, the local fractional extension (LFE) was introduced in parallel to AFS for the area.

LFE measures how much the distance between cells increases going from the contracted to the stretched condition. The analysis of the index (Figure 48 and Figure 49) showed that, even considering a single position on the centreline of the heart, the local stretching of the tissue results different among the segments considered. Therefore, each region of the heart shows not only a single value of LFE, but a range. Considering the mean value in each position s, the LFE increases along the centreline of the heart and the final part of the myocardium undergoes the higher stretching.
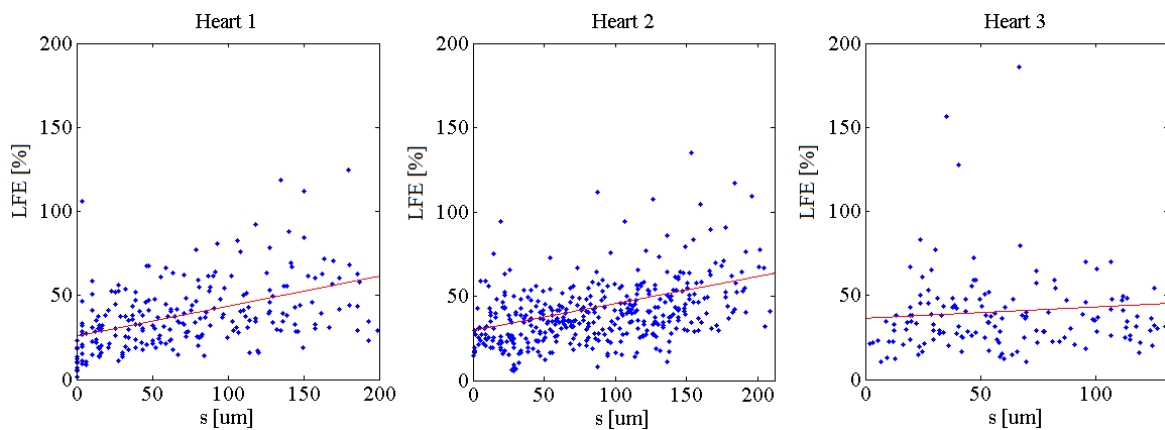
Figure 48: Myocardium local fractional extension (LFE) along the centreline in three hearts at 28 hpf. The mean stretching of the tissue progressively increases along the heart (red line) reaching the maximum at the end of the heart tube.
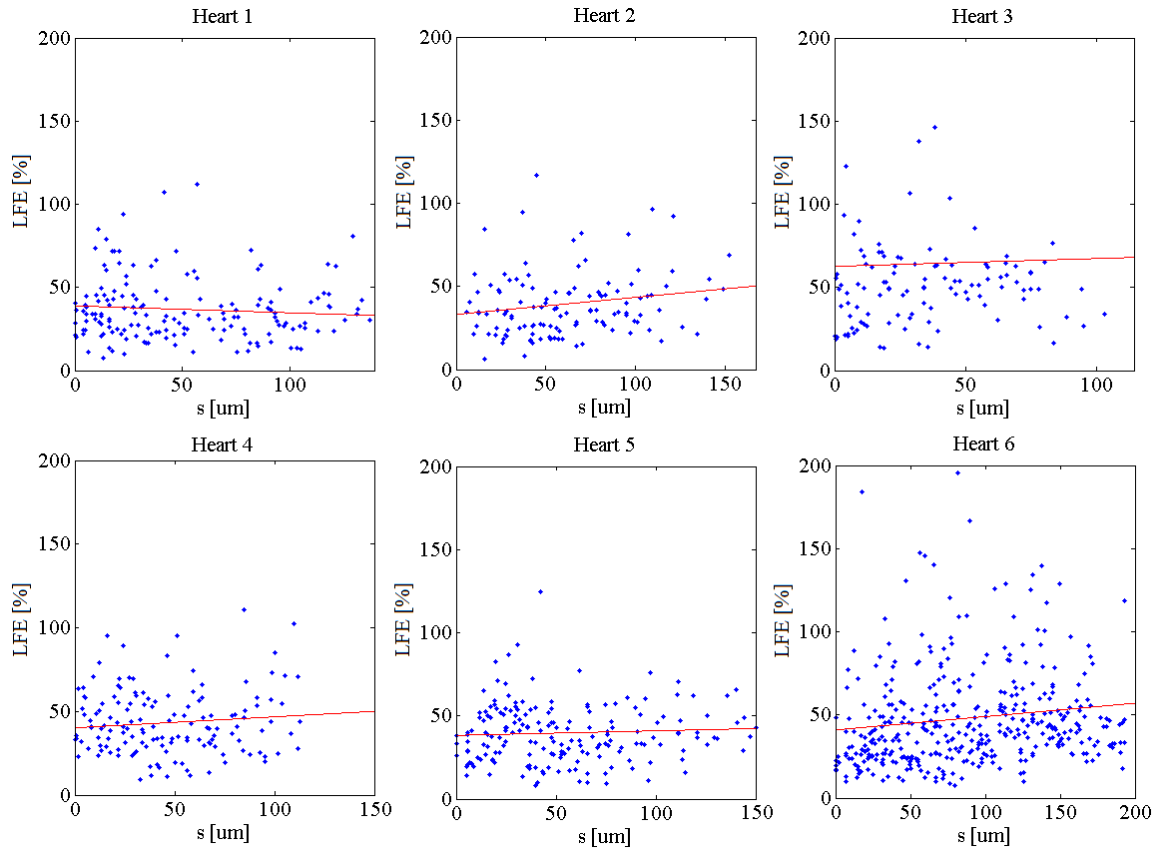
Figure 49: Myocardium local fractional extension (LFE) along the centreline in six hearts at 30 hpf. The mean stretching of the tissue (red line) progressively increases along the centreline (except for heart 1).

3.1.2 Endocardium

Endocardium dynamics at 28 hpf was studied using only the cross-sections area as a parameter (Figure 50). Results are similar for the two hearts analysed; however some differences can be observed. In heart 2, the contraction wave propagates linearly along the centreline; in heart 1 the pattern is more complex and the wave propagates changing speed several time with a pattern that resembles a step. In heart 1 the contraction wave starts while the outflow region is still contracted. In heart 2, on the contrary, the new contraction wave startes after the end of the previous one. As in the case of the myocardium, however, this can be due to the fact that the outflow region in heart 2 may not have been fully acquired since the centreline does not reach the same length of heart 1. This consideration is supported also by the analysis of the relaxation and contraction durations along the centreline (Figure 51). In heart 1, the duration of the relaxation decreases progressively from the inflow to the end of the centreline while the contraction duration increases and

reaches its maximum in the final part of the heart; in heart 2 the same trend is observed but the contraction duration never overcomes the duration of relaxation, probably because the outflow region is missing. On the contrary of the myocardium at 28 hpf, in which the relaxation duration was very homogeneous in the first half of the heart and then suddenly decreased (Figure 39), in the case of the endocardium the duration of relaxation and contraction respectively decreases and increases linearly.
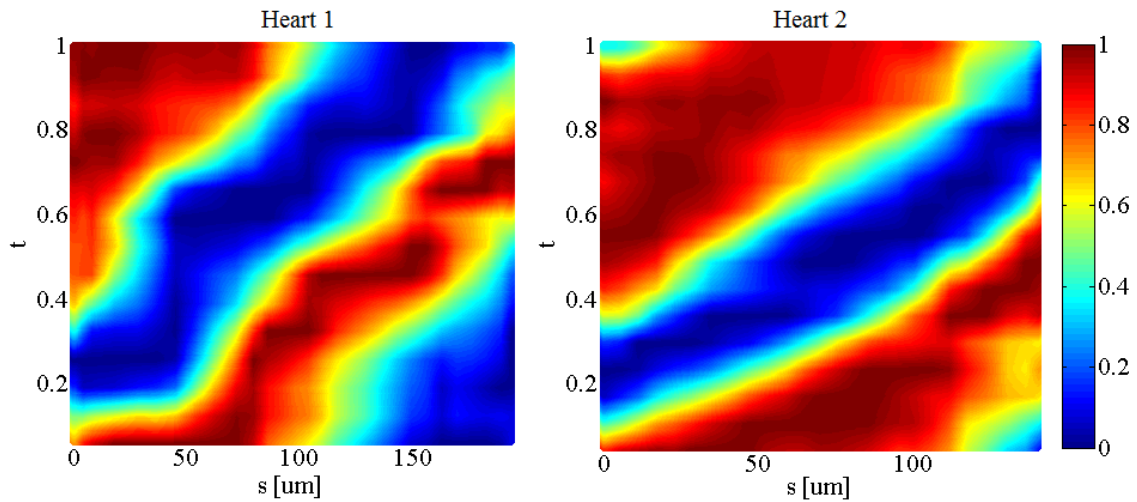
Figure 50: Endocardium dynamics at 28 hpf described using cross-sections areas in two hearts.
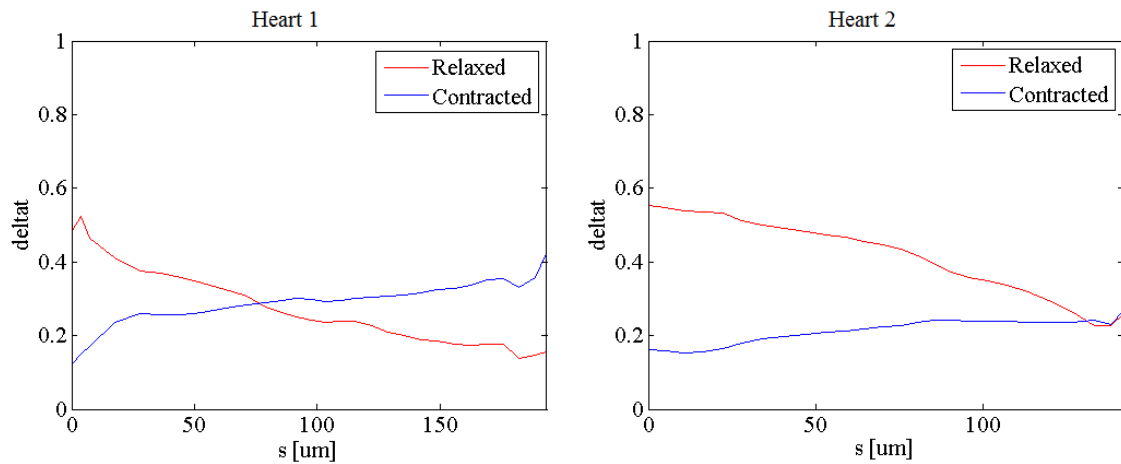
Figure 51: Duration of relaxation and contraction conditions along the centreline at 28 hpf. From the inflow to the end of the centreline, the durations of relaxation and contraction respectively decrease and increase almost linearly.

Different results between the two hearts were obtained also for the areas of the endocardium cross-sections along the heart (Figure 52). In heart 1, maximum, mean and

minimum area curves are more homogeneous than in heart 2, where, on the contrary, outflow and inflow regions are clearly the smallest and the biggest, respectively.
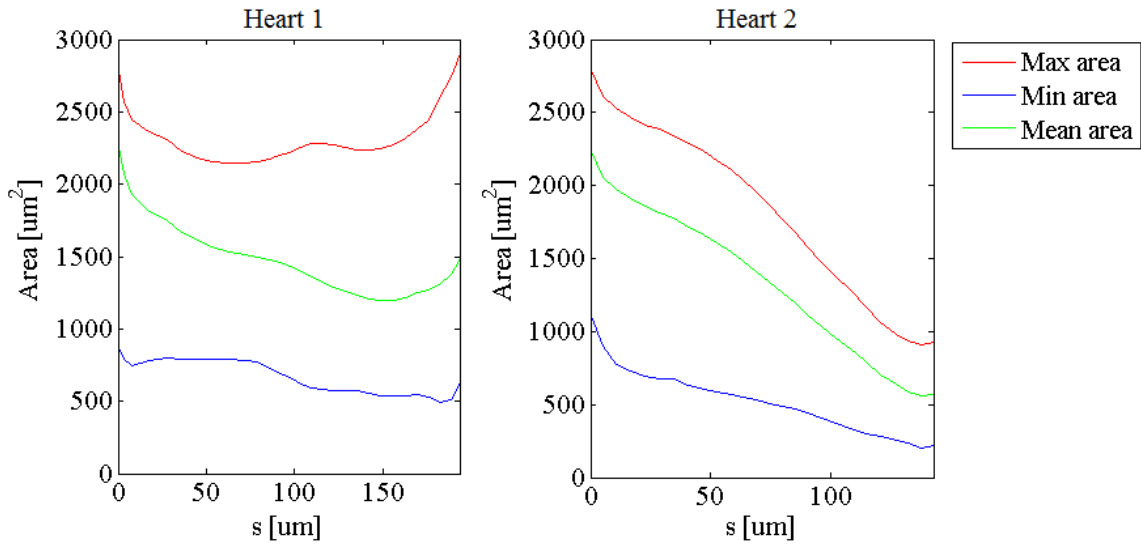
Figure 52: Maximum, mean and minimum area of endocardium cross-sections along the centreline in two hearts at 28 hpf. Outflow region has the smallest area (except for the maximum area in heart 1); areas values in the different regions are more homogeneous in heart 1.

As regards the area fractional shortening (Figure 53), AFS values are between -60% and -80%, that means higher than in myocardium (between -30% and -60% as shown in Figure 46 and Figure 47). The region that decreases its area the most during contraction is the final part of the heart in both the samples. The regions with the minimum AFS are at the 20-30% of the heart tube length in heart 1 and at the inflow in heart 2.
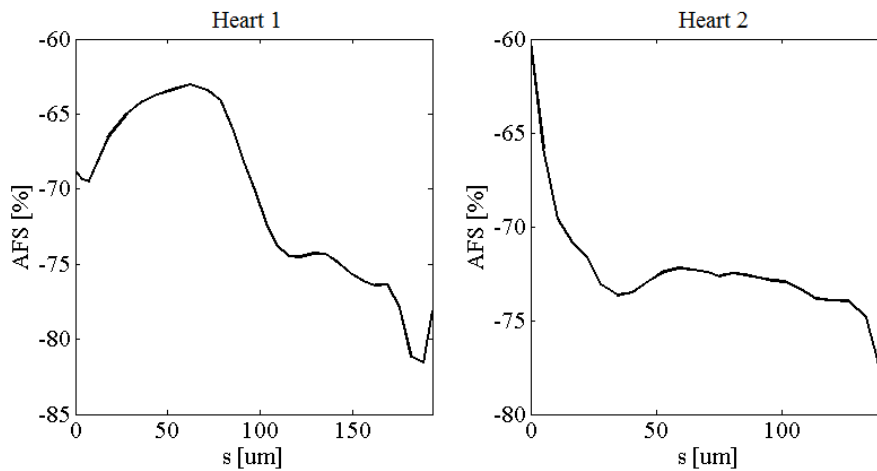
Figure 53: Endocardium area fractional shortening (AFS) along the centreline in two hearts at 28 hpf.

The results obtained from the analysis of the endocardium in the two hearts showed some differences. Since the myocardium dynamics in the same hearts, on the contrary, is very similar (Figure 54), these differences may be linked to the calculation of the cross-sections areas of the endocardium. Compared to the myocardium, in fact, the shape of the endocardium cross-sections (Figure 55) is more irregular and shows folds and evaginations during contraction that make ellipse fitting approximate.
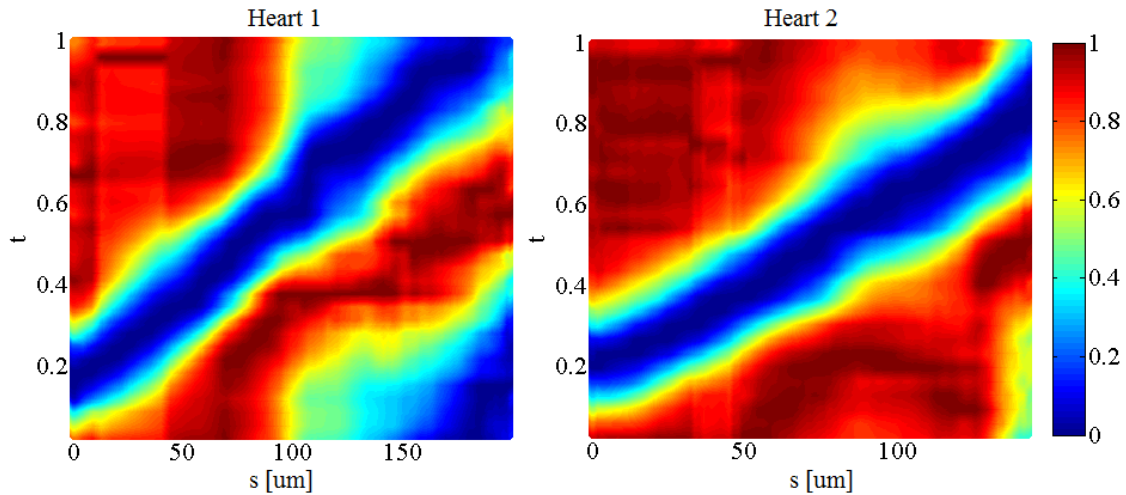
Figure 54: Myocardium dynamics in the same hearts used to study the endocardium dynamics.
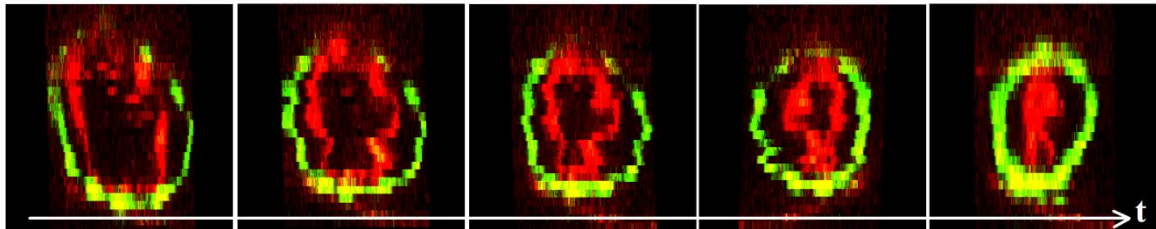
Figure 55: Example of myocardium (green) and endocardium (red) cross-section from expensed to contracted condition. Myocardium has an elliptical shape during the whole cardiac cycle. Endocardium shape is elliptical only when it is relaxed; during contraction it shows folds and evaginations.

3.1.3 Cardiac jelly

Cardiac jelly was studied in two hearts at 28 hpf using the difference between myocardium and endocardium cross-section areas as a parameter. Five equidistant cross-sections along the centreline s of the heart were considered, at the inflow (s=0%), at 25% of the length, in the middle (s=50%), at 75% and at the end (s=100%).

As regards the cardiac jelly area, the minimum values are at the inflow and at the outflow, while the maximum values are in the central part of the heart (Figure 56).
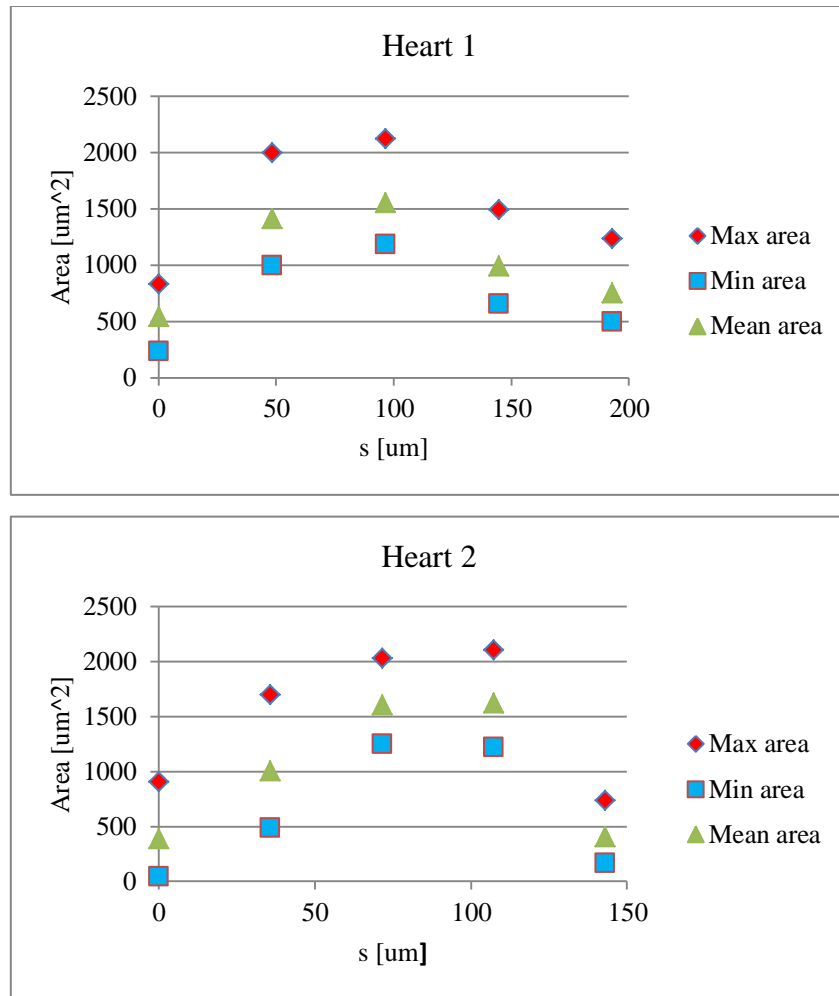
Figure 56: Maximum, mean and minimum area of the cardiac jelly in five equidistant cross-sections of the heart in two samples at 28 hpf. Outflow and inflow regions have the smallest area; the greatest amount of cardiac jelly is in the central part of the heart.

In Figure 57 and Figure 58 a comparison between the dynamics of myocardium, endocardium and cardiac jelly in the five cross-sections considered is shown. Endocardium and myocardium dynamics are very similar and contraction and relaxation of the two layers occur simultaneously in almost all the cases.

Cardiac jelly dynamics seems more complex. In general, the cardiac jelly area increases during the contraction of the endocardium and the myocardium and decreases during heart relaxation. This is in line with what the direct observation of the cross-sections of the endocardium and the myocardium suggests (Figure 59). However, in some cases a phase

shift is observable between heart contraction and maximum cardiac jelly area and between heart relaxation and minimum cardiac jelly area (e.g. $s=0\%$ and $s=50\%$ in Figure 57 and $s=75\%$ and $s=100\%$ in Figure 58). This phase shift appears when the myocardium and endocardium curves show deviations from each other.
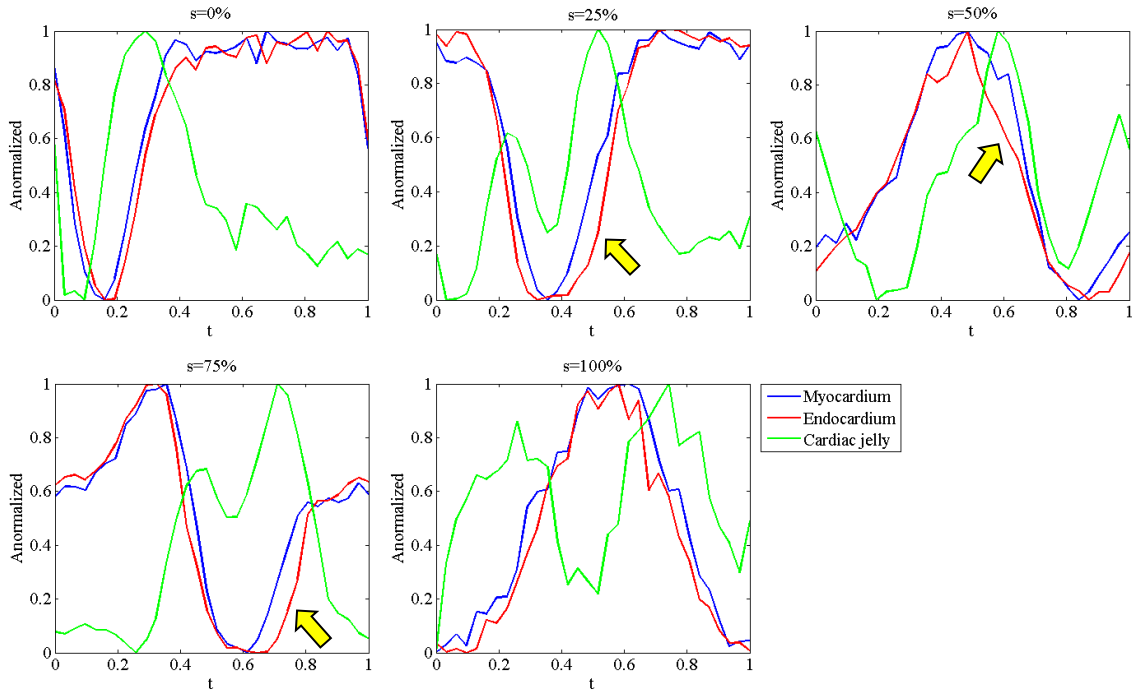
Figure 57: Comparison between myocardium, endocardium and cardiac jelly dynamics along the centreline of heart 1. Myocardium and endocardium curves are similar and contraction and relaxation of the two layers occur simultaneously. In general, the cardiac jelly area increases during heart contraction and decreases during heart relaxation. A phase shift between the cardiac jelly dynamics and the myocardium-endocardium dynamics appears when myocardium and endocardium curves deviate from each other (yellow arrows).
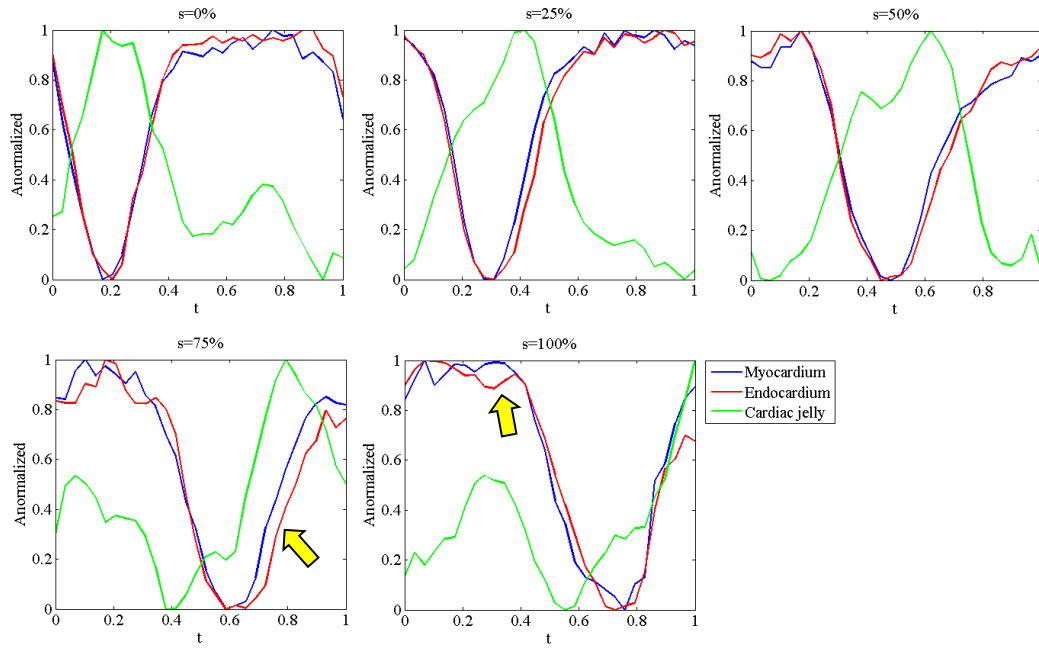
Figure 58: Comparison between myocardium, endocardium and cardiac jelly dynamics along the centreline of heart 2. Myocardium and endocardium curves are similar and contraction and relaxation of the two layers occur simultaneously. In general, the cardiac jelly is in counterphase to endocardium and myocardium but a phase shift appears when myocardium and endocardium curves deviate from each other (yellow arrows).
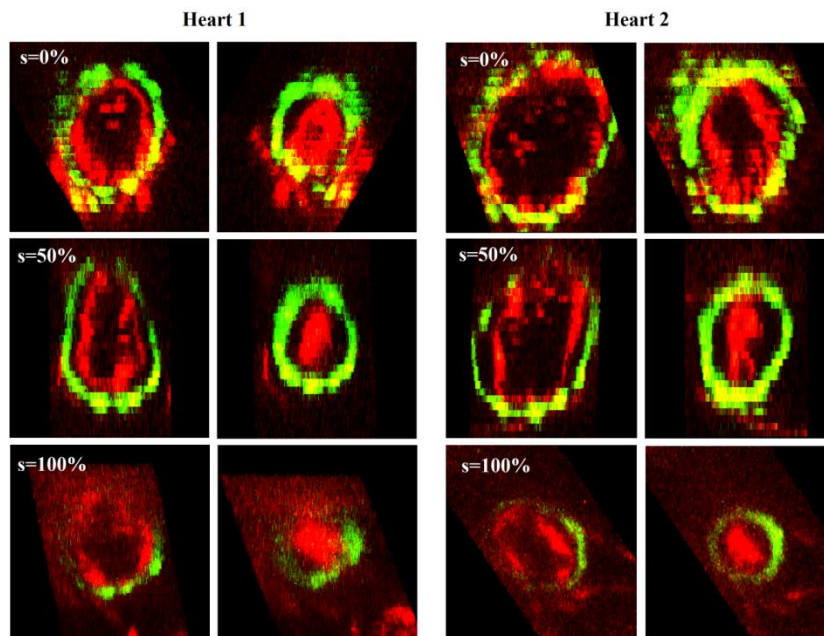
Figure 59: Cross-sections of myocardium (green) and endocardium (red) during relaxation (left) and contraction (right) at the inflow (s=0%), centre (s=50%) and outflow (s=100%) of the two hearts. Observing the cross-sections, the minimum area of the cardiac jelly seems to be reached during endocardium and myocardium relaxation and the maximum area during the contraction.

3.2 Red blood cells velocity

The analysis of red blood cells velocity was done in two hearts at 28 hpf. Erythrocytes were tracked in a single plane of the heart during the cardiac cycle and the mean velocities in different regions were calculated and compared.

Results are shown in Figure 60 (heart 1) and Figure 61 (heart 2). Positive values in velocity indicate red blood cells are moving forward (i.e. toward the outflow of the heart), negative values correspond to reversing flow.

In region 1 of both the samples, the velocity has a negative peak, indicating that backflows are present. In the central part of the planes considered, the negative peak is present only in heart 2. In region 3, velocity is never negative and reversing flows are not present anymore in both the hearts.

From the observation of the acquired images of the two hearts (see Movie 1 and 2), the regurgitation seems to occur during the contraction of the inflow and might be due to the lower occlusion of the endocardial lumen in this region, visible from the direct observation of the endocardium cross-section (in s=0% in Figure 59 the endocardial lumen results not completely occluded during the contraction).
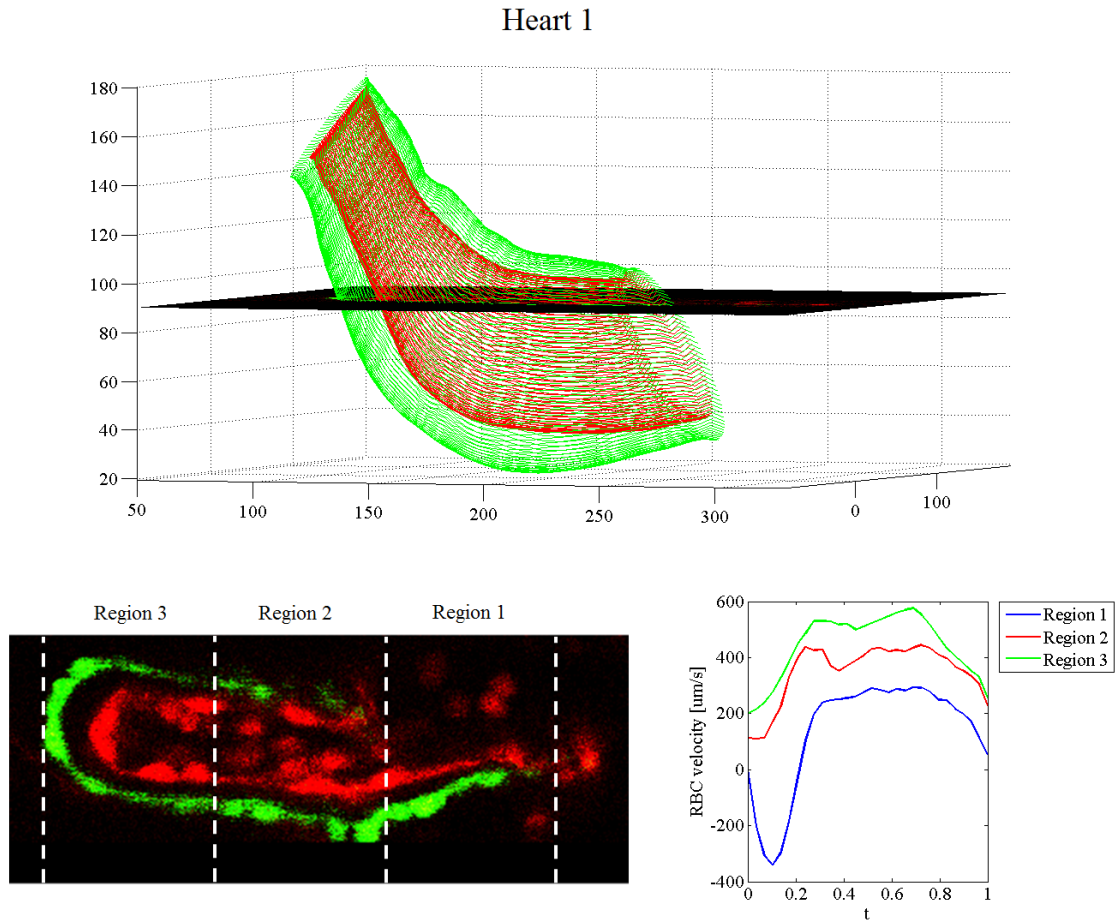
Figure 60: Red blood cells (RBC) velocity in one plane in heart 1. The plane was chosen to visualize most of the heart length (above) and was cut in three regions (left below). In region 1 (inflow region), RBCs travel slower than in the other regions (maximum velocity ≈ 250 µm/s) and backward movements are present (negative peak in t=0.1); in region 2 and 3 the velocity increases (maximum velocity ≈ 400 µm/s and 600 µm/s, respectively) and no reversing flows are observable (minimum velocity ≈ 100 µm/s and 200 µm/s, respectively).
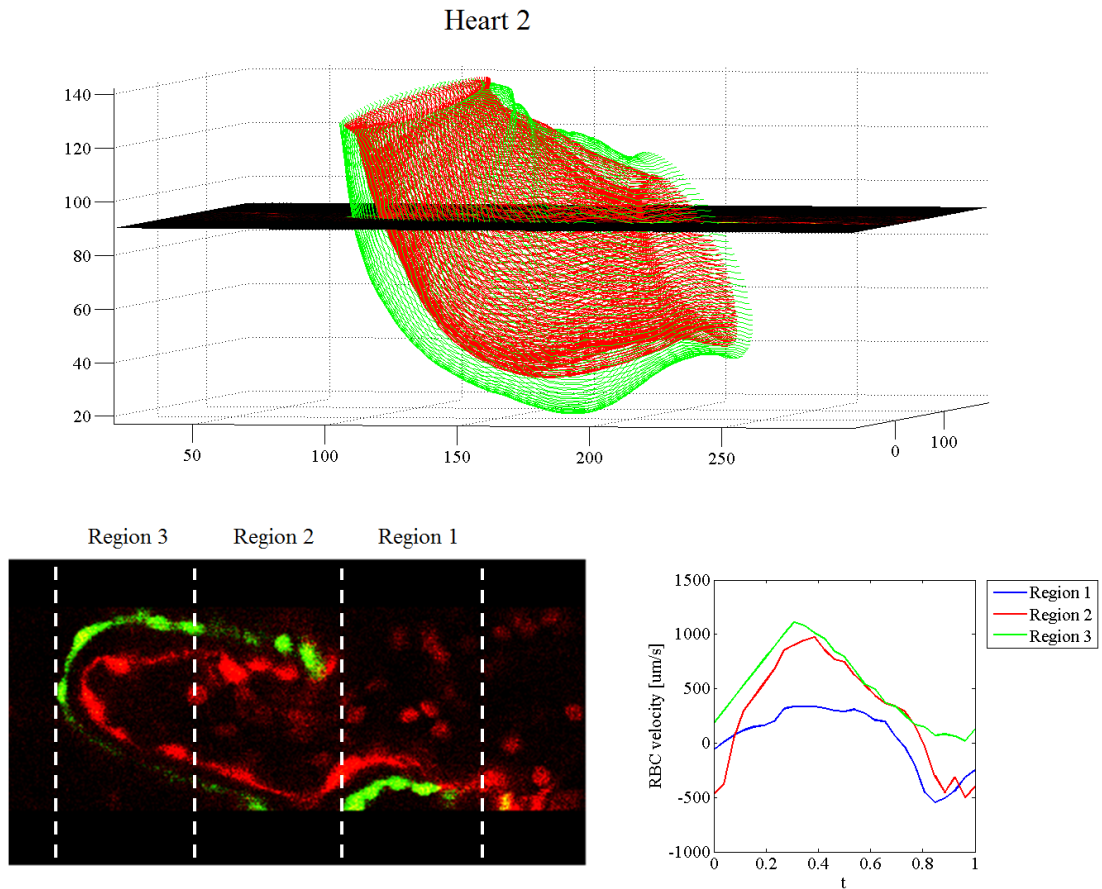
Figure 61: Red blood cells (RBC) velocity in one plane of heart 2. The plane was chosen to visualize most of the heart length (above) and was cut in three regions (left below). In region 1, RBC maximum velocity is lower than in the other regions (≈ 250 μm/s) and backward movements are present (negative peak in t=0.85); in region 2 the velocity increases (maximum velocity ≈ 1000 μm/s) and reversing flows are still observable (negative peak in t=0.9-0.95); in region 3 maximum velocity reaches the highest values (≈ 1100 μm/s) and there are not reversing flows (minimum velocity ≈ 0 μm/s).

3.3 Calcium dynamics in myocardium

3.3.1 Non-beating heart

To study the calcium dynamics in the myocardium, a non-beating heart was considered at first and red and green fluorescence (*RFP* and *gcamp5.0* signals, respectively) in cardiomyocytes was compared. Since the former does not depend on the calcium in the cells, it was supposed to be constant during the cardiac cycle, while the latter was supposed to oscillate according to the calcium variations in the cardiomyocytes.

66

The analysis shows *gcamp5.0* signal changes over time while *RFP* intensity is almost constant over the cardiac cycle (Figure 62). The small oscillations visible in *RFP* signal are probably due to the manual tracking of the cardiomyocytes used to measure the colour intensity. Since the heart is not beating and there are no other external factors that affect the signals acquired (*RFP* signal is in fact constant as expected), *gcamp5.0* signal seems to represent only calcium variations in the myocardium as hypnotized.

Calcium dynamics (given by *gcamp5.0* intensity) is shown in Figure 63, with the same plot used for the heart dynamics. Calcium wave propagates along the centreline of the heart almost linearly, changing the conduction speed in the second half of the heart. A slowdown is visible between *s*=0.6 and *s*=0.7, where the slope of the dark red curve becomes higher, the wave speed increases between *s*=0.7 and *s*=0.8 and decreases again between *s*=0.8 and *s*=1 (Figure 64).

Figure 62: Comparison between *gcamp5.0* and *RFP* intensities over the cardiac cycle in different positions along the centreline of the non-beating heart. *Gcamp5.0* signal changes over time while *RFP* signal is almost constant.
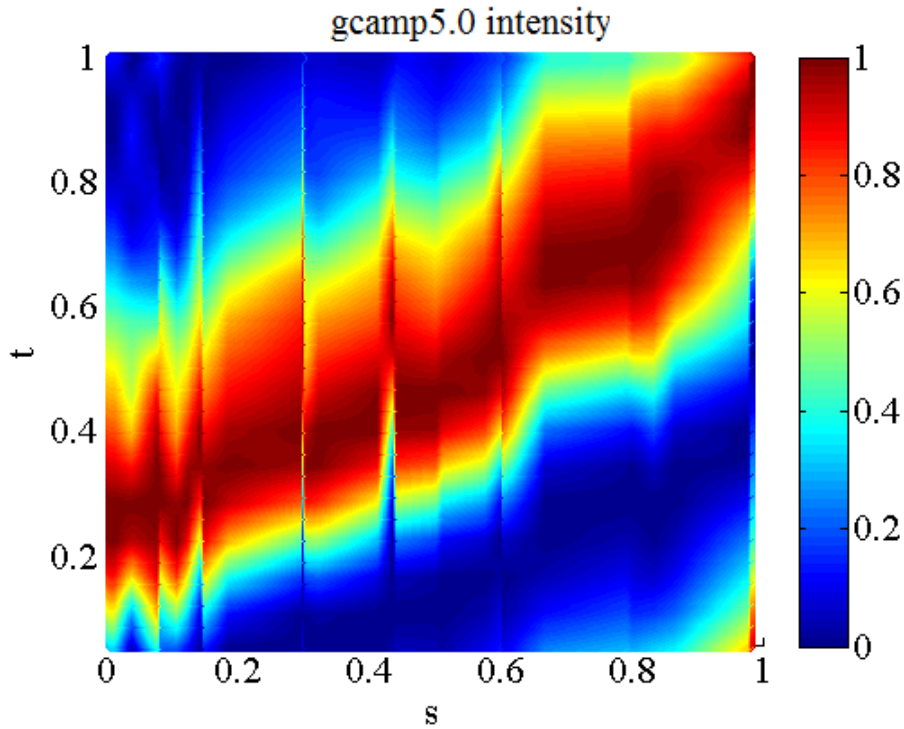
Figure 63: Dynamics of calcium, described by *gcamp5.0* signal, over the cardiac cycle along the non-beating heart. s on the x axis is the centreline (in this case normalized between 0 and 1), t on the y axis is the time over the cardiac cycle duration; the colorbar goes from 0 (minimum signal intensity) to 1 (maximum signal intensity). The calcium wave (dark red curve) propagates along the heart from the inflow to the outflow and the conduction speed changes in the second half of the heart, slowing in s=0.6, increasing between s=0.7 and s=0.8 and decreasing again between s=0.8 and s=1.
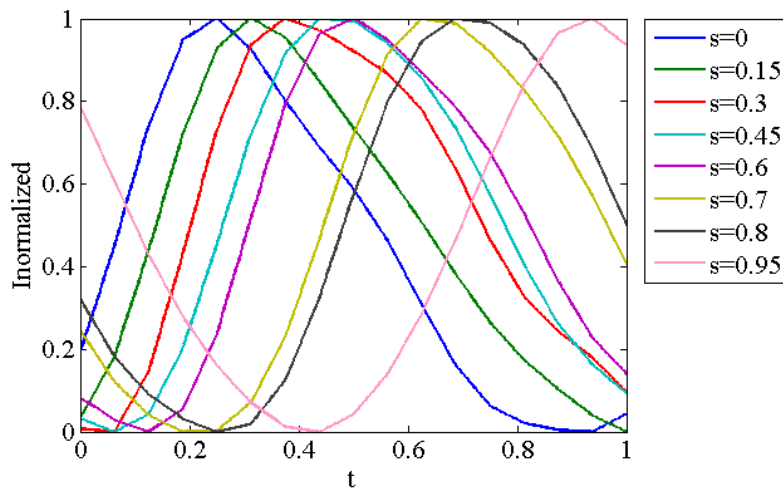
Figure 64: Calcium wave along the non-beating heart. The calcium wave propagation (corresponding to the positive peaks in the curves) shows a uniform speed until *s*=0.6, then it decreases between s=0.6 and s=0.7, increases between s=0.7 and s=0.8 and decreases again in the final part of the heart.

3.3.2 Beating heart

After proving the activity of the calcium reporter *gcamp5.0* in the non-beating heart of the fish, the same heart was analysed after restarting the contraction. During the acquisition, the heart was beating at 2.5 Hz (physiological heart rate).

In this case, *RFP* signal is not constant as in the non-beating heart but changes over time (Figure 65) and shows a dynamics very similar to *gcamp5.0*, with a wave that propagates along the heart tube (Figure 66). As previously explained, *RFP* signal is not supposed to change because the expression of the fluorescent protein in cardiomyocytes can be considered constant over time and no other factors affect the signal. The fact *RFP* signal changes in the beating heart and is constant in the non-beating heart means that the variations in the signal intensity are due to the heart movement. Going closer to and back from the light source of the microscope, the acquired signal results more or less intense. Since *RFP* and *gcamp5.0* signals are very similar and *RFP* intensity does not depend on calcium in the cells, it is not possible to assume that the wave described by *gcamp5.0* signal represents calcium propagation in the heart. By contrast, *gcamp5.0* signal seems to be linked to the movement of the heart too.
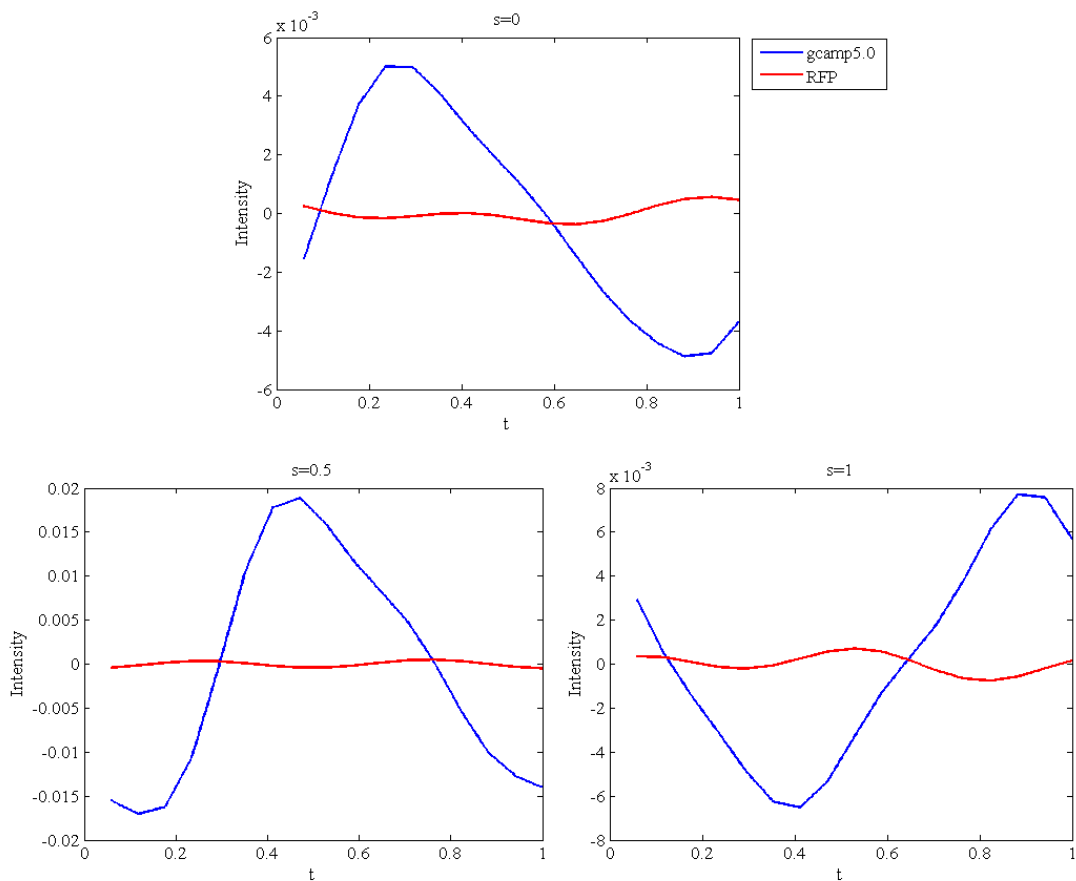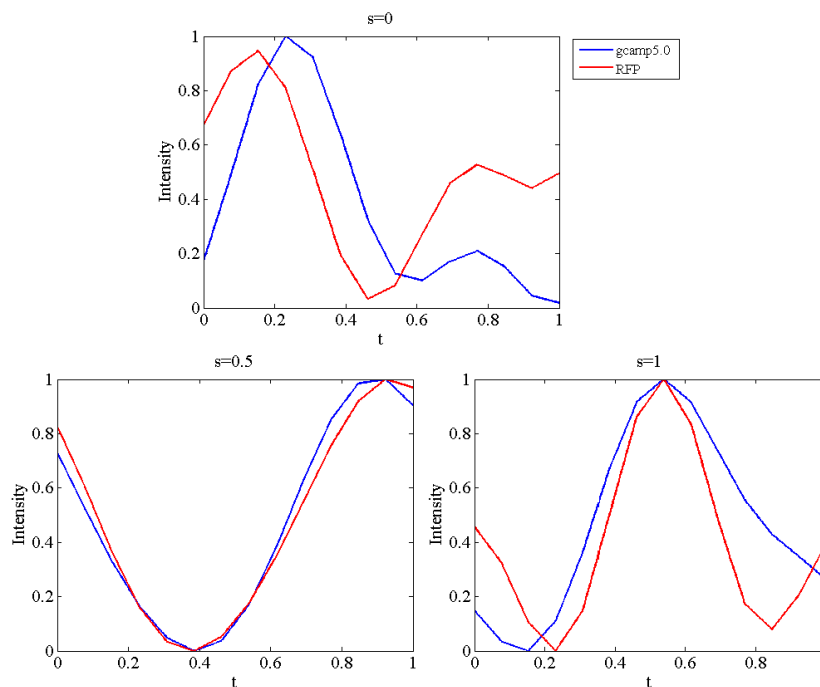

Figure 65: Comparison between *gcamp5.0* and *RFP* intensities over the cardiac cycle in different positions along the centreline of the beating heart. Both *gcamp5.0* and *RFP* signals change over time while the heart is beating.
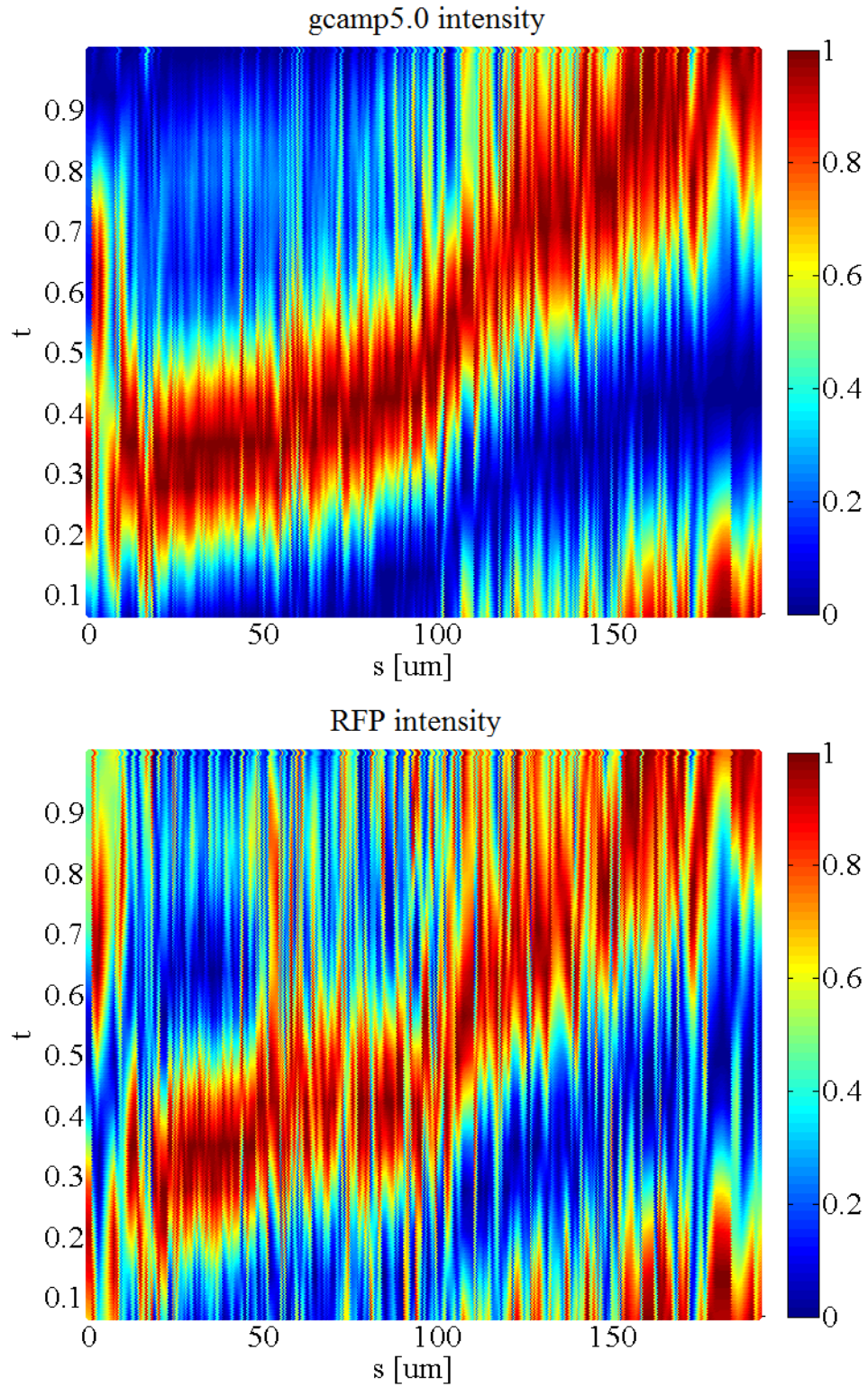
Figure 66: Dynamics of *gcamp5.0* (above) and *RFP* (below) signals over the cardiac cycle t along the centreline of the beating heart. The colorbar goes from 0 (minimum signal intensity) to 1 (maximum signal intensity). The two signals show a similar pattern attributable to the movement of the heart.

70

To remove the contribution of the heart movement from *gcamp5.0* signal, the ratio between *gcamp5.0* and *RFP* intensity was considered (<u>Figure 67</u>).
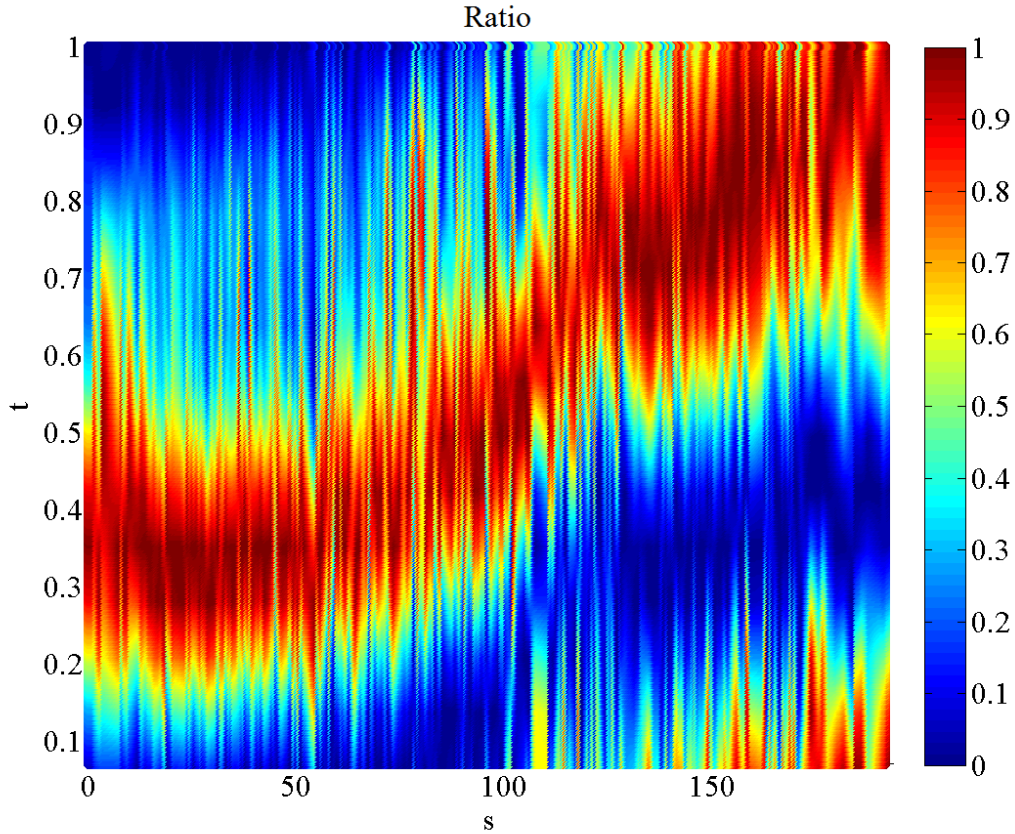
Figure 67: Dynamics of the ratio between *gcamp5.0* and *RFP* signals over the cardiac cycle along the centreline of the beating heart. The colorbar goes from 0 (minimum signal intensity) to 1 (maximum signal intensity).

3.3.3 Control heart

To verify that the ratio between the intensity of *gcamp5.0* and *RFP* deleted the contribution of the heart movement from the *gcamp5.0* signal, a heart expressing green (*eGFP*) and red (*RFP*) fluorescence in cardiomyocytes in a non-calcium dependent-manner was analysed. The two signals represent both the baseline signal of the myocardium and, since they were expressed in the same cells, their intensities were supposed to change over time because of the motion artefacts with a similar dynamics. From the analysis, this is confirmed (<u>Figure 68</u>). Thus the ratio between their intensities was supposed to be constant too. By contrast, the calculated ratio shows oscillations (<u>Figure 68</u>).
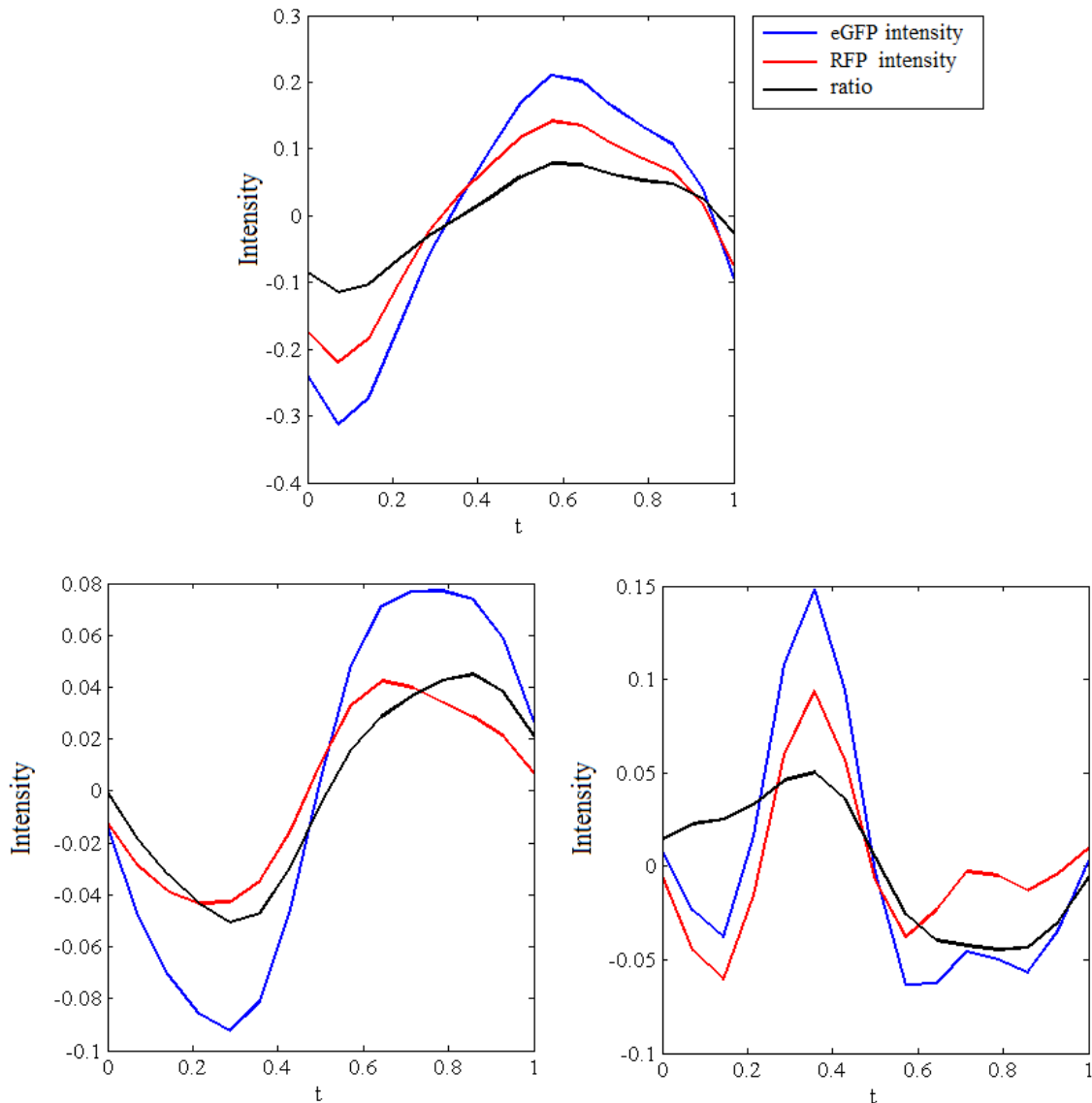
Figure 68: Examples of *eGFP*, *RFP* and ratio (*eGFP/RFP*) intensities over the cardiac cycle in three spots of the control heart. *eGFP* and *RFP* signals, respectively in blue and red, have a similar intensity profile but small differences are visible. These differences result in oscillations of the ratio.

Potential sources of this artefact include: the dimension of the spots used for the calculation of the cardiomyocytes intensity (Paragraph 2.3.4.1), the intensity of the signal itself (which depends on the proximity of the cell to the light source of the microscope and on the expression level of the fluorescent protein) and the velocity of the spots.

It turns out that the error, defined as the amplitude of the ratio oscillation, is not dependent on the dimension of the spots used to calculate cardiomyocytes fluorescence intensity (Figure 69 and Figure 70); it tends to be higher in spots with higher signals intensity

(Figure 71), but the error difference between spots with higher and lower intensity is not statistically significant (Figure 72), probably due to the small number of spots considered in the analysis. Instead, the amplitude of the movement artefacts depends significantly on the cell velocity: cardiomyocytes with a higher velocity show a statistically higher error than slower cardiomyocytes (Figure 73 and Figure 74).
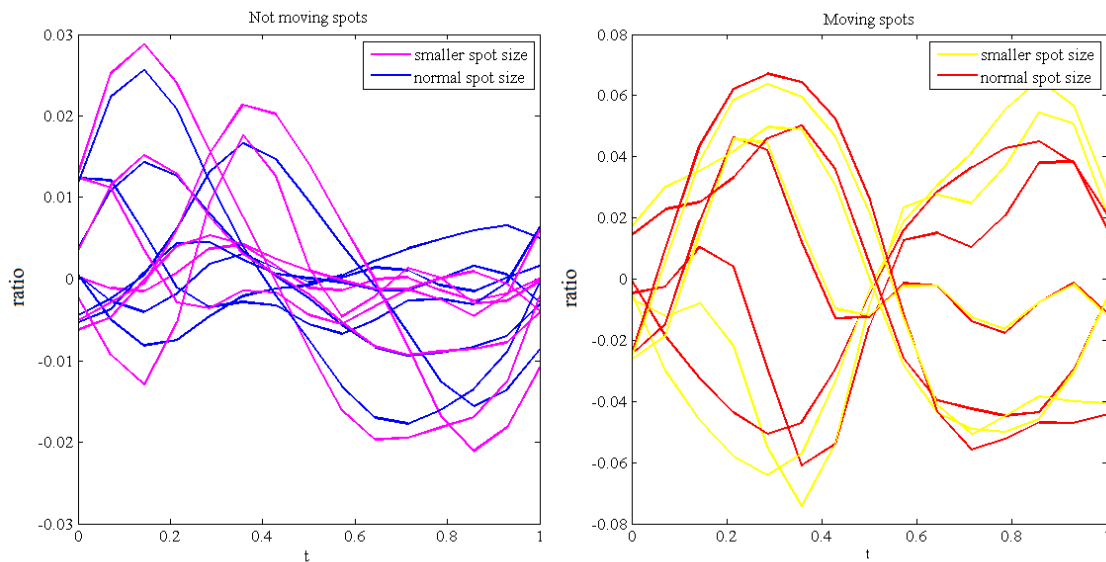
Figure 69: Ratio (*eGFP/RFP*) according to the spots size in not moving (left) and moving (right) cardiomyocytes. Ratio curves are almost the same independently of the spots size, indicating that the error (ratio amplitude) does not depend on the dimension of the spot.
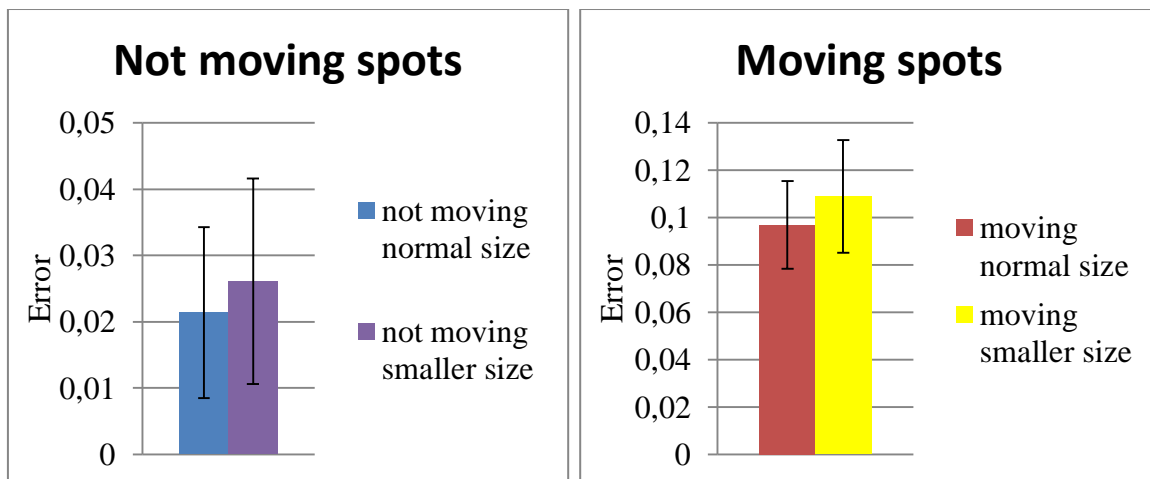
Figure 70: Error (amplitude of ratio oscillation) as a function of spots size in not moving (left) and moving (right) cardiomyocytes. Error in smaller and in normal size spots is not statistically different (p>0.05).
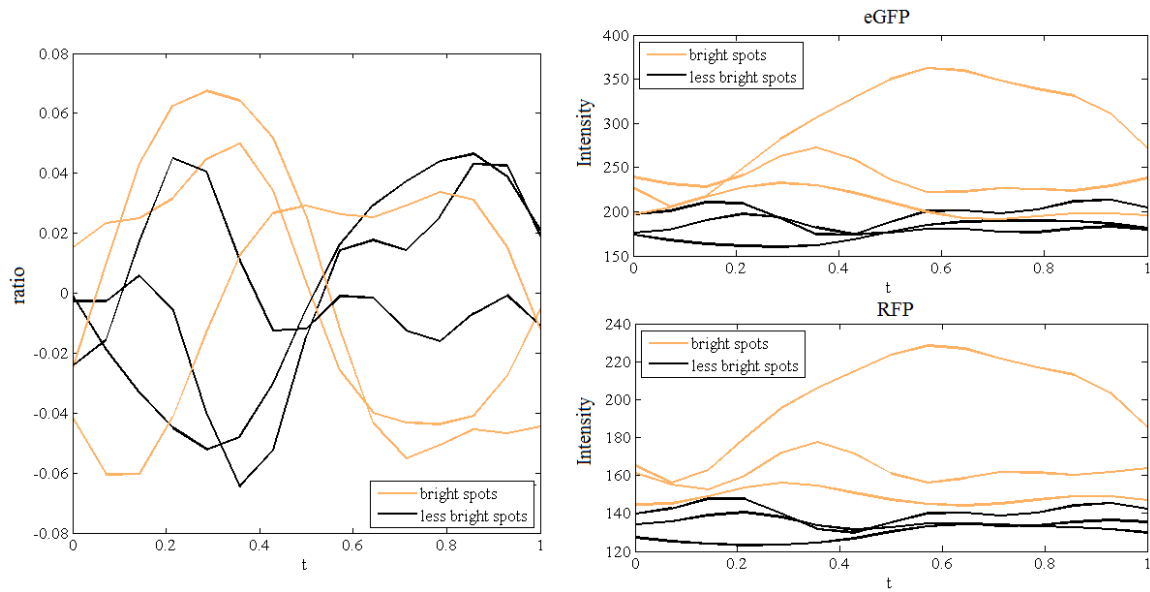
Figure 71: Ratio (*eGFP/RFP*) (left), *eGFP* and *RFP* intensities (right) in bright and less bright spots. The error (amplitude of ratio oscillation) is higher in brighter spots. The higher intensity of these spots can be due to their proximity to the light source of the microscope and to a higher expression of the fluorescent proteins in the cells.
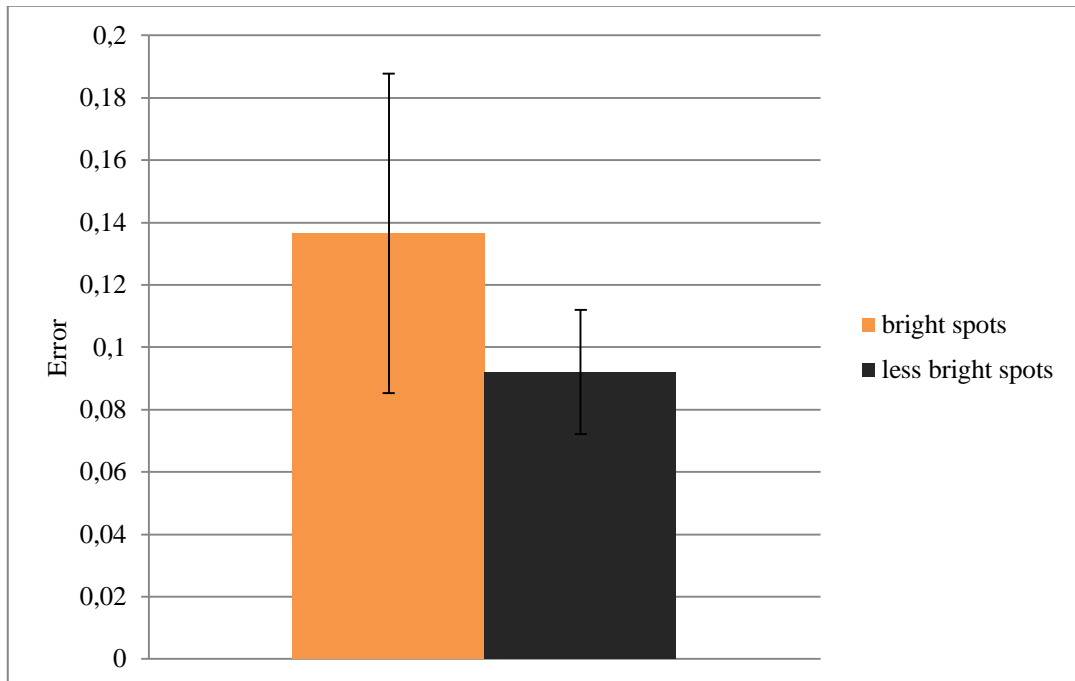
Figure 72: Error in spots with different red and green fluorescence signals intensities. Error seems higher in brighter spots but the difference is not statistically different (p>0.05).
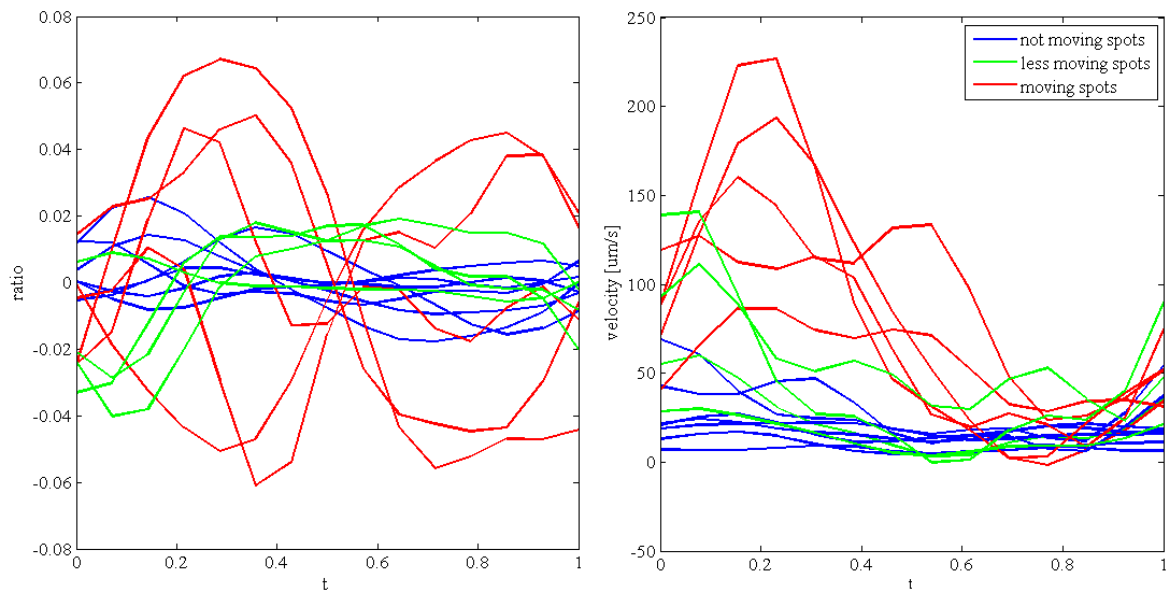
Figure 73: Correlation between ratio (*eGFP/RFP*) (left) and velocity (right) in not moving (blue), less moving (green) and moving (red) spots. The amplitude of the ratio oscillations is much higher in moving spots.
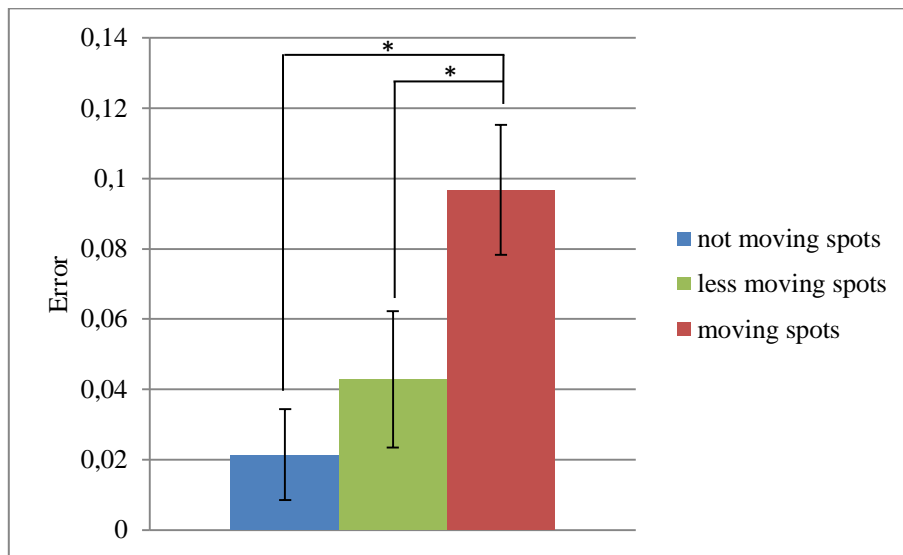
Figure 74: Error (amplitude of ratio oscillation) as a function of spots velocity. Error is significantly higher in moving spots than in not or less moving spots (* p<0.01).

75

These observations suggest that the oscillations due to the movements artefact cannot be completely removed. Therefore, only oscillations of the *gcamp5.0* intensity with amplitude larger than the discussed artefacts should be considered in the analysis of the beating heart. Therefore the dynamics of the calcium signal shown in Figure 67 was revised, deleting from the analysis the spots where the ratio between the two signals was smaller than a threshold defined as the highest error calculated in the control heart (0.14). The result so obtained is shown in Figure 75.
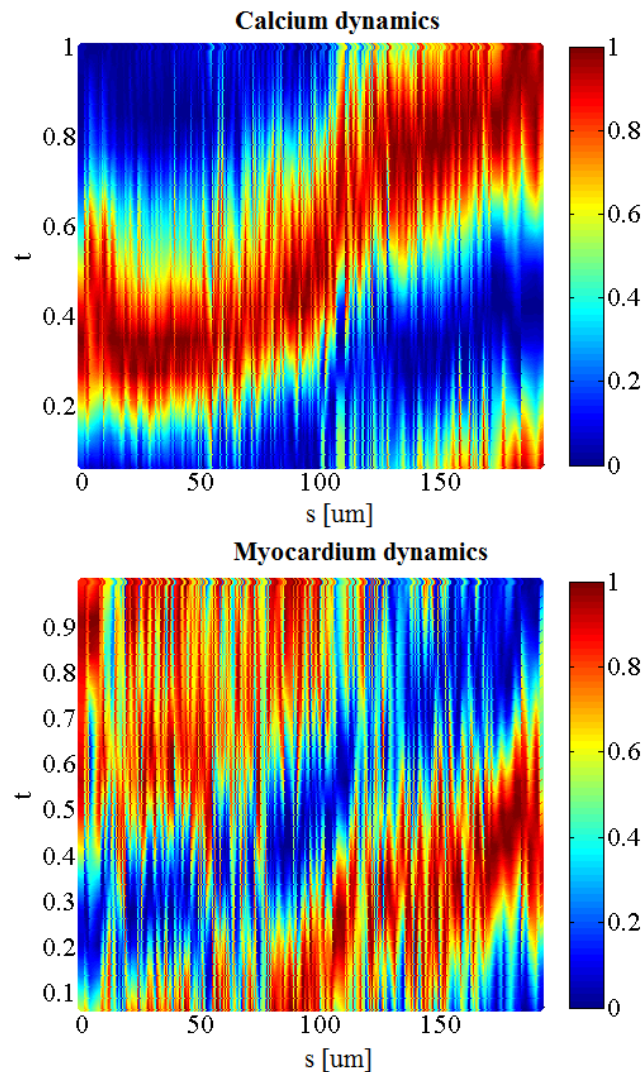
Figure 75: Dynamics of calcium (above) and myocardium (below) over the cardiac cycle along the centreline of the beating heart after deleting from the analysis the spots in which it is not possible to discriminate the information on the calcium from the error due to the movement artefact. 0 represents minimum signal intensity (above) and tissue contraction (below); 1 maximum signal intensity (above) and myocardium relaxation (below). The calcium wave is very similar to the contraction wave with a faster propagation at the inflow and at the outflow and a slower propagation in the central region.

76

The calcium wave in the myocardium is observable as the dark red curve in the panel above of Figure 75. The electric impulse starts at the inflow and propagates toward the outflow with different speed. In the central region, in fact, the propagation is slower, while at the inflow and at the outflow is faster.

3.3.4   Electromechanical coupling

To study the electromechanical coupling of the heart and to search for the feedback of the myocardium stretch on the calcium activity, the calcium wave was compared to the myocardium dynamics as given by studying the distance between neighbouring cardiomyocytes (Figure 75). The conduction pattern (red curve in the figure above) is very similar to the contraction wave (blue curve in the figure below) in the tissue: when the distance between cardiomyocytes reach the minimum, calcium signal is maximum, vice versa when the distance is maximum, the signal is minimum (Figure 76).
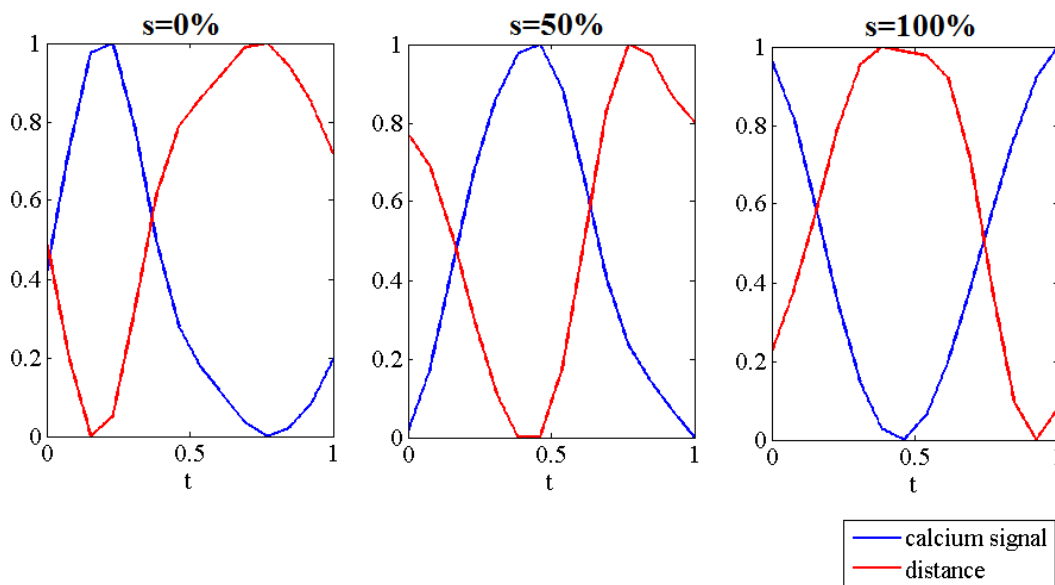
Figure 76: Comparison between calcium and myocardium dynamics in three cardiomyocytes of the beating heart at the inflow (s=0%), in the middle of the centreline (s=50%) and at the outflow (s=100%). The signals are in counterphase: the contraction of the tissue corresponds to the maximum in calcium intensity and the stretching to the minimum intensity.

Despite the fact that the contraction and the calcium signal are in generally in counterphase, some spots show a double peak in the calcium signal, one first peak associated to the contraction and a second peak arising during the stretching of the tissue. In some cases, the peak in the calcium signal corresponding to the stretching is smaller

than the peak associated to the contraction (<u>Figure 77</u>), but in some spots it is the opposite (<u>Figure 78</u>). The double peak in the calcium signal is not observed for s>63% of the centreline length.
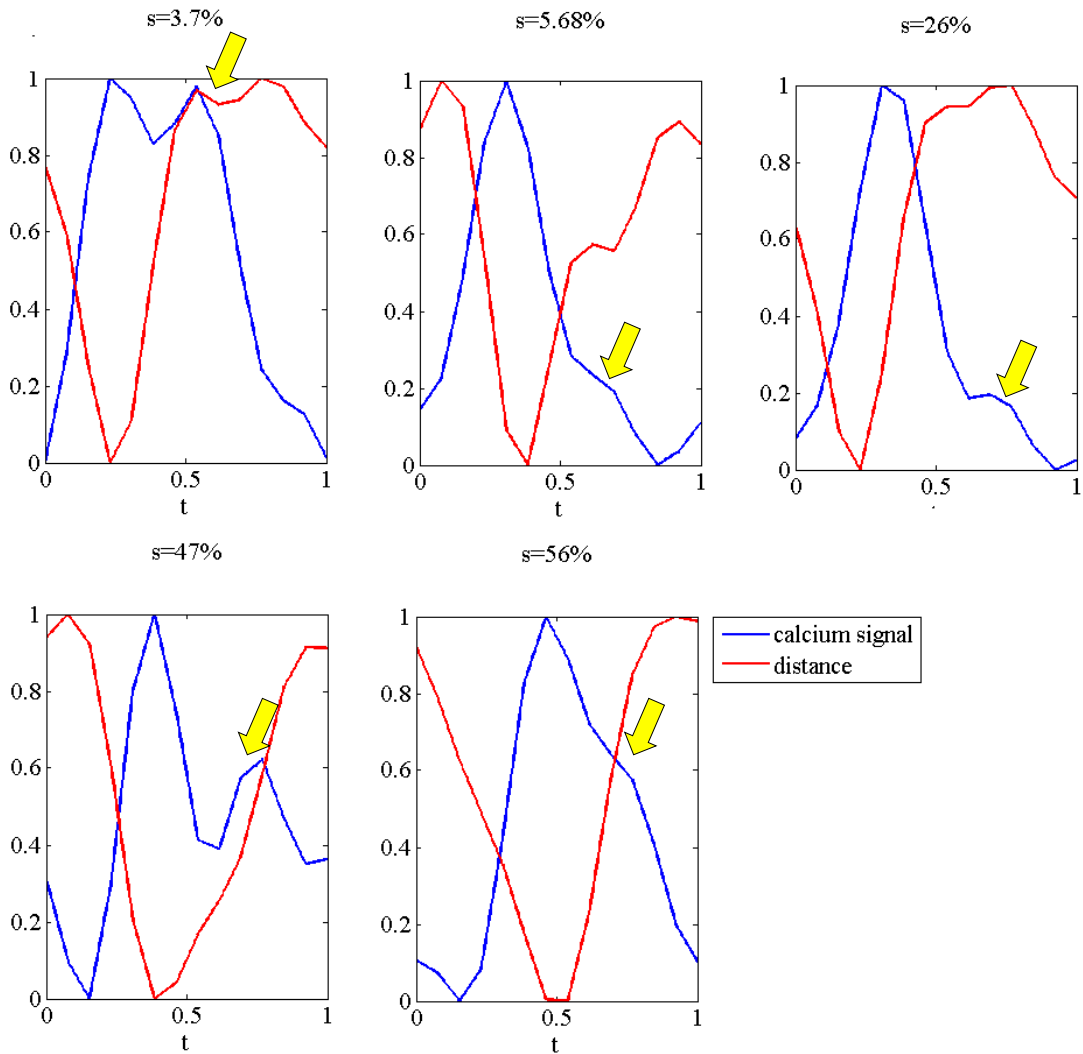
Figure 77: Double peak in calcium signal in five cardiomyocytes of the beating heart in different positions along the centreline. Calcium signal has a double peak, the higher corresponds to myocardium contraction (minimum distance), the other (yellow arrow) is smaller and corresponds to a stretched condition of the tissue.
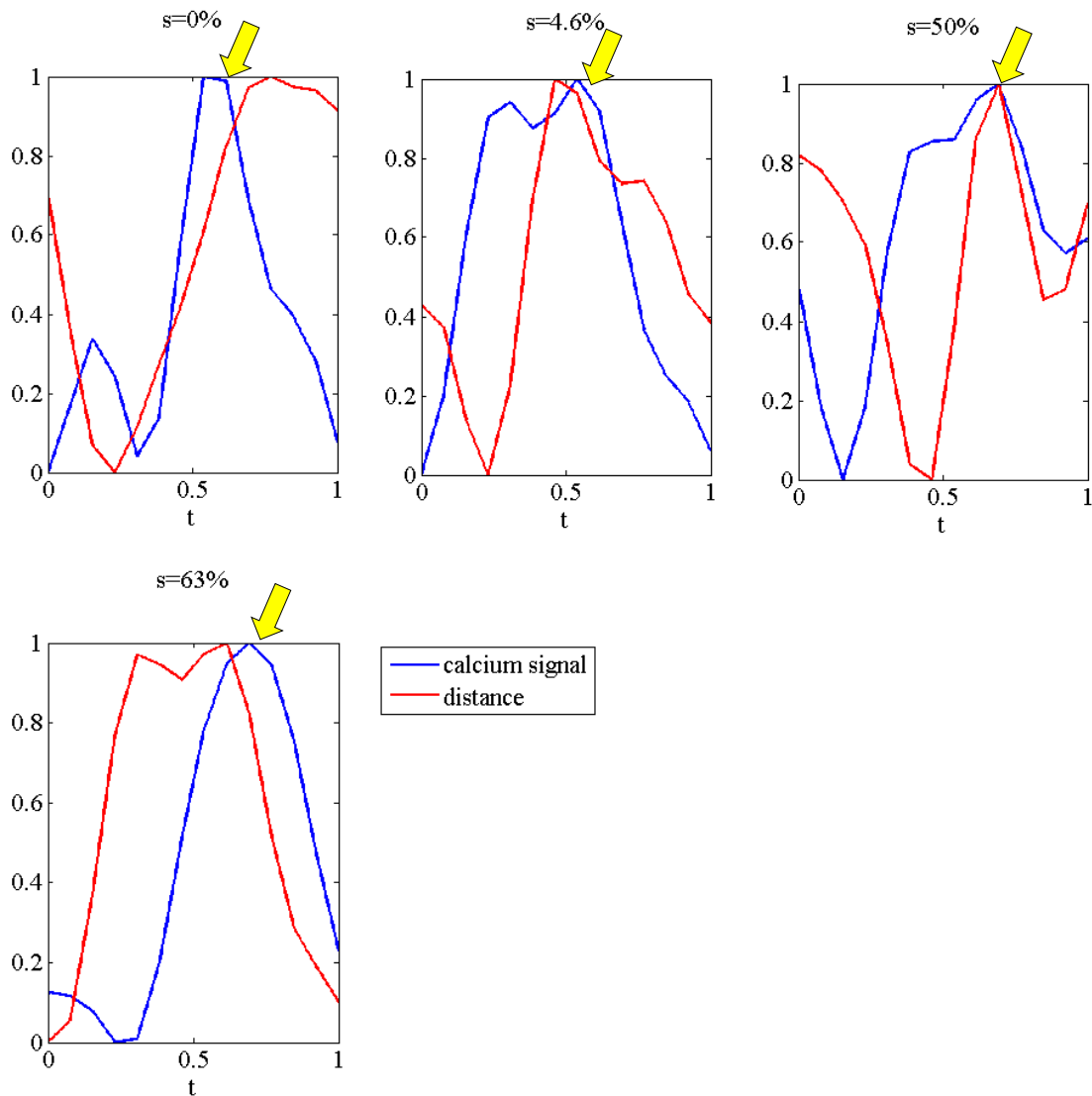
Figure 78: Double peak in calcium signal in four cardiomyocytes of the beating heart in different positions along the centreline. Calcium signal has a double peak, the smaller corresponds to myocardium contraction (minimum distance), the other (yellow arrow) is higher and corresponds to a stretched condition of the tissue.

4. Discussion

Congenital heart diseases arise when the physiological development of the organ is altered and the causes of these anomalies are mainly unknown. In the hope that one day early diagnosis and cure of these conditions will be possible, many researches are trying to clarify why and how cardiogenesis is impaired. In this context, the starting point is to consider the development and working mechanism of the heart under normal conditions. The study of the mechanics and electrophysiology of the embryonic heart is a fundamental step since they contribute to and are affected by pathological conditions.

In the present work, live imaging of the heart tube of 28-30 hpf zebrafish embryos was performed to investigate tissue dynamics and calcium signaling *in vivo* at early developmental stage.

The study of the beating heart should consider both the 3D geometry and the movement of the organ and since it is complex to deal with 4D (space + time) data, previous quantitative works limited the analysis of the heart to two spatial dimensions. On the contrary, the present work wants to consider the heart tube in 3D in order to further investigate its still unknown working mechanism. New dedicated tools were thus developed to analyse the 4D dataset resulting from the live imaging of the beating heart.

A semi-automatic method was implemented in Matlab to parametrize the geometry of the heart at each time step of the cardiac cycle, a fundamental step to assign to each region or cell of the heart a specific position and to study the heart in space and in time. The algorithm, that segments the cross-sections of the myocardium and the endocardium using ellipses, also quantifies the cross-sectional areas of the two layers over the cardiac cycle along the heart tube, giving a wide range of information on the anatomy and dynamics of the two layers of the heart.

Examples of the information obtained on the anatomy of the myocardium and endocardium are discussed in the following paragraph.

In the myocardium, the shape of the cross-sections is elliptical during relaxation and more circular during contraction. The endocardium is elliptical during relaxation but displays irregular contours and folds during contraction. Similar observations were made in chick heart tube at Hamburger and Hamilton developmental stage 13[6] by Garita *et al.* [39], who

---

[6] Chick embryos are usually staged according to Hamburger and Hamilton (HH). HH stage 13 corresponds to 1-2 days post fecundation in zebrafish (see Table 1).

suggested that these evaginations, present only in the endocardium, might help the lumen expanding during the filling and closing during the ejection. This hypothesis seems to be confirmed by the fact that the endocardium, going from the relaxed to the contracted condition, changes its area more than the myocardium. In the analysed hearts, in fact, the Area Fractional Shortening (AFS), index which represents how much in percentage the cross-sectional area changes from its maximum to its minimum value, was found between -30% and -60% in the myocardium and between -50% and -80% in the endocardium. Differences in AFS were found between samples and between regions of the heart. This was not observed by Garita *et al.* in the chicken embryo, where the AFS was almost constant along the heart tube (between -40% and -50% for the myocardium and around -80% for the endocardium). However, this might be due to differences in the observed developmental stage, which is not easily comparable between different animal models.

In the endocardium, larger and smaller AFS were measured respectively in the final part of the heart and at the inflow, and from the study of red blood cells velocity, regurgitations were found in the inflow region of the heart and seemed to disappear while proceeding towards the final part of the heart tube. Reversing flows are thus present in regions with lower cross-sectional constriction and absent where the shrinking is higher. These observations suggest that the constriction of the endocardial lumen is the main factor that guarantees the unidirectional blood flow in the valveless tube, as proposed by Hove *et al.* [13].

The developed algorithm was then used to quantify the dynamics of the myocardium and the endocardium. In order to extend the description to all the layers composing the heart and to investigate the relationships between them, also the third layer, i.e. the cardiac jelly, was considered.

The analysis of the cardiac jelly currently requires the definition by the user of the perimeters of the myocardium and endocardium cross-sections to reduce the artefacts due to the ellipse fitting of the endocardium and, to limit the manual work, the quantification of the cardiac jelly area was done only in few cross-sections along the heart. A new algorithm that better defines the cross-sections of the endocardium and calculates more precisely its cross-sectional areas might be developed in the future to extend the analysis of the cardiac jelly to the whole heart.

The results showed that the contraction wave in the myocardium propagates linearly along the tube, but a delay in the propagation was observed in the outflow region in most of the hearts analyses. This was never quantified at the developmental stage considered (28-30 hpf) by previous works in literature which are mainly based on qualitative observation of the contraction wave. The delay in the outflow region may reflect a transformation that is affecting only the final part of the heart at the developmental time considered (in this case it could be a transitory characteristic during the looping process not visible at earlier or later stages), or be a requirement for the pumping action. The delay at the outflow, in fact, might give time to the upstream region to fill with blood and lead to the simultaneous contraction of the inflow and outflow observed in many of the hearts analysed in order to help the pressure to increase in the central part of the tube in view of the systole.

Only in one of the studied hearts, the myocardium dynamics showed a different pattern, with higher wave velocity at the inflow and at the outflow and a slower propagation in the middle. This indicates that the heart was probably older than the others.

As regards endocardium dynamics, the results in the two hearts analysed showed some differences which may indicate that the developmental stage of the two hearts was not exactly the same. In particular the irregular dynamics observed in the endocardium of heart 1 in Figure 50 could suggest a contraction still immature in this heart. It is reported in literature, in fact, that the primitive heart has an asynchronous movement at the onset of the blood flow, replaced later by a regular contraction. The linear wave observed in heart 2 in Figure 50 may be the result of this maturation. Since the myocardium of the two hearts shows a similar contraction pattern, however, this seems not to be the case and also the possibility of a pathological condition of one of the two samples can be excluded. Therefore the differences in the endocardium dynamics are probably due to artefacts in the area calculation of the layer since the observed invaginations of the endocardial layer are not always well fitted by an ellipse.

From the study of the endocardium dynamics by Garita *et al.* in chick embryo, contraction wave seems to propagate from the inflow to the outflow with uniform speed except for the centre of the heart, where the contraction starts simultaneously with the inflow [39]. However the small number of cross-sections considered in that work (six) could hide a much more complex dynamics of the tissue and does not allow to draw conclusions about

the contraction wave speed. To obtain better results, the algorithm that fits endocardium cross-section should be optimized and a greater number of samples should be analysed.

Though not exactly in phase, myocardium and endocardium cross-sectional area change together and the contraction of the two layers occurs simultaneously, suggesting that the transmission of the force starting the contraction from myocardium to endocardium is immediate or faster than the time resolution of the confocal microscope used for the acquisition (and so not visible from the results of the analysis). As regards the cardiac jelly dynamics, area seems to change in counterphase to myocardium and endocardium, increasing during heart contraction and decreasing during relaxation, as previously shown also by Garita *et al.* and Forouhar *et al.* [38] [39]. The action of the cardiac jelly may thus help the expansion of the cross-sections of the two tissues after the systole and the contraction after the diastole, by accumulating and returning elastic energy as a spring. However, in some cases the curves describing the dynamics of the myocardium and endocardium slightly deviate from each other while going from the contracted to the relaxed condition or vice versa, causing a peak in the cardiac jelly area and a phase shift between the instants of heart contraction and maximum cardiac jelly area. Other samples should be analysed to understand whether this phase shift is effectively present and functional in the heart or whether it is an artefact due to the area calculation of the layers of the heart.

Furthermore, the analysis of myocardium and endocardium dynamics showed that the contraction and the relaxation of the two tissues is not instantaneous but each region of the heart remains in contracted and stretched condition for a certain time. The contraction and relaxation durations change along the heart tube: the first half of the heart remains expanded the longest (40-60% of the entire cardiac cycle in the myocardium and 50-60% in the endocardium) and contracted the shortest (20% in both the tissues) while the outflow region remains contracted the longest (30-40% in both the tissues) and expanded the shortest (20% in the myocardium and 20-30% in the endocardium). The inversion occurs progressively along the centreline with a linear pattern in the endocardium; in the myocardium, the relaxation and contraction durations are almost constant in the first half of the heart, in the centre of the tube they respectively decrease and increase in a sharp way and they remain constant in the final region. The more regular transition observed in the endocardium may be due to a smoothing action of the cardiac jelly. The increase in the

contraction time going from the inflow to the outflow of the heart was observed also in the chick endocardium by Garita *et al.* [39], who suggested that the longer contraction status of the outflow region of the heart may allow the upstream region to be filled with blood and the longer relaxation in the first part of the tube could help the blood enter the tube and the pressure increase for the ejection.

The most ambitious goal of the work was the development of a method to quantify and compare for the first time *in vivo* the dynamics and the calcium oscillations in the myocardium in order to investigate the electro-mechanical coupling of the heart.
A combination of existent and newly developed algorithms was thus exploited to quantify the relationship between stretching and calcium in each cell.
Since the electric impulse propagation in a beating heart had never been quantified before, at first a non-beating heart, in which the electro-mechanical isolation was reversibly achieved by drugs as reported in literature [20], was considered to test the activity of the *gcamp5.0* calcium reporter.
The calcium wave observed started from the inflow of the heart, supporting the observation that the cardiomyocytes in this region possess a pacemaker phenotype [3], and propagated to the outflow with change in speed in the second half of the heart: the velocity in this region was found to decrease, increase and decrease again. A linear calcium wave with faster propagation in the final region of the tube was previously reported by Chi *et al.* [20] in a 2D analysis.
After considering the calcium dynamics in the non-beating heart, the same heart in beating conditions was studied and the baseline signal of the myocardium (*RFP* signal) was used to remove the artefacts due to the movement of the heart that affects the *gcamp5.0* signal. The calcium signal was thus calculated as the ratio between *gcamp5.0* and *RFP* signals.
The strategy adopted was verified in one control heart and the results showed that the movement artefact is not completely removable. An error in the ratio signal is unavoidably present, probably due to the fact that the *gcamp5.0* and *RFP* signals are acquired separately during the imaging, that means in consecutive cardiac cycles, and synchronized in the post-acquisition process. Cardiac cycles are not exactly identical to each other, so after the synchronization, small differences between the two signals always appear. However, since the error resulted below a certain threshold in the control heart, the maximum value of these differences in the control heart was used as a threshold in the beating heart of the

calcium reporter line to remove from the analysis those cardiomyocytes in which the ratio between *gcamp5.0* and *RFP* signal was comparable with the error of the control. The calcium wave obtained with this strategy shows a pattern very similar to the contraction of the myocardium and propagates from the inflow to the outflow of the heart with higher speed in the first and final part of the tube and lower velocity in the middle. Both the contraction and the conduction waves in the heart analysed suggest that the heart was not at 28-30 hpf, but older. In fact, after the atrioventricular canal formation, a delay in the contraction and electric conduction waves develops in the atrioventricular region and the propagation accelerates in the ventricular region of the heart [4][20].

The discrepancies observed between the beating and non-beating heart suggest that the conduction pattern might be different in the two conditions, though these differences may also be due to the fact that the heart was acquired at different developmental times. It was, in fact, necessary to wait between the acquisitions of the non-beating and beating heart that the stopped heart restarted the contraction. Therefore, the comparison between the electric impulse propagation with and without the heart movement has to be repeated in other samples trying to reduce the time lapse between the two acquisitions. This could help to study the effect of the stretching of the myocardium on the calcium.

In the beating heart, the conduction and contraction waves were found in counterphase in almost all the cardiomyocytes: the calcium reached the maximum level during the contraction of the tissue as expected from the normal mechanism of electromechanical coupling. It is known, in fact, that the contraction in muscles occurs thanks to the calcium release from the sarcoplasmic reticulum [26-28]. In some cardiomyocytes, however, an increase in calcium was observed also in correspondence to a stretched condition of the myocardium.

This suggest that a mechanotransduction mechanism similar to the stretched-dependent calcium activation previously documented in adult cardiomyocytes [29-32] may be in action also in the embryonic heart. From the results obtained the mechanism seemed to be absent close to the outflow of the heart. A larger amount of samples should be considered to verify these preliminary observations and to understand if the stretched-dependent calcium increase is localized in specific regions of the heart.

5. Conclusion

In the present work, tissue dynamics and calcium signaling of the zebrafish primitive heart tube were investigated on the basis of quantitative live imaging of the beating heart. New tools were developed *ad hoc* to deal with the complex 4D dataset and to quantify the dynamics of the three layers composing the heart and of the calcium in the myocardium.

The algorithms implemented for the analysis of the heart dynamics allow an efficient semi-automatic analysis of the myocardium, though it could be further optimized for the endocardium and the jelly layers. In fact, the method here proposed, based on the fitting of the heart cross-sections with ellipses, gives good results in the analysis of the myocardium, but seems not to fully describe the endocardium and this hampers an automatic study of the cardiac jelly.

Despite these limitations, the application of these algorithms to several hearts at 28-30 hpf showed that they represent a valid method for a preliminary study of the heart, giving access to several information.

For example, anatomical data can be extracted and the results obtained are in general consistent with the works available in literature on the chick model at the same developmental stage, confirming that zebrafish is a proper model to study the early stages of heart development, though the mature heart of the animal is different from mammal and avian hearts.

Furthermore the dynamics of the myocardium and the endocardium over the cardiac cycle can be described in a (i) quantitative and (ii) three-dimensional way and (iii) along the whole length of the heart tube, three characteristics that hardly coexisted in the previous works in literature. These data can be, then, compared to study the relationships between the layers of the heart.

The results obtained are still preliminary and to further investigate the working mechanism of the valveless heart at early developmental stage, a more detailed study should be done on the cardiac jelly layer since it seems to play a fundamental role in the pumping action. In addition, more attention should be definitely paid to the fluid dynamics of the heart. In the present work, the analysis of red blood cells velocity was, in fact, two-dimensional and limited to a single plane of the heart. Since the 3D analysis of the blood flow with the method here proposed is impossible and on the base of direct measurements is complex, the flow in the heart could be predicted through *in silico* models. In this contest, mesh-free

methods offer the great advantage of not requiring the challenging discretization of the moving flow domain. Meshless methods based on the dynamics of the heart wall have already been applied to predict the haemodynamics of the embryonic heart, but using a 2D description of the wall dynamics [24] [49].

Thanks to the segmentation algorithm developed in the present work, the quantification of the 3D dynamics of the endocardial lumen over the cardiac cycle is possible and the data obtained could be used in the future as boundary conditions for 3D simulations of the embryonic heart.

The method developed to analyse the calcium dynamics in the myocardium of the beating heart and to compare it with the dynamics of the tissue opens the door to a future detailed investigation of the coupling between electric impulse and mechanics of the layer *in vivo*. In fact, the presented results on the stretched-dependent calcium activation obtained are promising and the mechanotransduction mechanism should be investigated further.

Since the analysis of the calcium response to stretch is complicated by the normal relationship between the intracellular calcium and the contraction of the heart, other actors involved in the mechanotransduction pathway could be considered. Several studies in literature have already explained how the mechano-electric feedback can be blocked by acting with drugs on microtubules, NOX enzymes and ROS production [29] [32]. If the calcium peaks observed in the present work disappeared after arresting the mechanotransduction process by removing the action of one of these components, the existence of the stretched-dependent calcium response could be verified.

Another option would be to alter the stretching of the myocardium *in vivo* and compare the calcium signal in presence of the physiological and the altered stretching. A preliminary test was tempted trying to stretch the whole embryo by applying an external load and simultaneously monitoring calcium activity under the fluorescent microscope. However the experiment is still under optimization phase.

The great advantage of the developed tools is that the analysis can be easily applied to a large number of samples and potentially extended to hearts at different developmental stages and in pathological conditions. In the present work, in fact, the algorithms were applied to characterize the heart in physiological conditions, which is a starting point for further studies on abnormal (pathological) hearts. Therefore it would be very interesting, in the future, to repeat the study in embryos in which the normal cardiogenesis process is

genetically altered. For example, silent heart mutants could be considered to study in three-dimensions how the absence of contraction affects the electric impulse propagation; or embryos with perturbed blood fluid mechanics could be analysed to understand whether the shear stress exerted by the blood flow on the endocardium wall, which have been shown to affect the normal development of the heart at 48 hpf [24], alters the dynamics of the tissue at early stages of development and whether this affects the behaviour of the myocardium and cardiac jelly too.

In conclusion, the developed tools and the live imaging approach could be potentially applied in several contexts and provide additional information on the working mechanisms of the primitive heart, on the mechanotransduction processes involved in its development and on the causes and consequences of altered conditions of the heart in cardiogenesis. The deepening of all these aspects, in the future, may further the current knowledge on congenital heart diseases.

Bibliography

[1] Mozaffarian *et al*., Heart Disease and Stroke Statistics—2016 Update: A report from the American Heart Association, *Circulation,* 2016, 133(4), e38-e360

[2] Kamino *et al*., Localization of pacemaker activity in early embryonic heart monitored using voltage-sensitive dye, *Nature*, 1981, 290, 595-597

[3] Christoffels *et al.*, Development of the Pacemaker Tissues of the Heart, *Circulation Research*, 2010, 106, 240-254

[4] Boselli *et al.*, Blood flow mechanics in cardiovascular development, *Cellular and Molecular Life Science*, 2015, 72(13), 2545-59

[5] Iaizzo, Handbook of Cardiac Anatomy, Physiology, and Devices (Current Clinical Oncology), Springer 2nd ed. 2009

[6] Moorman *et al.*, Development of the heart: formation of the cardiac chambers and arterial trunks, *Heart* 2003, 89, 806–814

[7] Dhanantwari *et al.*, Human Cardiac Development in the First Trimester A High-Resolution Magnetic Resonance Imaging and Episcopic Fluorescence Image Capture Atlas, *Circulation*, 2009, 120, 343-351

[8] Lindsey *et al.*, Mechanical regulation of cardiac development, *Frontiers in Physiology*, 5, 1-15

[9] Kowalski *et al*., Investigating developmental cardiovascular biomechanics and the origins of congenital heart defects, *Frontiers in Physiology*, 2014 5, 408-408

[10] OpenStax, Anatomy & Physiology, 2014 [Online]. Available: http://cnx.org/contents/14fb4ad7-39a1-4eee-ab6e-3ef2482e3e22@6.27 [Accessed: 10-02-2016].

[11] Cohen *et al*., A house with many rooms: how the heart got its chambers with *foxn4, Genes & Development*, 2008, 22(6), 706–710

[12] Nerurkar *et al*., Morphogenetic adaptation of the looping embryonic heart to altered mechanical loads, *Developmental Dynamics*, 2006, 235(7), 1822-9

[13] Hove *et al*., Intracardiac fluid forces are an essential epigenetic factor for embryonic cardiogenesis, Nature, 2003, 421, 172-177

[14] Damon *et al*., Patterns of muscular strain in the embryonic heart wall, *Developmental Dynamics*, 2009, 238, 1535-1546

[15] Liu *et al*., A dual role for ErbB2 signaling in cardiac trabeculation, *Development*, 2010, 137, 3867-3875

[16] Auman *et al.,* Functional modulation of cardiac form through regionally confined cell shape changes, *PLOS biology*, 2007, 5, 53

[17] Hierck *et al*., Fluid shear stress and inner curvature remodelling of the embryonic heart. Choosing the right lane!, *the Scientific World Journal*, 2008, 8, 212-22

[18] Yalcin *et al*., Hemodynamic patterning of the avian atrioventricular valve, *Developmental Dynamics*, 2011, 240, 23-35

[19] Reckova *et al*., Haemodynamics is a key epigenetic factor in development of the cardiac conduction system, *Circulation Research*, 2003, 93, 77-85

[20] Chi *et al*., Genetic and physiologic dissection of the vertebrate cardiac conduction system, *PLOS Biology*, 2008, 6, 1006-1017

[21] Janmey *et al*., Mechanisms of mechanical signaling in development and disease, *Journal of Cell Science*, 2011, 124, 9-18

[22] Menon *et al*., Altered Hemodynamics in the Embryonic Heart Affects Outflow Valve Development, *Journal of Cardiovascular Development and Disease*, 2015, 2, 108-124

[23] Balachandran *et al*., Cyclic strain induces dual-mode endothelial mesenchymal transformation of the cardiac valve, *Proceedings of the National Academy of Science of the United States of America*, 2011, 108, 19943-19948

[24] Heckel *et al.*, Oscillatory flow modulates mechanosensitive klf2a expression through trpv4 and trpp2 during heart valve development, *Current Biology*, 2015, 25, 1354-61

[25] Butcher *et al.*, Transition in early embryonic atrioventricular valvular function correspond with changes in cushion biomechanics that are predictable by tissue composition, *Circulation Research*, 100, 1503-1511

[26] Fearnley *et al.*, Calcium Signaling in Cardiac Myocytes, *Cold spring harbor perspectives in biology*, 2011, 3, a004242

[27] Haustein *et al.*, Excitation-Contraction Coupling in Zebrafish Ventricular Myocardium Is Regulated by Trans-Sarcolemmal Ca2+ Influx and Sarcoplasmic Reticulum Ca2+Release, *PLoS One*, 2015; 10(5), e0125654

[28] Shiels *et al.,* The Sarcoplasmic Reticulum and the Evolution of the Vertebrate Heart, *Physiology*, 2014, 29(6), 456-469

[29] Prosser *et al.*, X-ROS Signaling: Rapid Mechano-Chemo Transduction in Heart, *Science*, 2011, 333, 1440-45

[30] Iribe *et al.*, Axial stretch enhances sarcoplasmic reticulum Ca^{2+} leak and cellular Ca^{2+} reuptake in guinea pig ventricular myocytes: experiments and models, *Progress in biophysics and molecular biology*, 2008, 97, 298-311

[31] Iribe *et al.*, Axial stretch of rat single ventricular cardiomyocytes causes an acute and transient increase in Ca^{2+} spark rate, *Circulation research*, 2009, 104, 787-95

[32] Prosser *et al.*, X-ROS Signaling in heart and skeletal muscle: stretch-dependent local ROS regulates $[Ca^{2+}]_i$, *Journal of Molecular and Cellular Cardiology*, 2013, 58, 172-181

[33] Vermot *et al.*, Reversing Blood Flows Act through klf2a to Ensure Normal Valvulogenesis in the Developing Heart, Plos Biology, 2009, 7 (11)

[34] Goetz *et al.*, Endothelial Cilia Mediate Low Flow Sensing during Zebrafish Vascular Development, *Cell Reports*, 2014, 6, 799–808

[35] Bakkers, Zebrafish as a model to study cardiac development and human cardiac disease, *Cardiovascular Research,* 2011, 91, 279-288

[36] Leica Microsystems, Principle of Light Sheet Imaging, [Online]. Available: http://www.leica-microsystems.com/products/confocal-microscopes/details/product/leica-tcs-sp8-dls/ [Accessed: 14-02-2016]

[37] Manner *et al*., How does the tubular embryonic heart work? Looking for the physical mechanism generating unidirectional blood flow in the valveless embryonic heart tube, *Developmental Dynamics*, 2010, 239, 1035-1046

[38] Forouhar *et al*., The embryonic vertebrate heart tube is a dynamic suction pump, *Science*, 2006, 312

[39] Garita *et al*., Blood flow dynamics of one cardiac cycle and relationship to mechanotransduction and trabeculation during heart looping, A*merican Journal of Physiology - Heart and Circulatory Physiology*, 2011, 300

[40] Midgett *et al.*, Blood flow through the embryonic heart outflow tract during cardiac looping in HH13-HH18 chicken embryos, *Journal of Royal Society Interface*, 2015, 12

[41] Asakawa *et al.,* Genetic dissection of neural circuits by Tol2 transposon-mediated Gal4 gene and enhancer trapping in zebrafish, *Proceedings of the National Academy of Sciences of the United States of America,* 2008, 105(4), 1255-60

[42] Halpern *et al*., Gal4/UAS Transgenic Tools and Their Application to Zebrafish, *Zebrafish*, 2008, 5(2), 97-110

[43] Cold Spring Harbor Laboratory Press, Embryo medium for zebrafish, 2011, [Online]. Available: http://cshprotocols.cshlp.org/content/2011/7/pdb.rec12471.short [Accessed: 01-03-2016]

[44] JoVE Science Education Database, Zebrafish Breeding and Embryo Handling, 2016, [Online]. Available: http://www.jove.com/science-education/5150/zebrafish-breeding-and-embryo-handling [Accessed: 20-02-2016]

[45] Fishforscience.comTv, Sorting dead from live zebrafish embryos, [Online]. Available: https://www.youtube.com/watch?v=dIY9zKQJNk0 [Accessed: 15-02-2016]

[46] Fishforscience.comTv, Dechorionating zebrafish embryos, 2009, [Online]. Available: https://www.youtube.com/watch?v=3LbYTEu1Fo8 [Accessed: 15-02-2016]

[47] Liebling *et al.*, Double time-scale image reconstruction of the beating and developing embryonic zebrafish heart, *The International Symposium on Biomedical Imaging,* 2008, 855-858

[48] Liebling *et al.*, Four-dimensional cardiac imaging in living embryos via postacquisition synchronization of nongated slice sequences, *Journal of Biomedical Optics*, 2005, 10

[49] Boselli *et al.*, Live imaging and modeling for shear stress quantification in the embryonic zebrafish heart, *Methods*, 2016, 94, 129-34